การศึกษาลักษณะจำเพาะของรอยแยกในแอ่งกักเก็บโดยใช้กระบวนการหยั่งทางธรณีฟิสิกส์

Characterization of Reservoir Fractures Using Conventional Geophysical Logging

ไพฑูรย์ ละอองสกุล

Paitoon Laongsakul

วิทยานิพนธ์นี้เป็นส่วนหนึ่งของการศึกษาตามหลักสูตรปริญญา

วิทยาศาสตรมหาบัณฑิต สาขาวิชาธรณีฟิสิกส์

มหาวิทยาลัยสงขลานครินทร์

A Thesis Submitted in Partial Fulfillment of the Requirements for the Degree of Master of Science in Environmental Management
Prince of Songkla University
2010

Thesis Title	Characterization of Reservoir Fractures Using Conventional Geophysical Logging
Author	Mr. Paitoon Laongsakul
Major Program	Geophysics

Major Advisor:

……
(Dr. Helmut Dürrast)

Examining Committee:

…….Chairperson
(Dr. Prajak Saeung)

…….
(Dr. Sawasdee Yordkhayhun)

.....…….
(Asst. Prof. Dr. Warawutti Lohawijarn)

.....……....
(Dr. Helmut Dürrast)

The Graduate School, Prince of Songkla University, has approved this thesis as partial fulfillment of the requirements for the Master of Science Degree in Geophysics

...……..…….....
(Prof. Dr. Amornrat Phongdara)
Dean of Graduate School

Thesis Title	Characterization of Reservoir Fractures Using Conventional Geophysical Logging
Author	Mr. Paitoon Laongsakul
Major Program	Geophysics
Academic Year	2010

ABSTRACT

In hydrocarbon exploration fractures play an important role as possible pathways for the hydrocarbon flow and by this enhancing the overall formation's permeability. Advanced logging methods for fracture analysis, like the acoustic borehole televiewer and Formation Microscanner (FMS) are available, but these are additional and expensive tools. However, open and with water or hydrocarbon filled fractures are also sensitive to electrical methods and other conventional logging methods. For this study conventional logging data (e.g. electric, seismic) were available plus additional fracture information from FMS. Taking into account the borehole environment the result shown that the Micro-Spherically Focused Log (MSFL®) indicate fractures by showing low resistivity spikes opposite open fractures, and high resistivity spikes opposite sealed ones. Compressional and shear wave velocities are reduced when passing trough the fracture zone, which are assumed to be perpendicular to borehole axis. The photoelectric absorption curve exhibit a very sharp peak in front of a fracture filled with barite loaded mud cake. The density log shows low density spikes that are not seen by the neutron log, usually where fractures, large vugs, or caverns exist. Borehole breakouts can also cause the same effect, but fractures are often present when this occurs. From the results and advanced understanding a fracture checklist is given for future application in similar lithologies. Further, a fracture index was developed and calculated for this well, which shows a relatively good correlation to fracture zones that are likely the main fluid pathways rather than single fractures. Finally, conventional logging tools are promising for fracture characterization with further research needed in this direction.

ACKNOWLEDGEMENTS

This work could have been completed only with the help and support from many people during my period of study.

Thanks to the Graduate School for financial support for this research project, the Department of Physics, Faculty of Science Prince of Songkhla University, Thailand, and the oil and gas exploration company for the logging data.

I would like to express my deepest gratitude to my advisors, Dr. Helmut Dürrast and also Assistant Professor Dr. Warrawutti Loharwijarn and Associate Professor Dr. Tripob Bhongsuwan for their valuable supervision, suggestions, supports, encouragement, guidance, and criticism throughout the course of my study.

Very special thanks to Dr. Sawasdee Yordkhayhun and Dr. Kamhaeng Wattanasen for their suggestion and comments during my research.

I am very grateful to my friends in Geophysics Laboratory, Department of Physics, and Faculty of Science, Prince of Songkla University for their practical help, providing the wonderful environment and friendship during the time of this study.

Finally, I would like to express my sincere gratitude and appreciation to my dear parents who are always on my mind and also the members of my family for their love, cheerfulness devotion and encouragement throughout my life.

Hatyai, October 2010

Paitoon Laongsaku;

CONTENTS

LIST OF FIGURES

Figure .....Page

LIST OF TABLES

Chapter 1

Introduction

1.1 Literature review

1.1.1 Fractures

Fractures are mechanical breaks in rocks involving discontinuities in displacement across surfaces or narrow zones. Fracture is a term used for all types of generic discontinuities (Bates and Jackson, 1980).

However, different kinds of fractures exist, with different geometries, mechanical effects, and flow properties. Based on the nature of the displacement discontinuity, commonly encountered fractures can be classified into three geologically based major groups, (a) dilating fractures, (b) shearing fractures, and (c) closing fractures or pressure solution surfaces are in sedimentary rock that are welded together by solution that occurs at the contact surfaces of grains (Bates and Jackson, 1980).

Dilating fractures, which are also referred to as joints, can be idealized as two rough surfaces with normal displacement discontinuity, which the surfaces have moved away from each other in a direction perpendicular to the surfaces. Shear fractures, which are also referred to as faults, are shear displacement discontinuities where the fracture surfaces move predominantly parallel to each other. Pressure solution surfaces are also referred to as stylolites where the sense of the displacement discontinuity is opposite that of dilating fractures (Fletcher and Pollard, 1981).

Fracture Orientation

Joints and faults are fundamentally different in terms of their associated stress fields; see Figure 1.1 (Pollard and Segall, 1987). Fracture orientations are relative to the principal stress orientations. Stress is defined as the force per unit area acting on a plane. Any stress state at a point in a solid body can be described completely by the orientations and magnitudes of three stresses called principal stresses. The principal stresses are oriented perpendicular to each other and to the three planes of no resolved shear stress at the point. Figure 1.1 shows a block of rock having constant stress

throughout. The symbol σ designates compressive or tensile stress. The principal stresses are defined with σ1 > σ2 > σ3. Compressive stress and shortening strain are considered positive in rock mechanics and structural geology because in the earth all three principal stresses are always compressive. Joints are somehow different because they are one of the most common types of natural rock fracture even though they require an effectively tensile driving stress. Pore fluid pressure drives most joints by producing tensile effective stress through poroelastic loading of flaws that are orders of magnitude larger than typical pores (Lacazette, 2001).

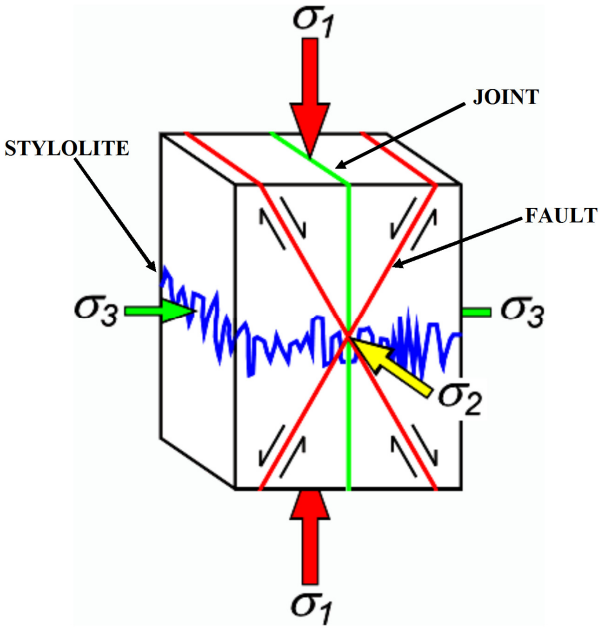

Figure 1.1 Fracture orientations relative to the principal stress orientations for different type of fractures (Pollard and Segall, 1987).

Figure 1.1 shows that the tip of a growing joint is always perpendicular to σ3 at the joint tip during propagation and curved joints indicate temporal and/or spatial variations in the orientation of σ3 during joint growth. Faults in virgin rocks form in each lithology with an approximately constant angle between σ1 and the two conjugate fault orientations around 25° to 40° but is normally about 30°. Pre–existing discontinuities with a wide range of orientations can be activated as faults if they are not oriented perpendicular to a principal stress. Deformation bands also tend to form

at 30° to σ1 but can be formed at any angle <90°. Stylolites and compaction bands form perpendicular to σ1.

Fracture aperture

Fracture aperture refers to the width of the opening between opposing walls of fractures, as measured perpendicular to the fracture surface (Luthi and Souhaite, 1990). For joints, the opening is filled with gases and/or fluids, whereas for veins the volume is filled with solid mineral crystals. It is important to distinguish between mechanical and hydraulic aperture. The mechanical aperture is a geometric property of the fracture; i.e., the physical measurement of the gap between two planar surfaces (see Figure 1.2, 1.3, and 1.4).

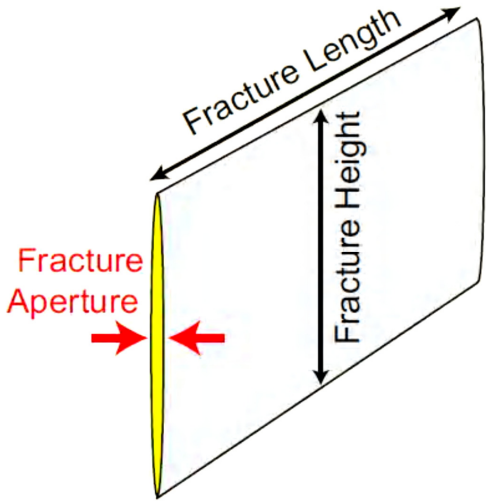

Figure 1.2 Schematic drawing showing components of fracture geometry, including length, height and mechanical aperture (after Luthi and Souhaite, 1990).

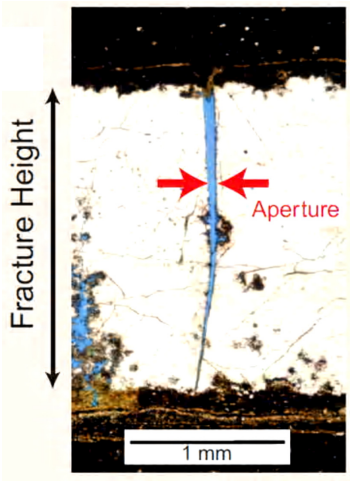

Figure 1.3 Thin section image of a small bed-confined fracture showing fracture aperture and height (after Luthi and Souhaite, 1990).

Figure 1.4 Outcrop of a large fracture in massive sandstone showing fracture aperture and length (after Luthi and Souhaite, 1990).

Fractures in hydrocarbon reservoir

In fractured reservoirs, the low permeability rock matrix holds the storage for the hydrocarbons, while the high permeability fracture system provides the pathways to produce them (La Pointe and Dershowitz, 1994). The amount of hydrocarbon that can be produced is a function of the fracture network connectivity and geometry. Naturally fractured reservoirs contain induced porosity formed by tension or shear stresses causing fractures in a competent rock. The effect of fracture porosity on reservoir performance, however, is very large due to its enormous contribution to

permeability. Naturally fractured reservoirs behave differently than unfractured reservoirs with similar porosity, due to the relative high flow capacity of the secondary porosity system (Crain, 2003). This often provides high initial production rates with good production forecasts.

Hydraulic fractures

A natural hydraulic fracture is the certain rock joint that could have been formed under in situ conditions characterized by a pore pressure larger than the least compressive stress (Secor, 1969). Hence, hydraulic fracture plays as a fluids path way if it connect to hydrocarbon reservoir (see Figure 1.5).

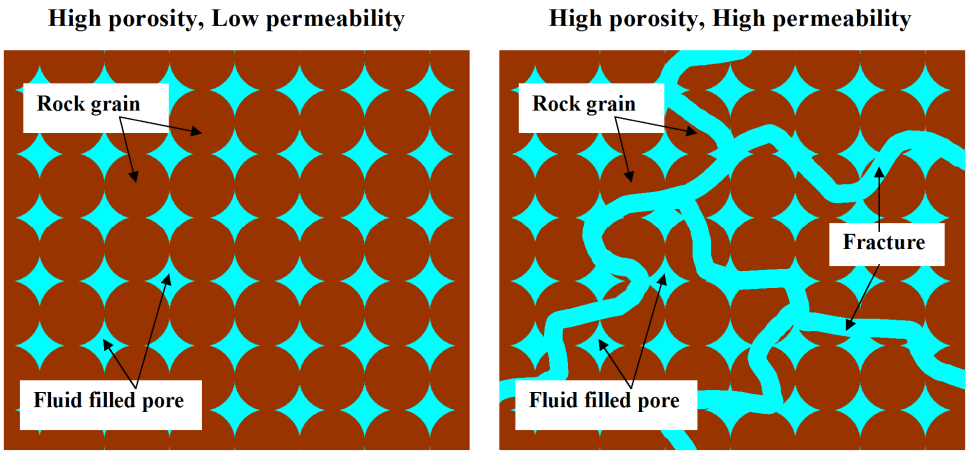

Figure 1.5 Fracture porosity increases permeability and fractures as fluids path way contribute to permeability. Left: without fracture; Right: with fractures.

1.1.2 Fracture detection methods

Fractures in the subsurface are zones of anomalous physical properties that can be detected remotely by various means, ranging from simple extrapolation of surface observations to sophisticated seismic and electromagnetic soundings. In general, methods that probe deeply into the subsurface have a poor ability to spatially resolve the locations of fractures and those with shorter ranges have correspondingly better resolutions. Geophysical fracture detection methods naturally divide themselves into three distinct scales, large scales associated with surface soundings, intermediate scales associated with surface to borehole and borehole to borehole soundings, and

small scales associated with measurements made on rocks immediately adjacent to a borehole or tunnel (National Academy of Sciences, 1996).

Surface methods

Shear wave splitting (SWS)

Seismic shear wave propagating through isotropic rocks containing stress aligned cracks behaves as if the rocks were anisotropic (Crampin, 1981; Hudson, 1981). This means that, regardless of its polarization at the source, a shear wave propagating through a cracked rock splits into two, a fast shear wave polarized parallel to the strike of the predominant cracks, and a slow one polarized perpendicular to it, which is time delayed by an amount proportional to the number of cracks per unit volume along the path between source and receiver (see Figure 1.6).

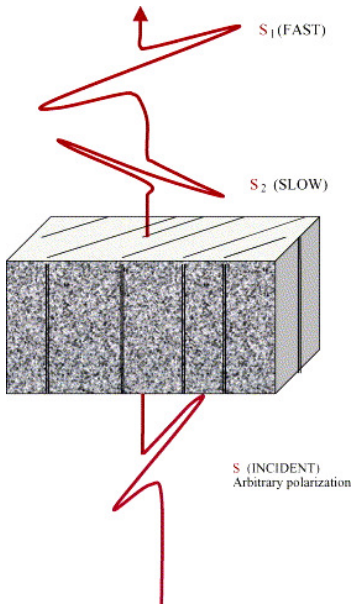

Figure 1.6 Schematic view of shear-wave splitting (Crampin and Hudson, 1981).

The shear wave splitting is attributed to structures as aligned cracks, joints and fractures which are oriented according to the stress field. Aligned fluid filled microcracks and preferentially oriented pore space causes extensive dilatancy anisotropy, which present in most types of rock (Crampin, 1986, 1989; Holmes et al., 1993). The analysis of horizontal component vertical seismic profile suggests that the shear wave splits in two orthogonal components when a fracture zone is intersected

(see Figure 1.7). The faster component polarizes parallel to the vertical fractures and the shear wave is perpendicular to the fractures and travels at a slower velocity. Thus shear wave splitting can be clearly characterized using the particle motion or polarization diagrams of S-wave arrivals on three component geophones.

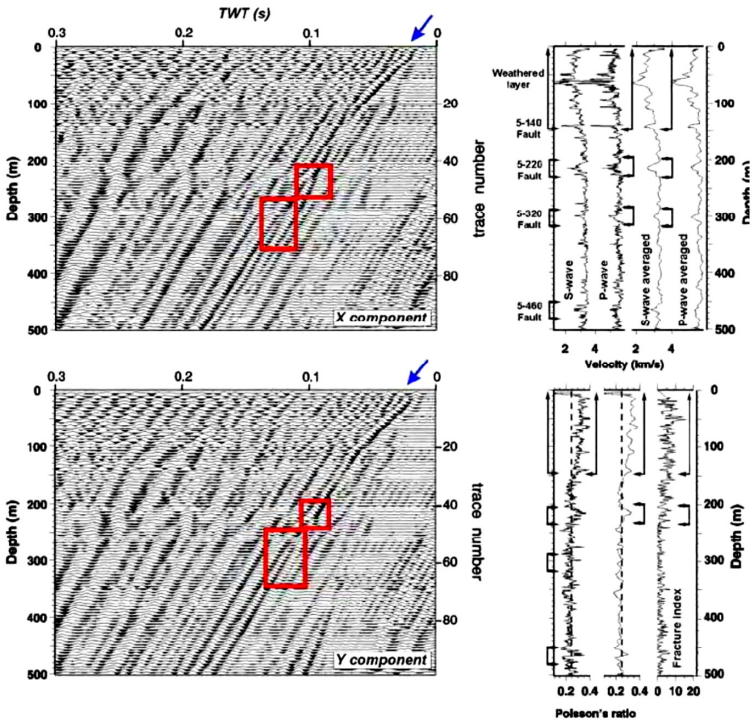

Figure 1.7 Illustration of the horizontal component in a vertical seismic profile, with squares mark the depth level where the shear wave arrivals split into two wavelets. These depths correlate with recognized fault zones derived from the fracture index, P and S-wave velocity and Poisson's ratio logs. Both horizontal components (X, Y) illustrate these effects (Holmes et al., 1993).

Borehole methods

Formation microscanner (FMS)

The FMS produces high resolution microresistivity images. This tool consists of four orthogonal imaging pad, each containing 16 microelectrodes (see Figure 1.8). The pads, which are in direct contact with the borehole wall, emit a focused current into the formation. The current intensity fluctuations are measured, then converted to color images that reflect microresistivity variations: the lighter the color, the greater

the resistivity (Ekstrom et al., 1987). These images have a vertical resolution of ~0.5 cm and a measurement interval of 0.25 cm (Serra, 1989). Roughly 30% of a 25 cm–diameter borehole is imaged. Through this the formation can be viewed in its complete state, such as bedding, fracturing, and slump folding can be resolved, and the fact that the images are oriented means that fabric can be analyzed and bed orientations measured.

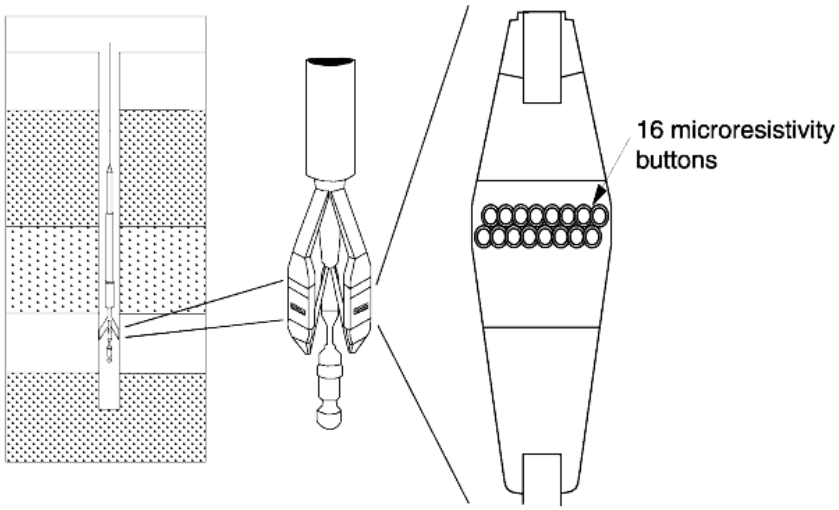

Figure 1.8 Schematic diagram of the Formation Microscanner (Lovell et al., 1998).

Figure 1.9 shows the steps of fracture characterization by FMS log, a sinusoid matched to these conductive intervals defines a unique orientation. This fracture measured in the core dips 58° but the independently picked sinusoid, blue lines in all FMS images indicates a dip of 60° (Haggas et al., 2001).

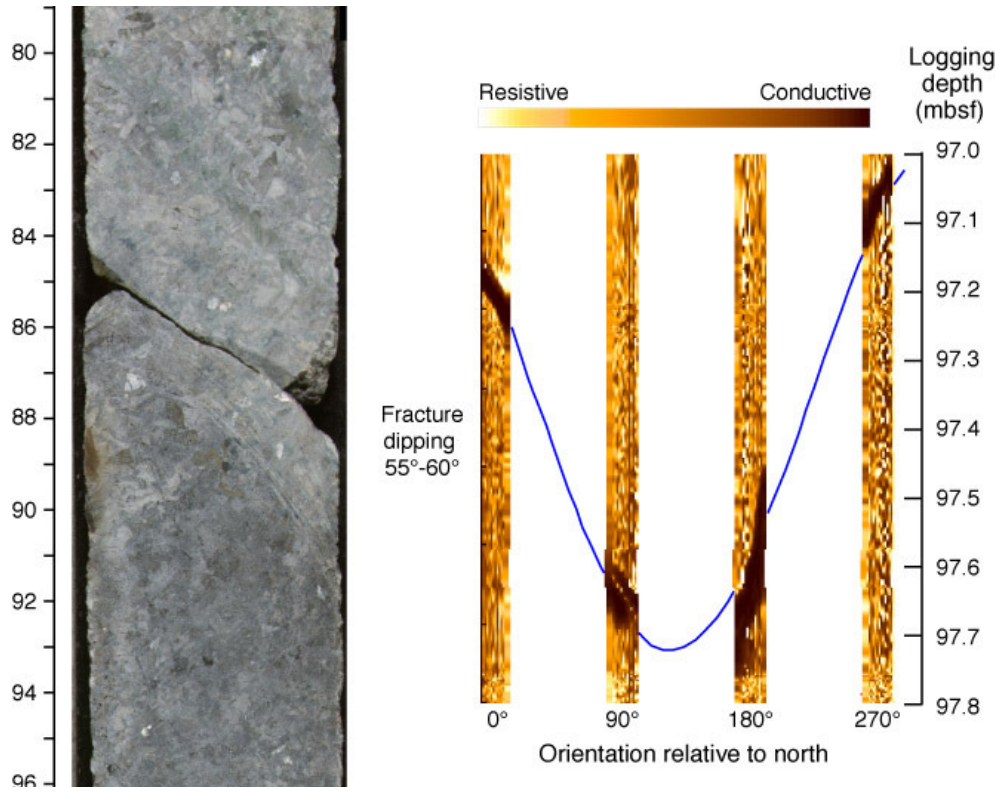

Figure 1.9 Example of a fracture that is highly conductive relative to the surrounding resistive formation (Haggas et al., 2001).

Dipole shear sonic imager (DSI)

The DSI employs a combination of monopole and dipole transducers (see Figure 1.10) to make accurate measurements of sonic wave propagation in a wide variety of lithologies (Schlumberger, 1995). In addition high quality determination of compressional wave velocity, the DSI excites a flexural mode in the borehole that can be used to determine shear wave velocity in all types of formations. When the formation shear velocity is less than the borehole fluid velocity, particularly in unconsolidated sediments, the flexural wave travels at shear wave velocity and is the most reliable means to estimate a shear velocity log. The configuration of the DSI also allows recording of cross line dipole waveforms. These modes can be used to estimate shear wave splitting caused by preferred mineral or structural orientations in consolidated formations. A low frequency source enables Stoneley waveforms to be acquired as well.

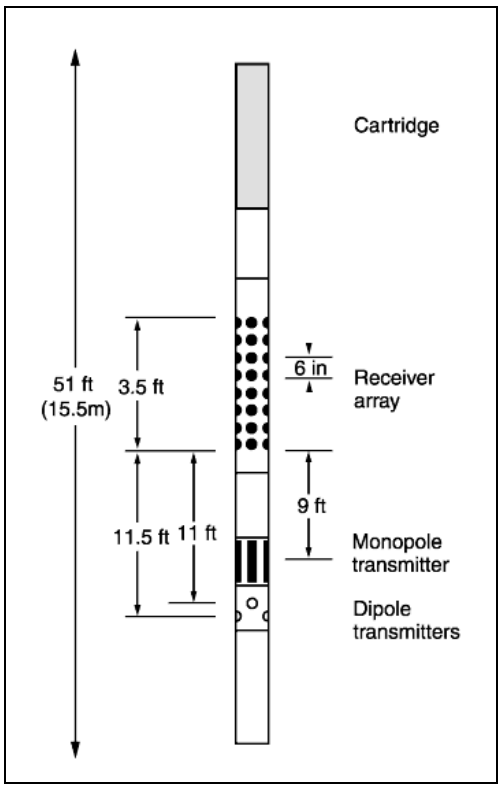

Figure 1.10 Dipoles shear sonic imager (Schlumberger, 1995).

Fracture characterization of dipole shear sonic logs is usually found by waveform correlation and not by first arrival detection although both methods are available (Crain, 2003). Therefore, it is less likely to skip a cycle due to low amplitude. Amplitude curves are presented as a matter of routine, so fractures can be identified by low compressional and shear amplitudes. Sonic curves on the array or dipole sonic can disappear or be shown as straight lines where amplitude is too low to obtain a waveform correlation (see Figure 1.11).

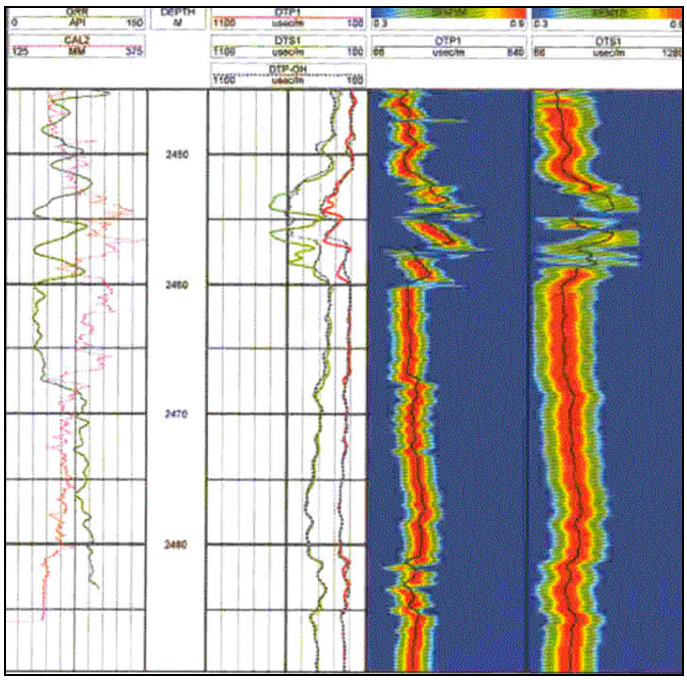

Figure 1.11 Example of DSI data: Fractures are indicated where the high amplitudes which are shown in red color on the image log disappear (Crain, 2003).

Borehole televiewer (BHTV)

The BHTV uses an ultrasonic beam with center band frequency of 500 KHz to 1.5 MHz and a beam diameter of 0.5 to 1.0 cm. The BHTV operates by scanning the borehole wall at a rate of about three revolutions per second while the probe is steadily drawn along the borehole. The transducer is fired at a rapid rate and serves as both the source of the acoustic pulse and the receiver for the reflected signal. The BHTV image is oriented with respect to the local magnetic field by a downhole magnetometer. The image is split along the apparent north azimuth and unwrapped for display (Rosenbom and Jakobsen, 2004)**.**

The intersection of the fracture with the borehole wall scatters acoustic energy, producing dark sinusoidal features on the image. The image allows interpret the strike and dip of fractures, although deviation surveys are required to determine the local orientation of the borehole, so that measured orientations can be corrected for borehole orientation and for deviation between local magnetic field and true north (Kierstein, 1984; Lau, 1983). The apparent thickness of the linear feature identified on the BHTV log may be taken as a qualitative indicator of fracture aperture. However,

this thickness depends on both the actual fracture aperture and the beam width and represents the fracture where it has been affected by drilling. For these reasons the interpretation of fractures using BHTV logs is at best semi-quantitative (see Figure 1.12).

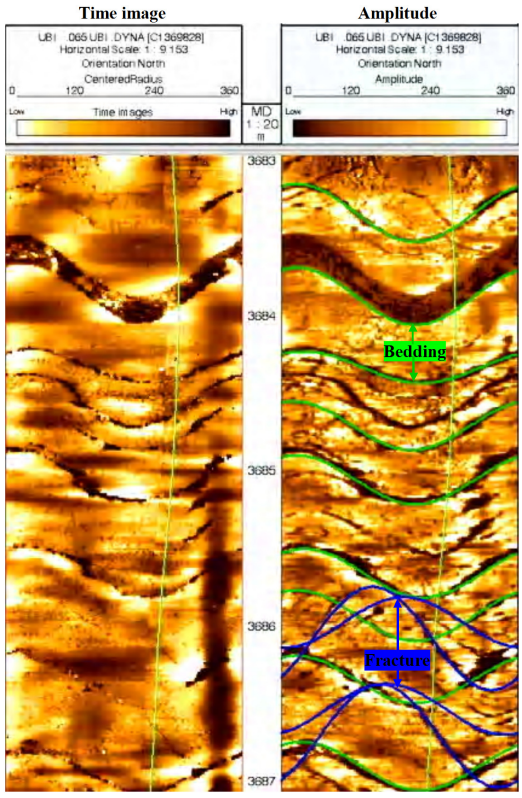

Figure 1.12 Example of a BHTV log showing a borehole image using amplitudes of the acoustic impedance. Dip angles are calculated from the image show both bedding and fracture dips (Crain, 2003).

Natural Gamma Ray (NGR) Logging

The GR log is a measurement of the natural radioactivity of the formations. It is useful for location of shale and non-shale beds and, most importantly, for general correlation. Natural gamma ray log tend to have a shallow depth of investigation less than 30 cm and will give depressed respond opposite large open fractures with a low gamma count. In general, however, gamma logs are inherently irregular in form and it is virtually impossible to distinguish between, for example, fractures and thin non-shalely beds. But rare exception occurs when, due to local geochemical conditions,

the faces of a fracture have become host to radioactive precipitates (Fertl, 1979; Fertl and Rieke, 1979). In such case, the fractures will give rise to sharp, anomalous high gamma reading which are particularly conspicuous in the spectral log corresponding to uranium sourced gamma ray emissions. Unfortunately, even with the availability of spectral gamma techniques, the types of response shown in Figure 1.13 are rarely definitive indicators of fracture presence, and other geophysical logs are usually required to confirm fracture interpretation.

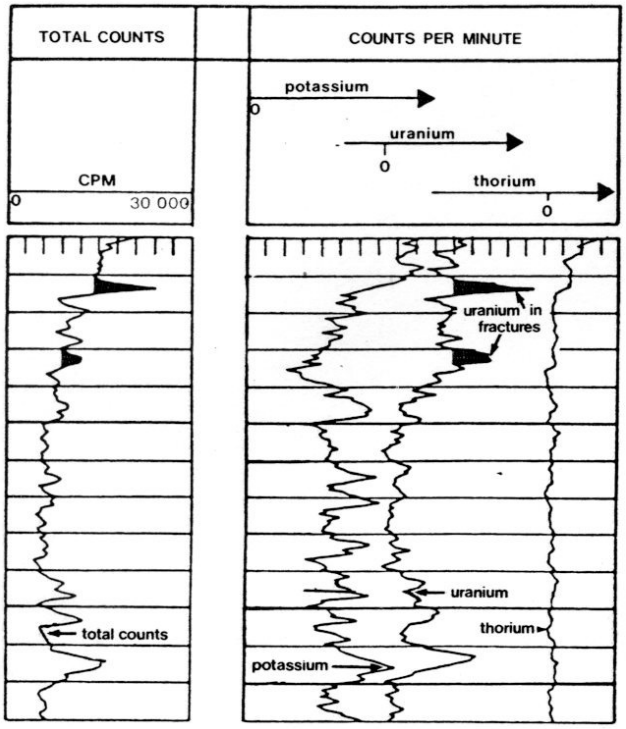

Figure 1.13 Comparison of total count gamma ray and spectral gamma log showing high levels of uranium associated with fractures in a sedimentary rock environment (Fertl, 1979; Rider, 1986).

Density Logging

Density logs are primarily used as porosity logs. Other uses include identification of minerals in evaporate deposits, detection of gas, determination of hydrocarbon density, evaluation of shaly sands and complex lithologies, determinations of oil shale yield, calculation of overburden pressure and rock mechanical properties (Schlumberger, 1989).

Because the density tool only looks at a small fraction of the borehole circumference, only a few of the fractures present will be logged. The depth of investigation is rather shallow, so mud cake and borehole rugosity can have an appreciable effect on the total measurement, despite the fact that it is a pad type contact device with some borehole compensation applied. However, if the density log shows high porosity spikes that are not seen by the neutron log, usually fractures, large vugs, or caverns exist. Broken out borehole also causes the same effected, but fractures are often present when this occurs. Both cases are shown in Figure 1.14 (Crain, 2003).

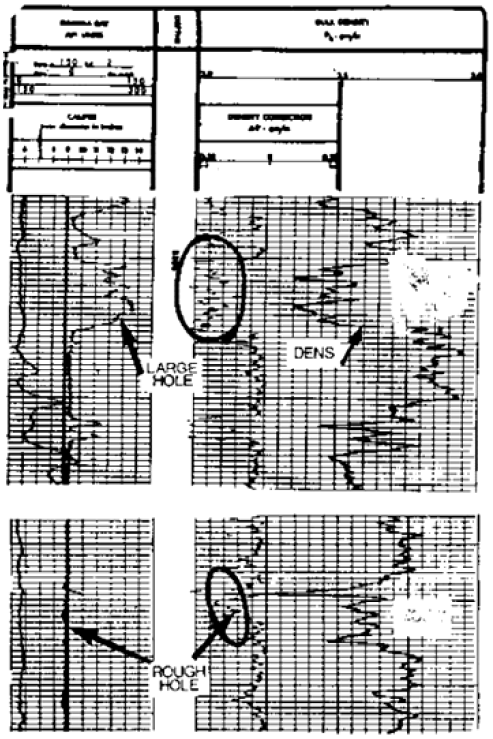

Figure 1.14 Density log spikes indicating fractures (from Crain, 2003).

When both sonic log and density or neutron log porosities are available, a direct comparison of the data can highlight difference which will confirm the presence of a secondary porosity component. Normally, this comparison is made with a parameter cross-plot or by overlaying the log on normalized scales (Schafer, 1979), see Figure 1.15.

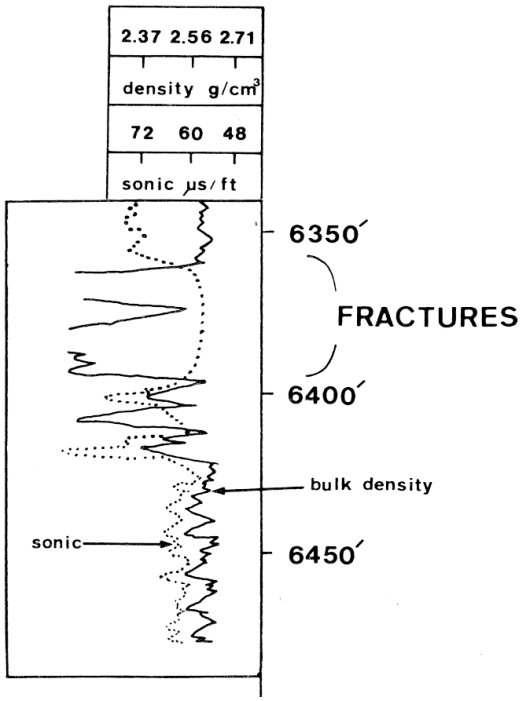

Figure 1.15 Fracture identification in the Austin Chalk, Texas, using bulk density and sonic logs (modified after Schafer, 1979; Rider, 1986).

Sonic Logging

Sonic log measure the speed of sound from the transmitter travel to formation and refracted back to the receiver. Accordingly, the first arrivals of sound energy at the receivers correspond to sound travel paths in the formation near the borehole wall (Schlumberger, 1989).

In the case of well logging, the borehole wall, formation bedding, borehole rugosity, and fractures can all represent significant acoustic discontinuities. Therefore, the phenomena of wave refraction, reflection, and conversion lead to the presence of many acoustic waves in the borehole when a sonic log is being run.

In some situation, fractures can attenuate the sonic signal to the extent that only second or third arrivals are detected by the receiver (Serra, 1984), Thus wave cycles are missed or skipped, and unwanted effect which shows up as abrupt increases in the interval transit time (see Figure 1.16).

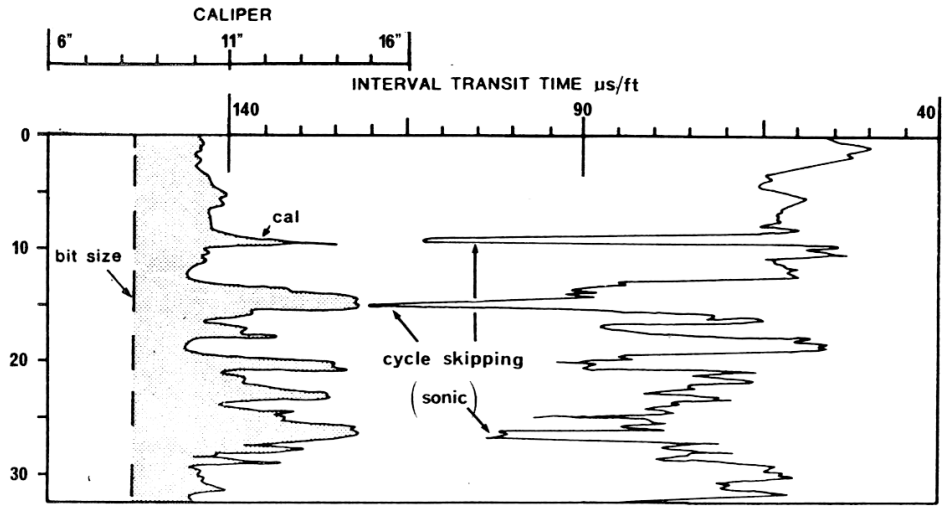

Figure 1.16 Cycle skipping on acoustic logs caused by fracturing (Rider, 1986). Note that this example is somehow idealized, as in many cases cycle skipping causes rapid and highly erratic deflections of the acoustic log.

Full wave form sonic logging

The full waveform sonic tool provides velocity and waveform data, but is designed for high resolution measurement of rock. Contrasting velocities can be used for stratigraphic interpretation, and direct calculation of formation porosity can be made from the P wave velocities. Under ideal conditions, S wave velocities may also be determined from the wave traces. In addition, waveform analysis can be used to economically locate fracture zones and, in cased holes, the waveform data can be used to evaluate the casing cement bond (Hughes, 2002).

Porosity, slowness and waveform quality are important sonic data. In Figure 1.17 low porosity zones are marked by decreased slowness and earlier waveform arrivals, in contrast to the high porosity zones or maybe the presence of fracture (Hughes, 2002).

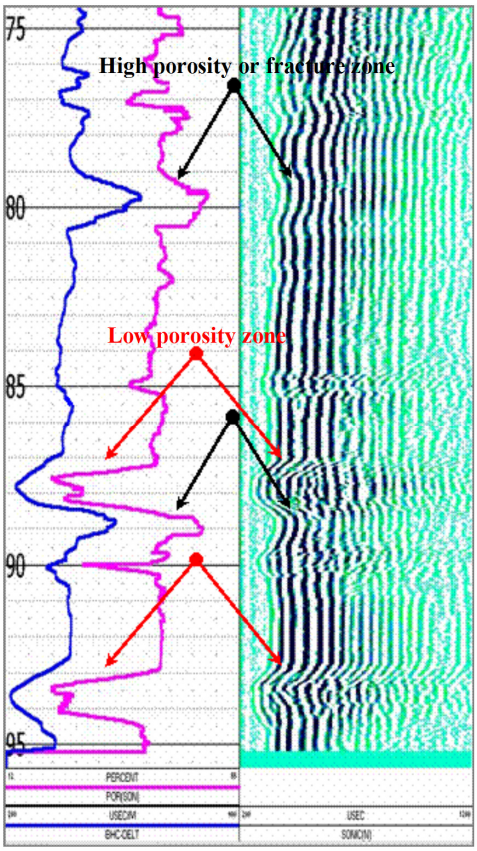

Figure 1.17 An example of low porosity zones are marked by decreased slowness and earlier waveform arrivals, in contrast to the high porosity zones or maybe the presence of fracture (Hughes, 2002).

Resistivity Logging

Microspherical focused log (MSFL), Laterolog shallow (LLs), and Laterolog deep (LLd) are available for this research. These tools are measure the resistivity of the formation in different depth of investigation.

Figure 1.18 shows an older well that do not have porosity, caliper, or gamma ray logs, the shallow resistivity log is used to find fractures. The shallow resistivity log may read the resistivity of drilling mud in washed out borehole sections caused by the presence of fracturing (Crain, 2003).

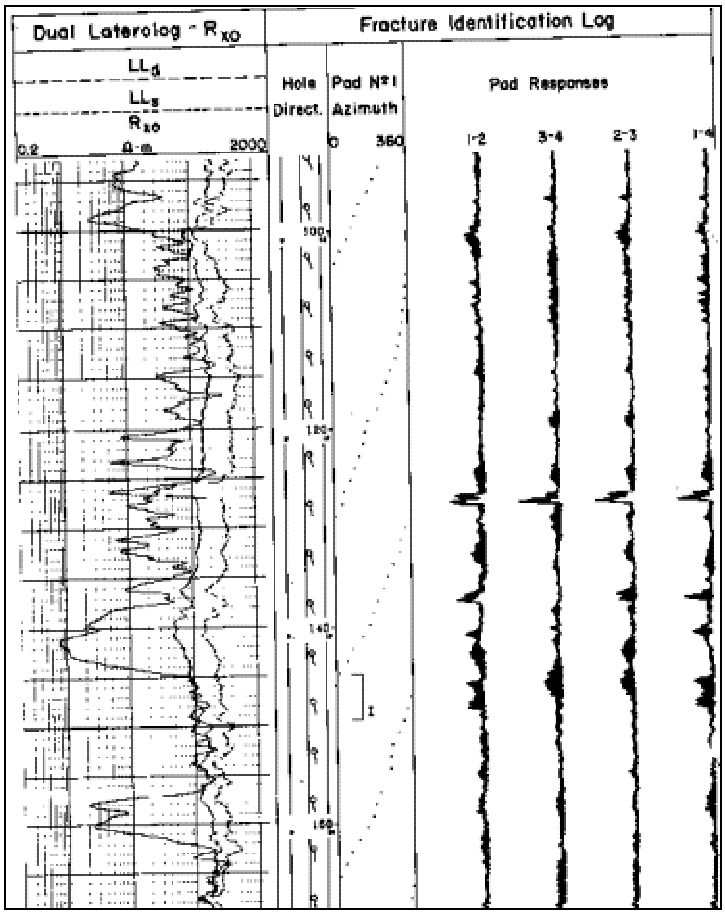

Figure 1.18 Sharp conductivity anomalies of the MSFL and shallow resistivity cross over indicating fractures (Crain, 2003).

Caliper Logging

Caliper log measure the average holes side by using caliper arm which connected to variable resistance push along to borehole wall and the changing electric signal can be transfer to holes size.

Caliper log is success to characterize the fracture by use a three arm caliper log for well CR-20 at Chalk River, Ontario, Canada, which can detected the fracture at zone A, B and C by show the bigger hole size compare temperature deflection indicative of fracture flow (see Figure 1.19).

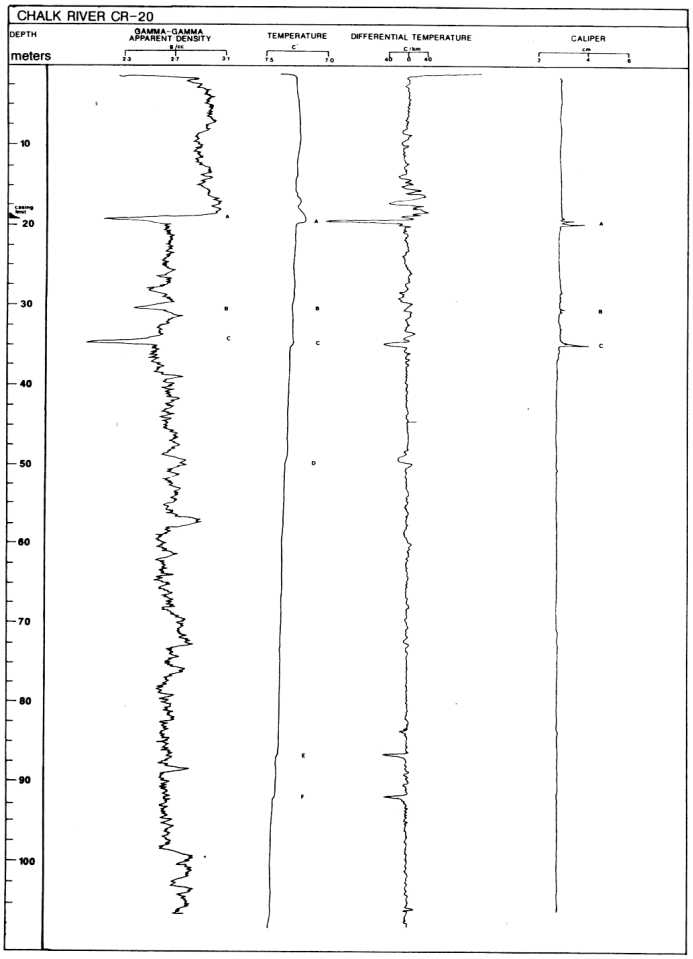

Figure 1.19 Illustrated geophysics borehole logs from CR-20 Borehole, Chalk River, Ontario, Canada, and fracture flow locations (Howard, 1990).

Photoelectric logging

Photoelectric absorption property is depending on the composition of lithology. Normally use for coal content determination but however, when weighted mud are used the large PE values greater than 5.0 is a fracture indicator (Crain, 2003). Barite has a very large photoelectric cross section, 267 as compared with 5.0 for limestone and 3.1 for dolomite. Thus the PE curve should exhibit a very sharp peak in front of a fracture filled with barite loaded mud cake.

In Figure 1.20, two very sharp peaks on the PE curve correspond to fractures. In light weight mud, an abnormally low PE value, less than 1.7, indicates, fractures, bad holes condition, or coal.

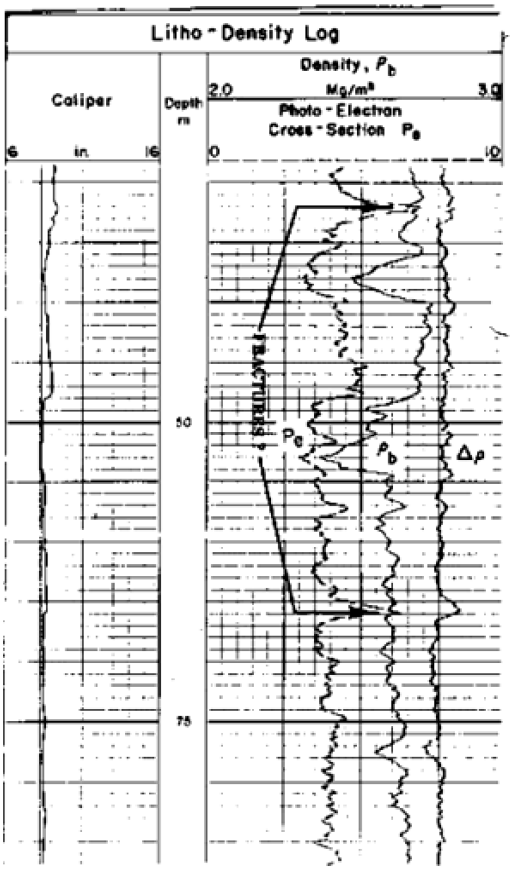

Figure 1.20 PE curve showing fractures in barite weighted mud (Crain, 2003).

1.1.3 Drilling before logging

Geophysical borehole logging involves measuring the physical properties of the surrounding medium with a sensor located in a borehole, hence before log performing the hole should be drilled by pumping the mud from surface to bit for removed cutting from the well bore, lubricated and cool the drilling bit, and maintain the excess of borehole pressure over formation pressure, normally water and oil based mud is available. During the drilling of the well the hydrostatic pressure of the mud column is usually greater than the pore pressure of the formations for prevents the well from blowing out. The resultant pressure differential between the mud column and formation forces mud filtrate into the permeable formation and the solid particles of the mud are deposited on the borehole wall and form a mud cake. Mud cake usually has a very low permeability and, once developed, considerably reduces the rate of further mud filtrate invasion.

Very close to the borehole most of the original fluid formation may be flushed away by the filtrate. This zone is referred to as the flushed zone. It contains, if the flushing is complete, only mud filtrate and if the formation was originally hydrocarbon bearing, only residual hydrocarbons.

Further out from the borehole, the displacement of the formation fluids by the mud filtrate is less and less complete, resulting in a transition from mud filtrate saturation to original formation water saturation. This zone is referred to as the transition or invaded zone. The extent or depth of the flushed and transition zones depends on many parameters. Among these are the type and characteristics of the drilling mud, the formation porosity, the formation permeability, the pressure differential, and the time since the formation was first drilled. Generally, higher formation porosity generated deeper the invasion. The undisturbed formation beyond the transition zone is referred to as the uninvaded zone.

From Figure 1.21 the borehole diameter is described by the outside diameter of the drilling bit. But the borehole diameter may bigger or smaller than the drilling bit diameter. Because of washout or collapse of shale and poorly cemented porous rock and built up of mud cake on porous and permeable formation.

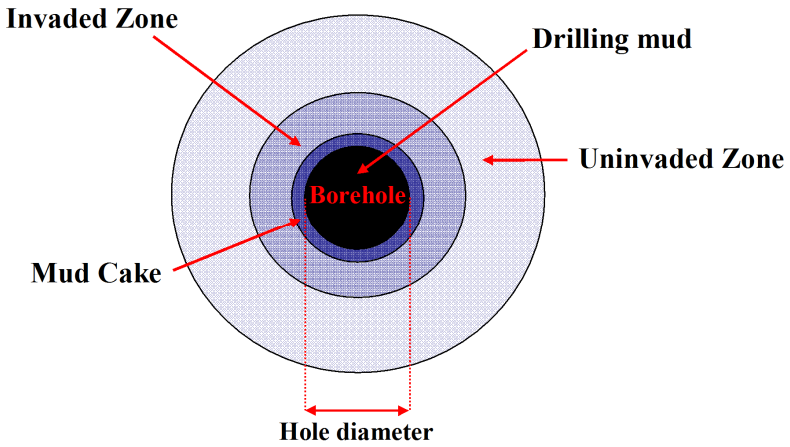

Figure 1.21 Schematic diagram of the borehole environment including mud cake, invaded zone, and uninvaded zone.

The drilling process can generate induced fractures that are created by drilling stress and they tend to form perpendicular to the least principal stress (see Figure

1.22). Induced fractures may connect the wellbore to natural fractures that would otherwise not contribute to flow capacity (Lacazette, 2001).

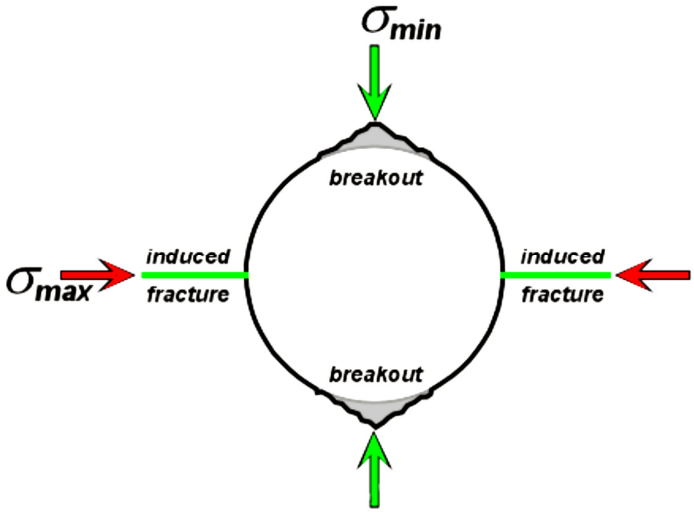

Figure 1.22 Schematic cross section of a wellbore showing the orientation of breakouts and induced hydraulic and centerline fractures relative to the borehole perpendicular in-situ earth stress components (Lacazette, 2001).

In order to perform a logging operation, the measuring instrument, often called a probe or sonde, is lowered into the borehole on the end of an insulated electrical cable (see Figure 1.23). The cable provides power to the downhole equipment. Additional wires in the cable carry the recorded measurement back to the surface. The cable itself is used as the depth measuring device, so that properties measured by the tools can be related to particular depths in the borehole. The winch of the logging cable is generally located on a special logging truck or container, which also carries the recorders, power sources, and auxiliary equipment. The parameters being logged are measured in situ as the sonde is moved along the borehole. The resulting signals from the sonde are transmitted through electrical conductors in the cable to the surface, where the continuous recording, or log, is made (Figure 1.27; Crain, 2003).

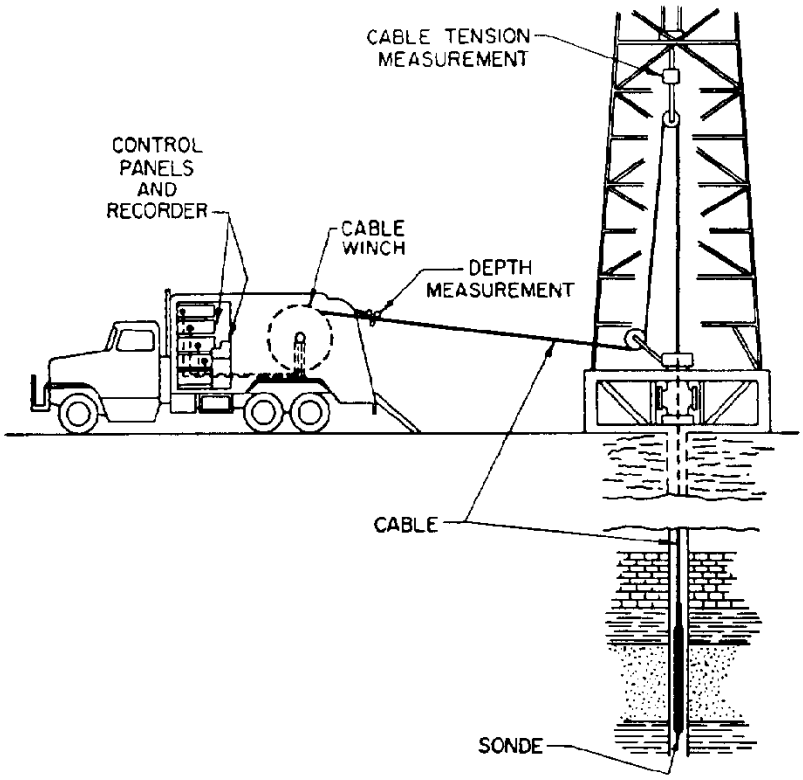

Figure 1.23 Schematic diagram of a wireline logging unit for operations at a well site (Schlumberger, 1989).

1.2 Objective

Geophysical logging is a standard method to obtain information from subsurface formations. Until today, several different and specialized tools are available serving many special purposes in logging. However, the logging constrains are time and the financial budget, and in many cases of them limited. Therefore, the aim is to get as much information from the conventional logging data as possible is still valid.

This study will evaluate the potential of conventional logging methods in identifying fractures in a well drilled in a fractured reservoir. Fractures are usually identified and evaluated by several techniques, with the most common being core analysis, advanced logging methods, like FMS, BHTV, and DSI. Fracture networks in a reservoir are of importance as they can provide the flow paths for rapid transport or they can act as fluid flow barriers and therefore as seals. Previous studies have shown that conventional logging methods have a potential to identify fracture characteristics.

Applying conventional logging for fracture characterization is needed where reservoirs are separated into smaller structural hydrocarbon traps, like in the Gulf of Thailand. Each small structure requires a well to be drilled, but with a comparable small production. In this situation not much money will be spend for advanced logging. More information about the subsurface formation, here about fractures, from the standard methods might be useful and less expensive.

Chapter 2

Material and Methods

2.1 Material

2.1.1 Conventional logging data and methods

Two sets of logging data from one well, which were made available by an international petroleum exploration company, are in Ascii format with measurement values from different tools. The depth data of both data sets are arbitrary values and do not present the real logging depth of the geophysical data. Real depth data are not required for the objective of this study. The main formations in the well are sandstone, shale, and coal, and by this characterized as a clastic reservoir.

The first logging data set is measured depth between 2679.954-3694.938 m, sampling interval 15.2 cm. Table 2.1 is an example of logging data set 1, which includes depth, GR, RHOB, DT, MSFL, LLd, LLs, CALI, SS, SH, COAL, PEF, and NPOR, with

GR = Natural gamma ray (API),

RHOB = Bulk Density (g/cm^3),

DT = Delta Time of Sonic Compression Wave (μs/ft),

MSFL = Resistivity measured from Microspherical Focused Log (Ω.m),

LLd = Resistivity measured from Deep Laterolog (Ω.m),

LLs = Resistivity measured from Shallow Laterolog (Ω.m),

CALI = Caliper Log measured hole size (inch),

SS = Sandstone Content (decimal fraction or %),

SH = Shale Content (decimal fraction or %),

COAL = Coal Content (decimal fraction or %),

PEF = Photoelectric Measurement (barns/ê),

NPOR = Neutral Porosity (vol/vol or p.u.).

Table 2.1 Example of the logging data set 1.

M. DEPTH	GR	RHOB	DT	MSFL	LLD	LLS	CALI	SS	SH	COAL	PEF	NPOR
2679.954	15.47	2.93	160.1	249.4	6000	468.914	9.7	0	0	0	6.4	0.03
2680.106	15.35	2.93	159.4	279.6	6000	422.583	9.8	0	0	0	6.2	0.03
2680.259	13.89	2.93	159.9	289.0	6000	435.561	9.8	0	0	0	6.1	0.03
↓												
3694.938	11.09	2.95	168.8	286.8	6000	385.566	9.9	0	0	0	6.5	0.03

The second logging data set is measured between depths 2699.995 and 2931.998 m, with a sampling interval of 2.5 cm (see Table 2.2) and includes DEPTH, GR, DTCO, and DT4S, with

GR = Natural gamma ray (API),

DTCO = Delta Time of Sonic Compression Wave (μs/ft),

DT4S = Delta Time of Sonic Shear Wave (μs/ft).

Table 2.2 Example of the logging data set 2.

M. DEPTH	GR	DTCO	DT4S
2699.995	166.805	212.675	346.37
2700.02	169.623	212.822	347.033
2700.045	172.442	212.97	347.696
↓			
2931.998	176.708	212.717	348.762

The geophysical methods of the available logging data are described in the following paragraphs including the physical base and a general tool description.

Natural gamma ray log (GR)

GR log is a method of measuring naturally occurring gamma radiation to characterize the rock or sediment in a borehole. Different types of rock emit different amounts of natural gamma radiation. In particular, shale usually emitted more gamma rays than other sedimentary rocks, such as sandstone and coal. Gamma radiation is usually recorded in API units, which 1 CPS (count per second) = 1.04 API units.

Natural radioactivity is the spontaneous decay of the atoms of certain isotopes into other isotopes. If the resultant isotope is not stable, it undergoes further decay until a stable isotope forms. The decay process is usually accompanied by emissions of alpha (α), beta (β), and gamma (γ) radiation. Natural gamma ray radiation is one form of spontaneous radiation emitted by unstable nuclei. Gamma (γ) radiation may be considered either as an electromagnetic wave similar to visible light or X-rays, or as a particle of photon. Gamma rays are electromagnetic radiations emitted from an atomic nucleus during radioactive decay, with the wavelength of 10^{-9} to 10^{-11}cm (Ellis, 1987).

Isotopes naturally found on earth are usually those that are stable or have a decay time larger than, or at least a significant fraction of the age of the earth about 5 x 10^9 years. Isotopes with shorter halflifes mainly exist as decay products from longer lived isotopes, and, as in C14, from irradiation of the upper atmosphere.

Radioisotopes with a sufficiently long halflife, and whose decay produces an appreciable amount of gamma rays are Potassium ^{40}K with half life of 1.3 x 10^9 years, which emits 0 α, 1 β, and 1 γ-ray, Thorium ^{232}Th with half life of 1.4 x 10^{10} years, which emits 7 α, 5 β, and numerous γ-ray with different energies, and Uranium ^{238}U with halflife of 4.4 x 10^9 years, which emits 8 α, 6 β, and numerous γ-ray with different energies. Each of these elements emits gamma-rays with distinctive energy. Figure 2.1 shows the energies of emitted gamma ray from the three main isotopes. Potassium 40 decays directly to stable argon 40 with the emission of 1.46 MeV gamma ray. Uranium 238 and thorium 232 decay sequentially through a long sequence of various isotopes until a final stable isotope. The spectrum of the gamma rays emitted by these two isotopes consists of gamma ray of much different energy and forms a complete spectrum. The peak of thorium series can be found at 2.62 MeV and the Uranium series at 1.76 MeV (Rider, 1986).

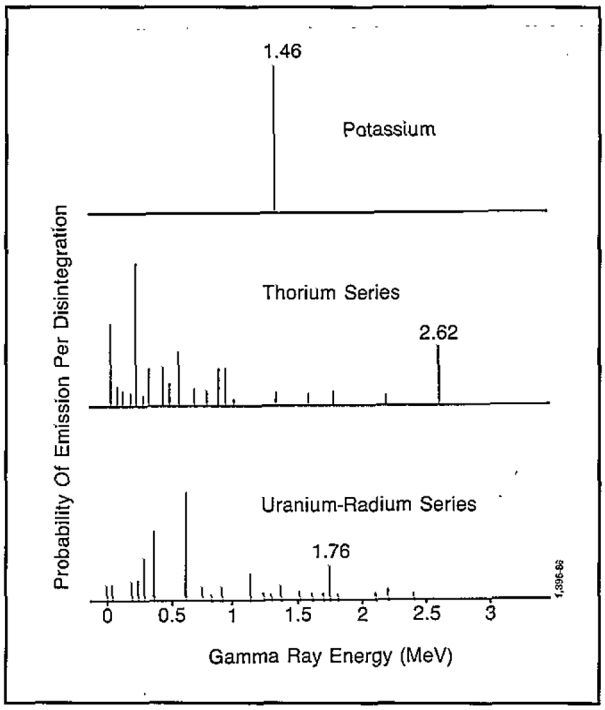

Figure 2.1 Illustrated the gamma ray emission spectra of radioactive minerals (Schlumberger, 1999).

Gamma-ray detectors use the sodium iodide (NaI) scintillation detector, which are usually composed of a NaI crystal coupled with a photomultiplier (Serra, 2004). When gamma ray from formation enters the crystal, it undergoes successive collisions with the atoms of the crystal, resulting in short flashes of light when the gamma ray is absorbed. The light is detected by the photomultiplier, which converts the energy into an electric pulse with amplitude proportional to the gamma-ray energy. The number of electric pulses is recorded in counts per seconds (CPS).

Bulk density log (RHOB)

RHOB records formation density in g/cm^3. The logging tool consists of a gamma ray source (Cs^{137}) and a detector shielded from the source so that it records backscattered gamma rays from the formation. The backscattering depends on the electron density of the formation, which is roughly proportional to the bulk density. The source and detector usually are mounted on a skid which is pressed against the borehole wall (Czubek, 1983).

A radioactive source, applied to the borehole wall in a shielded sidewall skid, emits medium energy gamma rays collide with the electrons in the formation. At each collision a gamma ray loses some, but not all, of energy to the electron, and then continues with diminished energy. This type of interaction is known as Compton scattering. The scattered gamma rays reaching the detector, at a fixed distance from the source, are counted as an indication of formation density (see Figure 2.2).

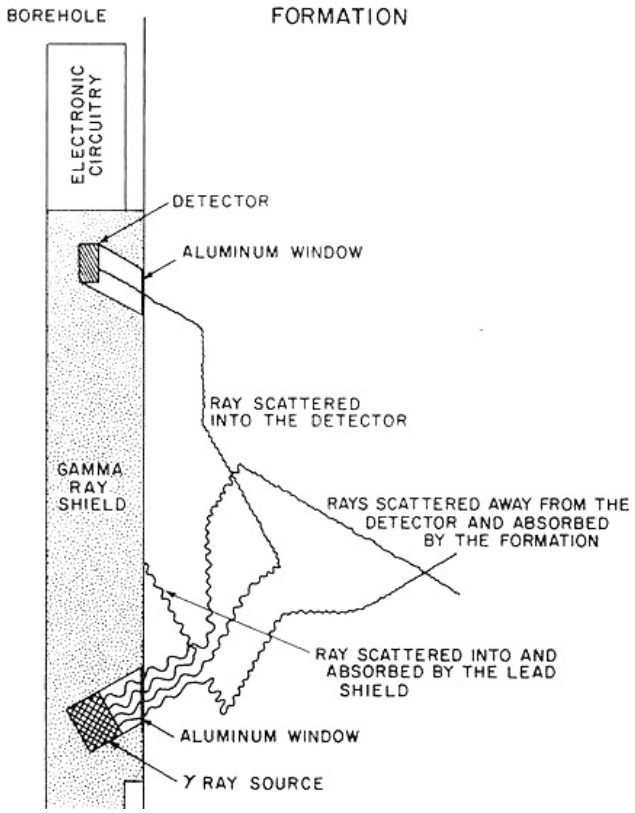

Figure 2.2 Schematic diagram of the density log show scatter gamma ray reaching the detector (Bassiouni, 1994).

The number of Compton scattering collisions is related directly to the number of electrons in the formation. Consequently, the response of the density tool is determined essentially by the electron density of the formation. Electron density, ρ_e, is related to the true bulk density, ρ_b, which, in turn, depends on the density of the rock matrix material, the formation porosity, and the density of the fluids filling the

pores. For a substance consisting of a single element, the electron density index, ρ_e, is related to the bulk density, ρ_b,

$$\rho_e = \rho_b\left(\frac{2Z}{A}\right)$$

where for common elements in sedimentary rocks $\frac{2Z}{A} \cong 1$, so that $\rho_e \approx \rho_b$, ρ_b is the actual bulk density, Z is the atomic number (number of electrons per atom), A is the atomic weight (ρ_b/A is proportional to the number of atoms per cubic centimeter of the substance). For a molecular substance, the electron density index is related to the bulk density:

$$\rho_e = \rho_b 2\left(\frac{\sum Z's}{Mol.Wt.}\right)$$

where $\sum Z's$ is the sum of the atomic numbers of atoms making up the molecule (equal to the number of electrons per molecule) and *Mol. Wt.* is the molecular weight. In the compensated formation density tool (FDC), two detectors of differing spacing and depth of investigation are used, as shown on Figure 2.3.

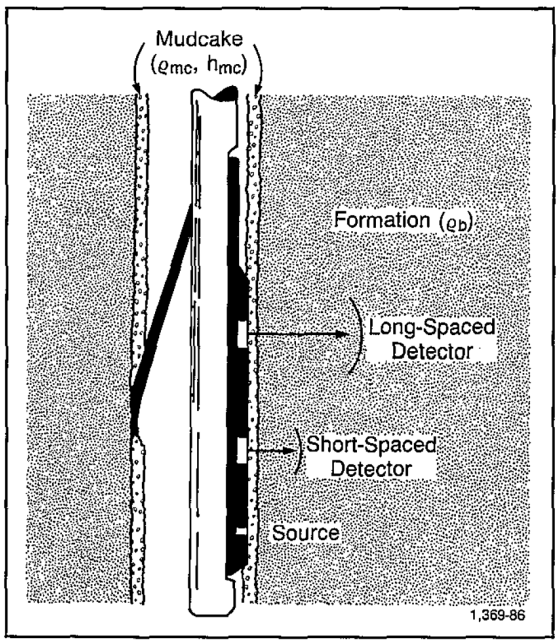

Figure 2.3 Schematic drawing of the dual spacing Formation Density Logging Device (Wti et al., 1964).

Delta time (DT)

The principle of the technique is measuring the difference in slowness using a single transmitter and two receivers. This transit time difference, or delta time (*Dt* or Δt), is defined as the slowness and is typically reported as time per unit distance generally μs/ft or μs/m, it is, by definition, the inverse of velocity (Keys, 1988).

The transmitter emits sound waves into the formation and measures the time taken to detect at a receiver of known distance from the transmitter. The first arrival is the compressional or P–wave, which travels adjacent to the borehole as shown in Figure 2.4. It is this arrival that is used to measure the individual travel times T1, T2, T3, and T4. Two receivers for each transmitter eliminate the borehole signal. The transit time DT is computed from these travel times as shown in the equation below. This particular arrangement of sonic tool transmitters and receivers is known as the standard BHC Sonic tool and compensates for borehole washouts and also for tool tilting in real time while logging.

$$DT_{LOG} = \left[\frac{(T1 - T2) + (T3 - T4)}{2} \right]$$

The amplitude of shear wave usually has slightly larger than the compressional wave, but smaller than Stoneley waves. The various arrivals in the received sonic signal can be seen in Figure 2.5.

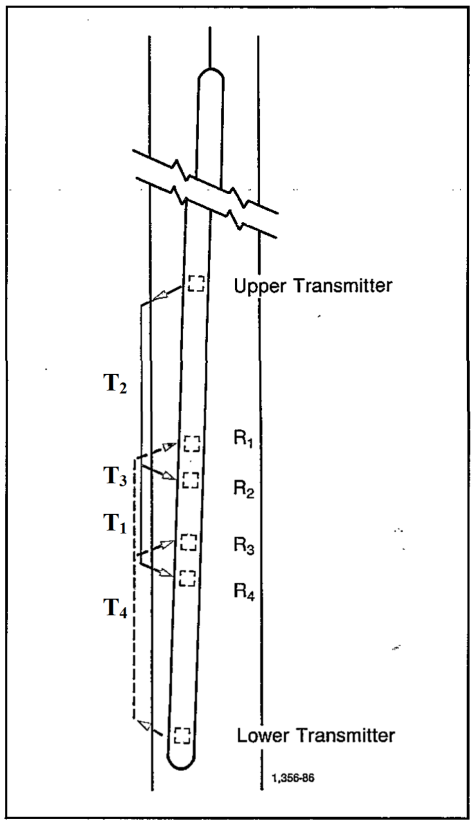

Figure 2.4 Schematic picture of the BHC sonde, showing ray paths for the two transmitters and receiver sets (Kokesh et al., 1965).

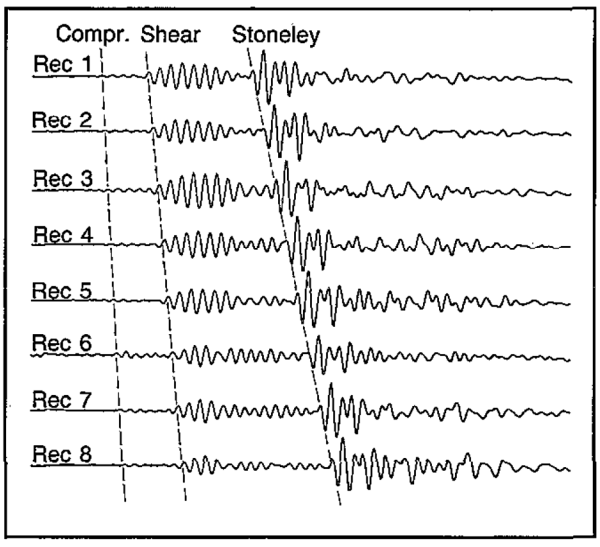

Figure 2.5 Example waveforms from an eight–receiver array sonic tool showing the arrival of the different wave trains with dashed lines (Crain, 2003).

Resistivity log

Microspherical focused log (MSFL), Laterolog deep (LLd), Laterolog shallow (LLs) are available for resistivity measurement of the formation. LLd is used for deep investigation of the uninvaded zone. LLs is used for shallow investigation of the invaded zone, and MSFL measures resistivity of flushed zone. The unit of resistivity is normally used ohm.meter (Ω.m).

Figure 2.6 is a sketch of the tool showing the electrode array used for the two laterolog devices and MSFL. Both use the same electrodes and have the same current beam thickness, but have different focusing to provide their different depth of investigation characteristics. Figure 2.6 illustrates the focusing used by the LLd and LLs device.

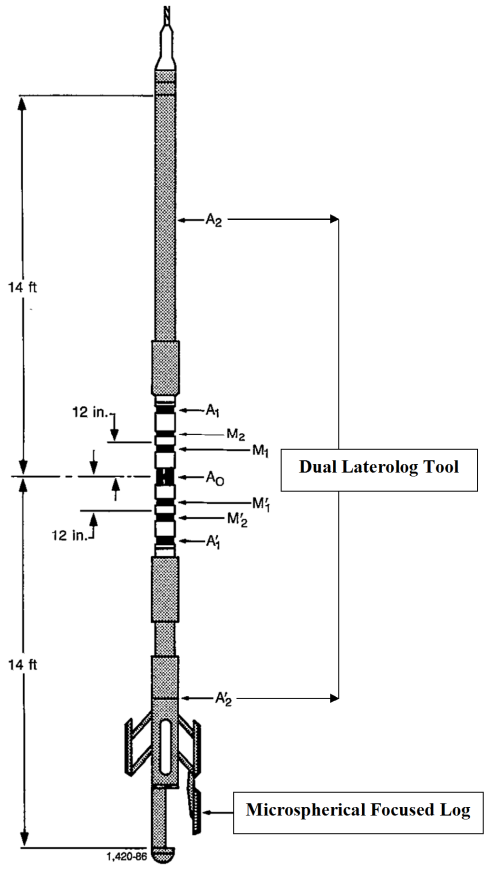

Figure 2.6 Schematic diagram of the Dual Laterolog tool (Schlumberger, 1989).

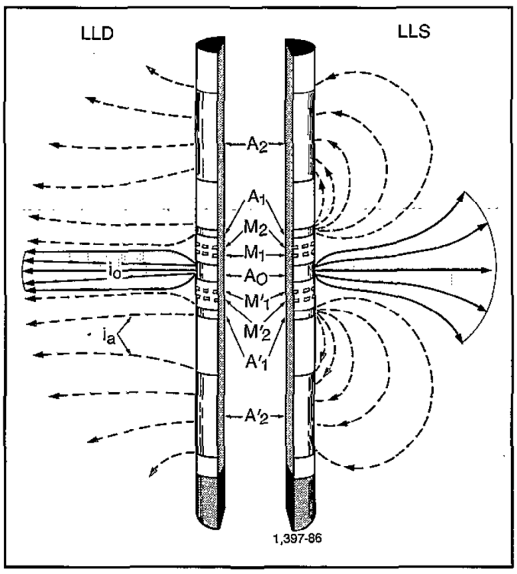

Figure 2.7 Schematic of the Dual Laterolog (Schlumberger, 1989).

The Microspherical focused log (MSFL) is a pad mounted spherically focused logging device. It has two distinct advantages over the other devices. The first is its combinability with other logging tools, such as Dual Laterolog (DLL) tools (see Figure 2.7). This eliminates the need for a separate logging run to obtain mud cake resistivity information. The second improvement is the tool response to very shallow zones in the presence of mud cake (Schlumberger, 1989).

The solution was found in an adaptation of the principle of spherical focusing in a sidewall pad device. By careful selection of electrodes bucking current controls, the MSFL measurement was designed for minimum mud cake effect without an undue increase in the depth of investigation. Figure 2.8 illustrates, schematically, the electrode arrangement and the current patterns of the MSFL tool.

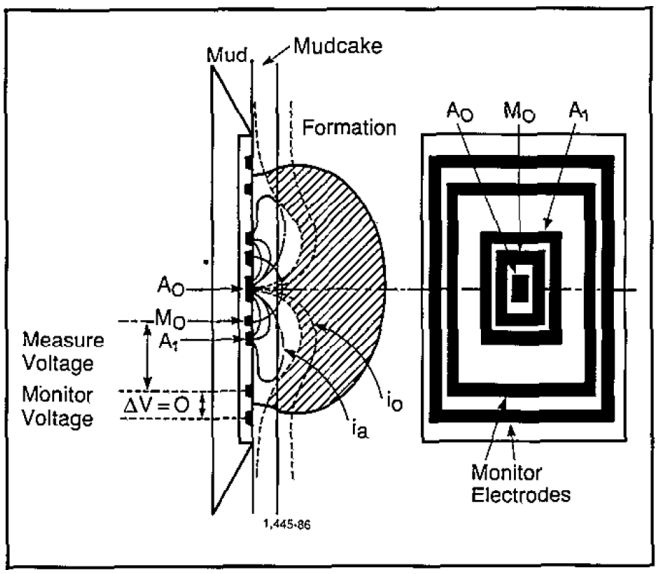

Figure 2.8 The electrode arrangement of MSFL device and current distribution (Schlumberger, 1989).

The surveying current from MSFL flows outward from a central electrode, A_0. Bucking currents, passing between the electrodes, A_0, and A_1, flow in the mud cake and, to some extent, in the formation. The measuring current, I_0, is thereby confined to a path directly into the formation, where it quickly bells out and returns to a remote electrode, B. To achieve this, the bucking current is adjusted to make the monitor voltage equal to zero. By forcing the measure current to flow directly into the formation, the effect of mud cake resistivity on tool response is minimized but the tool still has a very shallow depth of investigation (Schlumberger, 1989).

The MSFL and dual laterolog (LLs and LLd) has been designed to provide resistivity measurements in wells drilled with highly conductive drilling fluids. However, it is the contrast between the resistivity of the formation, and the resistivity of the drilling mud that is most important. Due to the high resistivity of most tight fractured reservoirs, the DLL and MSFL combination is the preferred resistivity log for such zones (Schlumberger, 1989).

Caliper log (CALI)

The simple mechanical caliper measures variations in borehole diameter with depth (Serra, 1979; Rider, 1986). The measurements are normally made by one or

more articulated arms or feelers pressed against the borehole wall. In most caliper tools, lateral movement of the arms in translated into vertical movement of pin attached to a variable resistance potentiometer (see Figure 2.9). Alternatively the arms are linked to a capacitor which alters the output of an oscillator. In either case, the generated output can be calibrated to produce a direct measurement of variation in holes diameter. The use of caliper tool to locate fractures requires that the fractures be either open or sufficiently enlarged by drilling to permit a change in borehole diameter to be detected by the tip of caliper arm. For this reason, caliper tool capable of resolving regular changes in borehole diameter of just a few millimeters may not be capable of detecting discrete fractures of comparable width.

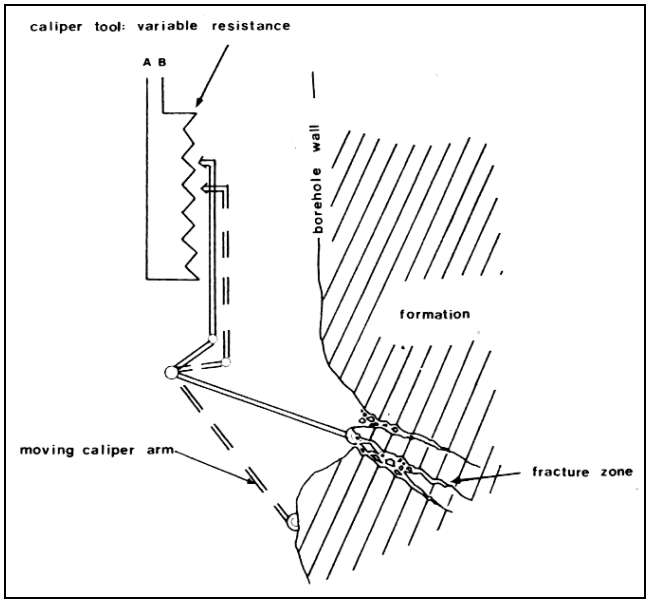

Figure 2.9 The schematic representation of the caliper tool showing translation of mechanical movement to an electric signal using a potentiometer (Serra, 1979; Rider, 1986).

Most caliper tools are classified according to the number and configuration of the arms that are in contact with the borehole wall. A one armed caliper uses a single arm which can only respond to roughness along one side of the borehole. A three arms caliper tend to provide a more accurate measurement of borehole diameter but may cause some confusion since, in most of these tools, the arms do not respond

independently, and single, steeply dipping fractures which intersect the hole over a range of depth, will give rise to three separate anomalies on the caliper log.

Shale (SH), Sandstone (SS) and Coal content (COAL)

SH, SS, and COAL are calculated values based on the natural gamma ray log as follow the simple equation,

$$Vshg = (GR - GR_0) / (GR_{100} - GR_0)$$

where GR = gamma ray log in zone of interest, borehole size corrected (API units)

GR_0 = gamma ray log reading in l00% clean zone (API units)

GR_{100} = gamma ray log reading in l00% shale (API units)

Vshg = shale volume from gamma ray log (fractional).

However, the equation above has a good result only in shalely sand formations; in case of other formations such as coal the calculation is more complicated and normally a complex equation and special computer software are applied.

Photoelectric log (PEF)

The photoelectric absorption is obtained from the low energy spectrum of the gamma ray, as measured in keV. The variable measured, photoelectric absorption cross section defined as a measure of the probability that a nuclear reaction will take place under specific conditions, between an incoming particle and its target (Holstein, 2007).

The atomic number, Z, is the number of electrons and can be related to the photoelectric absorption cross section index as:

$$P_e = \left(\frac{Z}{10}\right)^{3.6}$$

where P_e is in barns/ê

Neutron porosity log (NPOR)

NPOR measurement employs a neutron source to measure the hydrogen index in a reservoir, which is directly related to porosity. The hydrogen index (HI) of a

material is defined as the ratio of the concentration of hydrogen atoms per cm^3 in the material. As hydrogen atoms are present in both water and oil filled reservoirs, measurement of the amount allows estimation of the amount of liquid filled porosity.

Neutrons are typically emitted by a chemical source such as Americium Beryllium (Am-Be) or Plutonium Beryllium (Pu-Be), or generated by electronic neutron generators such as minitron. Fast neutrons are emitted by these sources with energy ranges from 4 MeV to 14 MeV, and inelastically interact with matter. Once slowed down to 2 MeV, they start to scatter elastically and slow down further until the neutrons reach a thermal energy level of about 0.025 eV. When thermal neutrons are then absorbed, gamma rays are emitted. A suitable detector, positioned at a certain distance from the source, can measure either epithermal neutron population, thermal neutron population, or the gamma rays emitted after the absorption (see Figure 2.10).

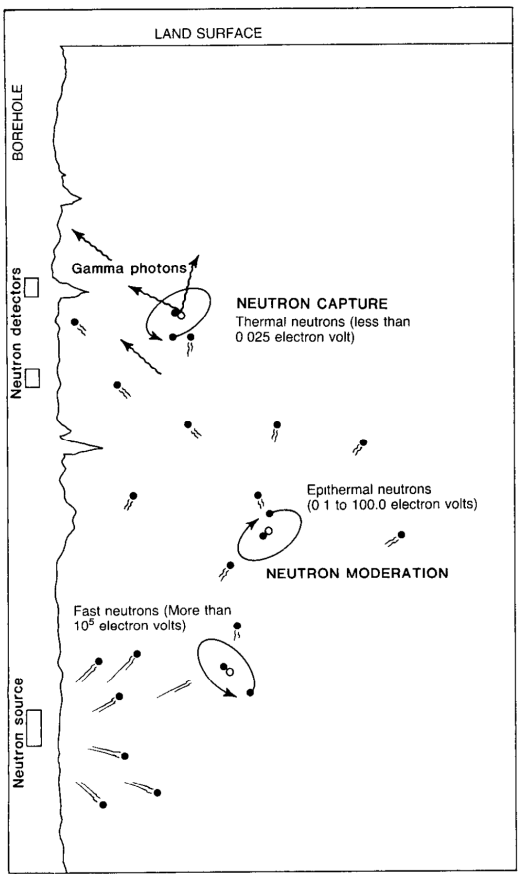

Figure 2.10 Neutron processes, from source to detectors, through rocks surrounding a borehole (Keys, 1990).

In neutron logging, the probe contains a source of neutrons, and detectors provide a record of the neutron interactions that occur in the vicinity of the borehole (see Figure 2.11). Mechanics of elastic collisions predict that the maximum energy transfer occurs during collisions of two particles of equal mass. Therefore, a hydrogen atom (H) will cause a neutron to slow down the most, as they are of roughly equal mass. As hydrogen is fundamentally associated to the amount of water and/or oil present in the pore space, measurement of neutron population within the investigated volume is directly linked to porosity.

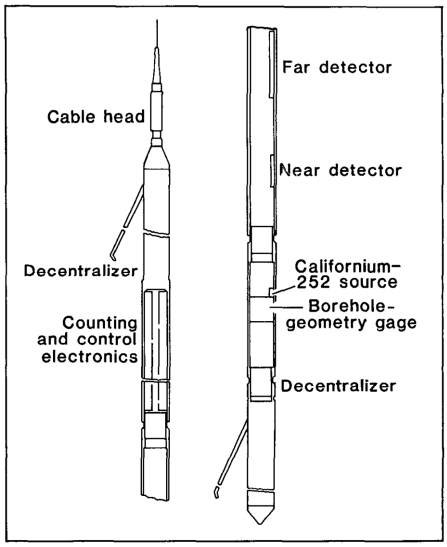

Figure 2.11 Probe for making compensated neutron porosity logs (Keys, 1990).

Delta time compression wave (DT) and Delta time shear wave (DT4S)

DT and DT4S are the measurement of the difference in transit times of compression wave and shear wave. This transit time difference is defined as the slowness and is typically reported as time per unit distance generally μs/ft, it is, by definition, the inverse of velocity.

2.1.2 Log presentation

Normally log presentation shown in term of depth and logging data as shown in Figure 2.12, A is depth (m) data plot with lithology, B is resistivity (Ω.m) data plot in log scale because of resistivity value some time have a big different between shallow and deep investigation, C is delta time compression wave and shear wave

(µs/ft) are available, D is caliper or hole size (inch) and photoelectric log (barns/ê), and the last, E is bulk density (g/cm^3) and neutral porosity log (vol/vol or p.u.).

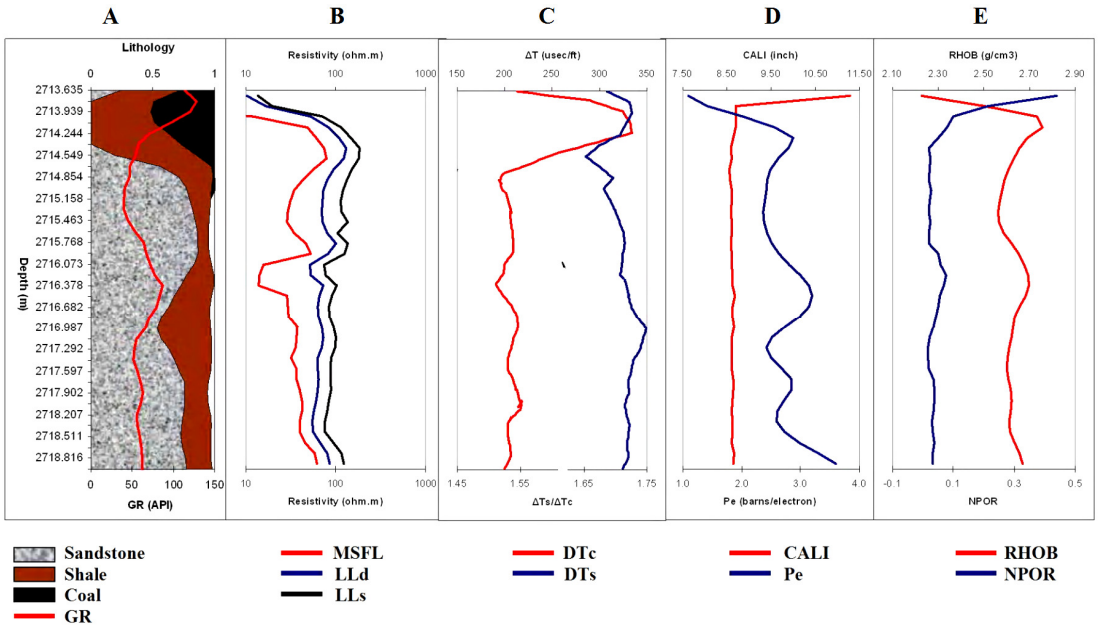

Figure 2.12 Presentation of log data with depth versus the different logging data.

2.1.3 Fracture data

Additionally to the logging data, fracture data from Formation Microscanner (FMS) were made available from the same well. The data were measured every 0.25 cm (sampling interval) and include depth of fracture plane or fracture zone, dip angle, azimuth, and also the label “resistive” or “conductive” from 2704.130 to 3695.400 m as shown in Table 2.3. The depth data here are also arbitrary, but the depth data match the logging data set 1 and set 2. The fracture orientation data are not used in this study as the borehole orientation and deviation with depth was not available.

Table 2.3 Fracture data from FMS (Formation MicroScanner) log. DIP = Dip Angle of fracture plane (^{o}). AZI = Azimuth of fracture plane (^{o}).

DEPTH	DIP	AZI	CODE	COMMENT
2715.11	68	287	20	Resistive fracture
2716.34	73	265	22	Conductive fracture
↓				
3695.400	59	346	22	Conductive fracture

Resistive fracture, normally filled with oil or gas but conductive fracture filled with water or brine. Fracture data is derived from the specialized tools called Formation Microscanner (FMS, see Chapter 1) which designed for mapping of bedding planes, fractures, faults, foliations, and other formation structures and dip determination. Figure 2.13 shown fracture plane, dip angle, azimuth and borehole axis.

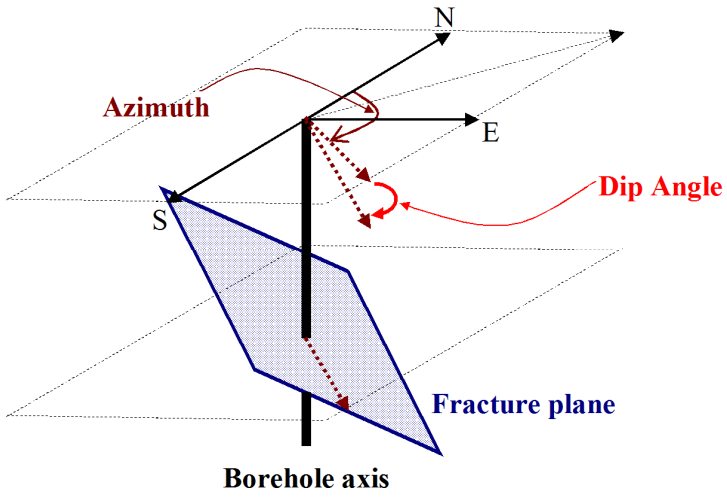

Figure 2.13 Illustration of the fracture plane, dip angle, azimuth and borehole axis.

2.1.4 Drilling mud properties

Additionally to the logging and fracture data, mud property data effect to logging tool such as mud resistivity were provided. The mud resistivity (Rm, in Ωm) at the surface with a temperature of 18 °C is about 0.075 Ωm and at 100 °C,

representing increasing depth, the mud resistivity is about 0.025 – 0.038 Ωm. The increase of the temperature with depth reflects the geothermal gradient. Figure 2.14 shows the resistivity of the mud related to increasing temperature in the borehole. Normally, drilling mud also contains barite that has an effect on the logging measurements. Barite, $BaSO_4$, is dissolved in the mud to increase the mud weight, respectively density, to maintain hydrostatic pressure in the wellbore and to control well stability. Barite has a high photoelectric absorption value of 267 barns/ê and hence it has an effect to the photoelectric log measurements.

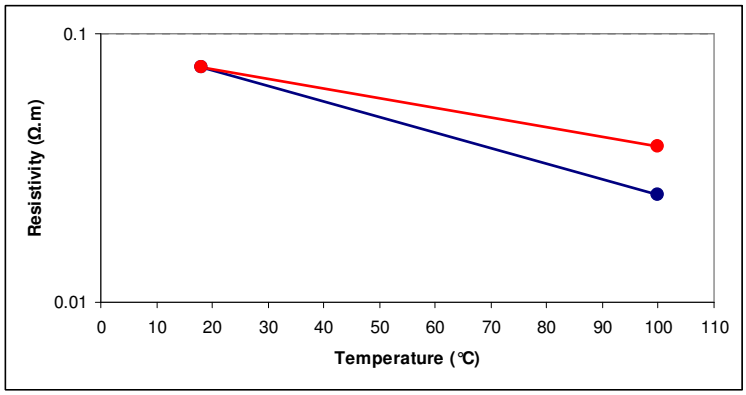

Figure 2.14 Mud resistivity (Ω.m) versus temperature (°C) from well measurements.

2.2 Methods

Geophysical well logging is a standard method to obtain information from subsurface formations. The aim of this research is to get as much fracture information from the conventional logging data as possible by compare with real fracture data derived from a Formation Microscanner (FMS).

Most conventional well logs respond in some way to the presence of fractures. Each major log type is discussed in the Table 2.5 with respect to its fracture response. Not all logs detect fractures in all situations, and very few see all fractures present in the logged interval and other borehole and formation responses will be superimposed on each log. Therefore, the main formations of the well, possible fluid contents, and the fracture characterization abilities of the available tools here will be discussed in detail below.

Then a qualitative modeling of the fracture response for the various available conventional logging tools will be performed in order to understand the possible response of these tools to fractures with different parameters.

2.2.1 Formation lithologies and fluids

Sandstone

Sandstone is a sedimentary rock composed mainly of sand-sized minerals or rock grains. Most sandstone is composed of quartz and/or feldspar because these are the most common minerals in the Earth's crust. Like sand, sandstone may be any color, but the most common colors are tan, brown, yellow, red, gray and white.

Sandstones are clastic in origin. They are formed from cemented grains that may either be fragments of a pre-existing rock or be mono-minerallic crystals. The cements binding these grains together are typically calcite, clays and silica. Grain sizes in sands are defined within the range of 0.0625 mm to 2 mm. Clays and sediments with smaller grain sizes not visible with the naked eye, including siltstones and shales, are typically called argillaceous sediments.

The formation of sandstone involves two principal stages. First, a layer or layers of sand accumulates as the result of sedimentation, either from water (as in a river, lake, or sea) or from air (as in a desert). Typically, sedimentation occurs by the sand settling out from suspension. Finally, once it has accumulated, the sand becomes sandstone when it is compacted by pressure of overlying deposits and cemented by the precipitation of minerals within the pore spaces between sand grains.

The most common cementing materials are silica and calcium carbonate, which are often derived either from dissolution or from alteration of the sand after it was buried. Colors will usually be tan or yellow (from a blend of the clear quartz with the dark amber feldspar content of the sand). A predominant additional colorant is iron oxide, which imparts reddish tints ranging from pink to dark, with additional manganese imparting a purplish hue.

The environment where it is deposited is crucial in determining the characteristics of the resulting sandstone, which, in finer detail, include its grain size, sorting and composition and, in more general detail, include the rock geometry and

sedimentary structures. Principal environments of deposition may be split between terrestrial and marine (Boggs, 2000).

Shale

Shale is a fine grained, clastic sedimentary rock composed of mud that is a mix of flakes of clay minerals and tiny fragments (silt-sized particles) of other minerals, especially quartz and calcite. The ratio of clay to other minerals is variable. Shale is characterized by breaks along thin laminate or parallel layering or bedding less than one centimeter in thickness, called fissility.

Shale typically exhibits varying degrees of fissility breaking into thin layers, often splintery and usually parallel to the otherwise indistinguishable bedding plane because of parallel orientation of clay mineral flakes.

Shales are typically composed of variable amounts of clay minerals and quartz grains and the typical color is gray. Addition of variable amounts of minor constituents alters the color of the rock. Black shale results from the presence of greater than one percent carbonaceous material and indicates a reducing environment. Red, brown and green colors are indicative of ferric oxide (hematite - reds), iron hydroxide (goethite browns and limonite - yellow), or micaceous minerals (chlorite, biotite and illite greens).

The process in the rock cycle which forms shale is compaction. The fine particles that compose shale can remain suspended in water long after the larger and denser particles of sand have deposited. Shales are typically deposited in very slow moving water and are often found in lakes and lagoon deposits, in river deltas, on floodplains and offshore from beach sands. They can also be deposited on the continental shelf, in relatively deep, quiet water (Tracy, 1996).

Coal

Coal is a readily combustible black or brownish black sedimentary rock normally occurring in rock strata in layers or veins called coal beds. The harder forms, such as anthracite coal, can be regarded as metamorphic rock because of later exposure to elevated temperature and pressure. Coal is composed primarily of carbon

along with variable quantities of other elements, chiefly sulfur, hydrogen, oxygen and nitrogen.

Coal begins as layers of plant matter accumulate at the bottom of a body of water. For the process to continue the plant matter must be protected from biodegradation and oxidization, usually by mud or acidic water. The wide shallow seas of the Carboniferous period provided such conditions. This trapped atmospheric carbon in the ground in immense peat bogs that eventually were covered over and deeply buried by sediments under which they metamorphosed into coal. Over time, the chemical and physical properties of the plant remains were changed by geological action to create a solid material (Licht and Dublin, 2005).

2.2.2 Fluid content in formation and fractures

Normally crude oil and natural gas are produced in source rocks. Source rocks refer to strata with a large organic component, which later turns to crude oil. Diatomite, a source rock, is a shaly rock that is composed mainly of the remains of diatoms (one celled plants) and radiolarians (protist). As the oil and gas are generated, depending on local conditions, the petroleum products will separate by density (Hyne, 2001).

If open fractures occur nearly permeable zone, and it will play as a fluids path way and fluids possible flow into the open fracture. Hence, fracture can be filled with any types of fluids that have enough pressure to flow in to the fracture.

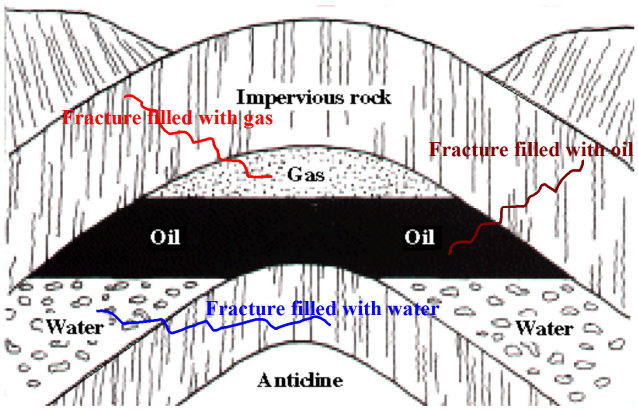

Figure 2.15 Illustration of fracture filled with different type of fluids (water, oil or gas).

Geophysical signature of the formations without fractures

In a normal sandstone formation, there is often no 100% clean sandstone or shale but they are mixed together, so it is necessary to determine an average value of the logging data response to each lithology, sandstone, shale and coal. In this topic a layer with a lithology value of more than ≥75% were used to determine the average value, maximum, minimum, and standard deviation. An example of average lithology values from logging data is shown in Table 2.4, here formations with shale content higher than 75%. Resistivity data are not determined because they are affected by many parameters, such as porosity and fluid content.

Table 2.4 Example of the minimum, maximum, average and STDEV values of shale formation with lithology content ≥75%.

	GR (API)	**RHOB (g/cm^3)**	**DT (µs/ft)**	**CALI (inch)**	**PEF (barns/electron)**	**NPOR (vol/vol)**
Shale						
Average	149	2.6	65.9	7.1	3.7	0.14
Maximum	293	2.8	121.6	13.1	6.7	0.55
Minimum	32	1.5	55.3	5.9	1.0	0.01
STDEV	30	0.1	8.0	1.0	0.6	0.05

The sandstone formations with sandstone content ≥75% were separated in different porosity classes, (a) smaller than 5%, (b) between 5% to 10%, and (c) higher than 10%. Table 2.5 shows an example of minimum, maximum, average and STDEV values of the sandstone formations with 0≤porosity≤5%. Porosity is derived from %SH + %SS + %COAL + %porosity = 100%.

Table 2.5 Example of minimum, maximum, average and STDEV values of sandstone formation with 0≤porosity≤5%.

	GR (API)	RHOB (g/cm^3)	DT (µs/ft)	CALI (inch)	PEF (barns/electron)	NPOR (vol/vol)
0≤porosity≤5%						
Average	57	2.62	60	7	2.7	0.03
Maximum	121	2.80	81	15	4.2	0.24
Minimum	30	2.39	51	5	1.0	0.00
STDEV	12	0.05	3	1	0.3	0.02

2.2.3 Parameters for qualitative fracture modeling

Fracture orientation

The fracture orientation is related to the principal stress; mainly the orientation and magnitude of the three principal stress directions (see Chapter 1). Figure 2.16 shows different fracture orientations with different inclination values related to a 2-dimensional vertical borehole.

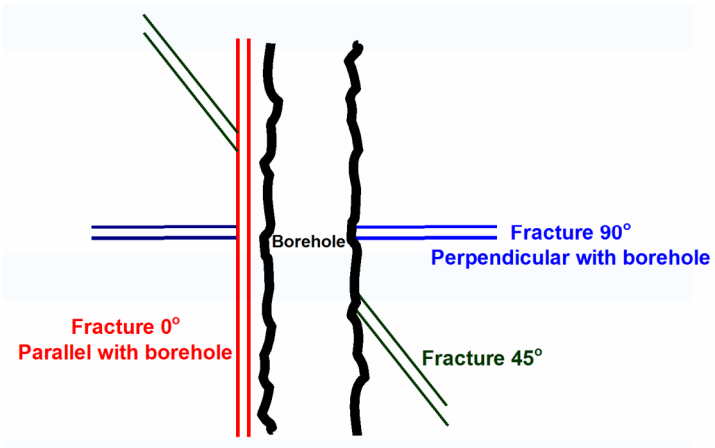

Figure 2.16 Schematic illustration of fracture orientation with different inclination in relation to a vertical borehole.

Fracture size

Fracture size is one parameter that should be under consideration because if a fracture is somehow smaller than the logging resolution it cannot be detected. Figure 2.17 shows different sizes or apertures of fracture compared to the borehole size.

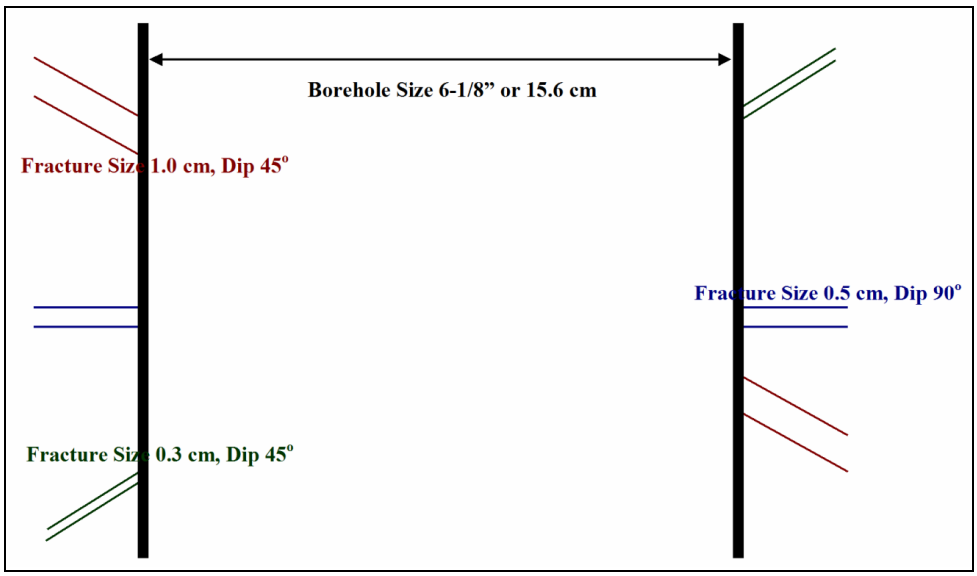

Figure 2.17 Schematic illustrations of fracture sizes 0.3, 0.5 and 1.0 cm compared to the borehole size 6-1/8 inch or 15.6 cm (scale 1:0.5cm).

A fault represented by a zone of intensely deformed rock is >1 cm thick. The thickness limitation is used for zones thick enough to be clearly distinguished in image logs (Lacazette, 2001). Deformation bands are mm-scale braided accumulations of crushed zones roughly 0.5-1 mm thick. Deformation band are important to the petroleum industry because they only form in highly porous (>15%) sandstones and chalks, which make good reservoirs. Deformation bands cause severe compartmentalization of oil fields in the North Sea, Indonesia, US and elsewhere (Antonellini and Aydin, 1995).

The distribution of fractures according to apparent aperture is shown in Figure 2.18. This plot represents the number of fracture of specific aperture that fall within the resolution capabilities of the BHTV tool. The frequency distribution of fractures aperture is clearly not random. Above 10-15 cm the frequency of a given apertures are inversely proportion to aperture. The drop of in frequency below apertures of 10 mm is largely a function of detection limit of tool and the resolution and technique used to measure apparent aperture and does not represent the true fracture distribution between 0-10 mm.

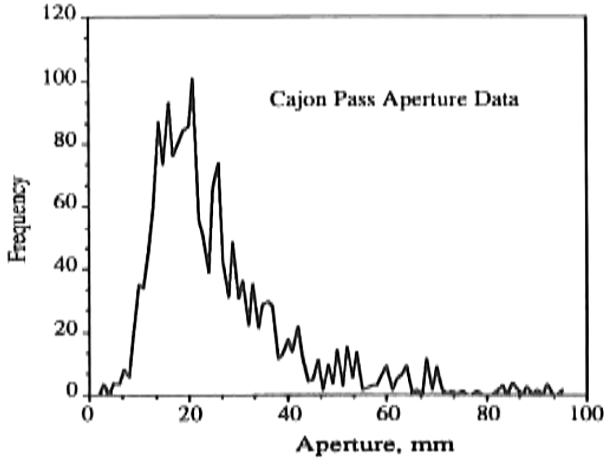

Figure 2.18 Fracture aperture distribution from the Cajon Pass scientific drill hole (Barton and Zoback, 1990).

Open or closed fractures

In an open fracture fluids can flow via the fracture to the borehole so a resistivity tool might detect the resistivity change due to the fluid presence. On the other hand, if a fracture is closed, the fluid cannot flow so a resistivity tool cannot detect any resistivity change related to a fluid. But if a closed fracture is filled with minerals of resistivity contrast to the formation, it might be detected by a resistivity log.

2.2.4 Qualitative modeling of geophysical fractures response

In order to understand the response of fractures in geophysical logging a qualitative approach was chosen as a quantitative modeling is hampered by the complexity of the different tools and borehole environment. In the following the geophysical response of the different tools in respect to fracture is discusses qualitatively.

Gamma ray log

Fractures can be identified by gamma ray log due to uranium salts that are soluble in both water and oil. Zones of high uranium content indicate fluid movement, subsequent mineral deposition, and thus a probable zone of permeability, usually a fractured zone (see Table 2.6).

Sonic log

In isotropy medium or unfractured medium, shear waves travel fastest when the direction of particle motion, called polarization, is parallel to the direction of greatest stiffness. Compressional waves have particle motion in the direction of propagation, but shear waves have particle motion in the perpendicular direction of propagation. This is the result why compressional wave velocity is faster than shear wave velocity.

In anisotropic medium or fractured zone, P-waves travel fastest in directions of polarization parallel to fractures, and travel more slowly when the polarization is perpendicular to fractures. This is the result why P-wave velocity reduced when it passing through the fracture zone which perpendicular to borehole axis. Also for shear wave velocity, if the fracture is parallel to the bore hole axis the shear waves travel near the borehole wall and do not 'see' the fractures. But if the fracture is perpendicular to the borehole axis both P– and S–waves are directly affected and the velocity will be reduced (see Table 2.6).

Another methods used for fracture characterization is utilizing the Vp/Vs or DTs/DTc ratio, which is the lateral strain divided by longitudinal strain, or P–wave velocity over shear wave velocity. A high DTs/DTc ratio indicates high stress level, which in turn indicates possible boundaries to a hydraulic fracture (Crain, 2004). Rocks with a high DTs/DTc ratio are more likely to have fractured zones than those with a low DTs/DTc ratio (see Table 2.6).

Resistivity log

MSFL indicates fractures by showing low resistivity spikes opposite open fractures, and high resistivity spikes opposite sealed fractures and tight or highly cemented layers. Another method, is to look for cross over of the shallow and deep resistivity. If mud resistivity is less than the formation resistivity, then the shallow resistivity curve will cross over the deep resistivity in a fractured interval and read lower resistivity, due to invasion of the fractures. Normally the shallow curve reads higher than the deep, except in salt mud systems. The shallow curve may also appear noisy or spiky (see Table 2.6).

Photoelectric log

Large Pe values, greater than 5.0 cu., especially when weighted muds are used, are a fracture indicator. Barite has a very large photoelectric cross section, 267 as compared with 5.0 for limestone and 3.1 for dolomite. Thus the Pe curve should exhibit a very sharp peak in front of a fracture filled with barite loaded mud cake. In light weight muds, an abnormally low Pe value, less than 1.7, indicates, fractures, bad hole condition, or coal (see Table 2.6).

Bulk density log

If the density log shows low density spikes that are not seen by the neutron log, usually fractures, large vugs, or caverns exist. Broken out borehole also causes the same effected, but fractures are often present when this occurs (see Table 2.6).

Neutron porosity

Neutron log is not a useful fracture indicator by itself. However, neutron porosity values are often compared with other sources to indicate either lithology or the possibility of fractures. The sidewall neutron log sees only a small portion of the borehole wall and may be affected by borehole break out in the same way as the density log. Break out is often associated with fractures (see Table 2.6).

Table 2.6 Summary of the qualitative fracture response for the logging tools used in this study.

Raw Data	**Log Name**	**Response**	**Description or Note**
GR	Gamma-Ray log	Anomalous (higher than normal trend)	Uranium salts are soluble in both water and oil; zones of high uranium content indicate fluid movement, subsequent mineral deposition, and thus a probable zone of permeability, usually a fractured zone.
MSFL, LLd, LLs	Resistivity log	Anomalous	- MSFL indicate fractures by showing low resistivity spikes opposite open fractures, and high resistivity spikes opposite sealed fractures and tight or highly cemented layers. - LLs may read the resistivity of drilling mud in washed out borehole sections - Cross over of the LLs and LLd
CALI	Caliper log	Size change	Sudden variations indicate a discrete feature
PE	Photoelectric log	High value with sharp drop	- Pe curve should exhibit a very sharp peak in front of a fracture filled with barite loaded mud cake - In light weight mud, an abnormally low Pe value, less than 1.7, indicates, fractures, bad holes condition, or coal.
Processed Data	**Log Name**	**Response**	**Description or Note**
RHOB	Bulk Density log	Low value	Combined with PE for open fracture.
NPOR	Neutral Porosity log	not a useful fracture indicator	
Vp/Vs or DTs/DTc		High value	Used for a stable borehole and known lithology

The qualitative modeling of the facture response of the conventional well logging tools available in this study is shown in a flow chart in Figure 2.18. As several of the conventional logging tool cannot detect fracture, like FMS or BHTV,

most well logs respond in some way to the presence of fractures. Not all logs detect fractures in all situations, and very few see all fractures present in the logged interval. Figure 2.18 shows the important fracture parameter needed for the qualitative modeling of the fracture response that are fracture size, fracture orientation, fluids filled and type of fractures.

The fracture size must be somehow larger than the sampling interval of the logging tools. However if a fracture is large enough to detected by the tool, the signal of CALI, DT, RHOB, DTs/DTc and PEF will deviate from the normal trend as the flow chart indicates. Fractures can be detected by the conventional logging tool only when the dip angle of the fracture plane is perpendicular or at any angle to the borehole axis but cannot be detected when the fracture plane is parallel to the borehole axis. Another parameter is the fracture filling. A fracture can be filled with hydrocarbon that gives very low resistivity values or with brine having then a conductive fracture. Sometimes a fracture filled with minerals or radioactive material then called closed fracture. If a fracture is filled with radioactive material, GR can detect it, but if filled with other mineral should be consider other log such as CALI, DT, RHOB, DTs/DTc and PEF.

The qualitative modeling of the facture response of the conventional well logging tools available in this study is shown in a flow chart in Figure 2.18. As several of the conventional logging tool cannot detect fracture, like FMS or BHTV, most well logs respond in some way to the presence of fractures. Not all logs detect fractures in all situations, and very few see all fractures present in the logged interval. Figure 2.18 shows the important fracture parameter needed for the qualitative modeling of the fracture response that are fracture size, fracture orientation, fluids filled and type of fractures.

The fracture size must be somehow larger than the sampling interval of the logging tools. However if a fracture is large enough to detected by the tool, the signal of CALI, DT, RHOB, DTs/DTc and PEF will deviate from the normal trend as the flow chart indicates. Fractures can be detected by the conventional logging tool only when the dip angle of the fracture plane is perpendicular or at any angle to the borehole axis but cannot be detected when the fracture plane is parallel to the borehole axis. Another parameter is the fracture filling. A fracture can be filled with

hydrocarbon that gives very low resistivity values or with brine having then a conductive fracture. Sometimes a fracture filled with minerals or radioactive material then called closed fracture. If a fracture is filled with radioactive material, GR can detect it, but if filled with other minerals should be consider other log such as CALI, DT, RHOB, DTs/DTc and PEF.

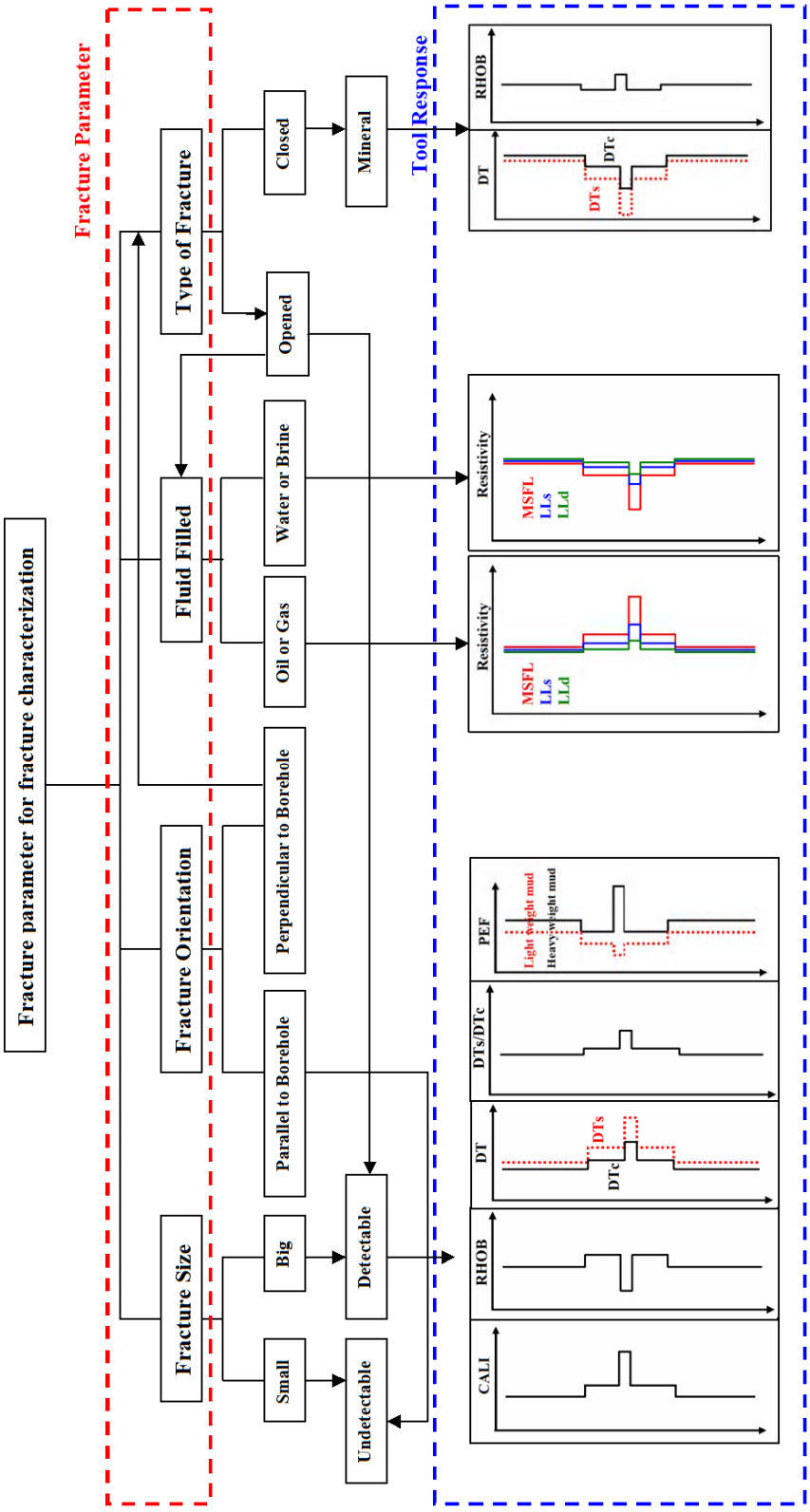

Figure 2.19 Flow chart for the qualitative modeling of the fracture response for the different fracture parameters and for the available conventional logging tools (tool response).

2.2.5 Correlation of fractures from conventional logging and FMS

As for the well of this study FMS fracture data are available, the last step in the analysis is the correlation with data from FMS and the conventional logging data. An example for this is shown for a fracture at the depth of 2716 m. The result shown that MSFL indicates the fractures by showing a low resistivity spike opposite of the open fracture (see Figure 2.19). From the data, DTc reduce but DTs increase and DTs/DTc or Poisson's ratio is higher, that means it is likely to have fractured zone at this depth. The photoelectric log (Pe) also show high value it can be possible that barite from mud filled in the fracture. The bulk density log (RHOB) shows high density spikes that are not seen by the neutron log (NPOR), usually fractures, large vugs, or caverns exist. Broken out borehole also causes the same effected, but fractures are often present when this occurs.

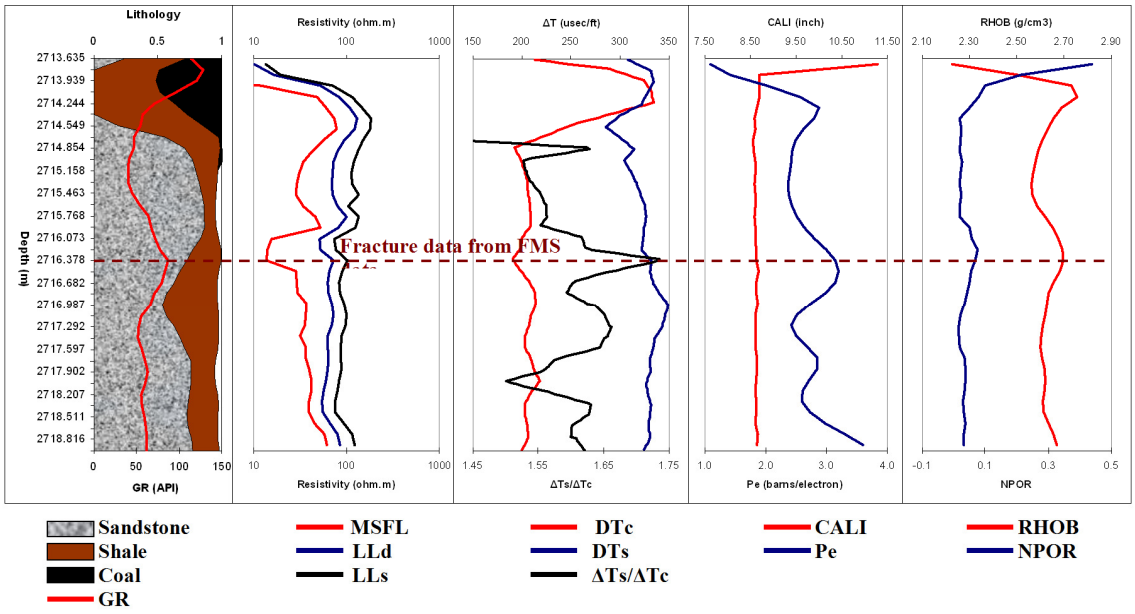

Figure 2.19 Example of a fracture zone at depth 2716 m with the FMS data combined with conventional logging data.

CHAPTER 3

Results

3.1 Characterization of main lithologies

From logging data set 1, there are three main lithologies including shale, sandstone and coal, which can be mixed together or interbeded with another. Therefore a lithology content value of higher than 75% was assigned for the main formations. For example, in depth interval 2712.568–2715.158 m the lithology content of sandstone higher than or equal 0.75 or 75%, so this layer is assigned sandstone formation, although it also contains coal and shale (see Figure 3.1).

Table 3.1 Example of logging data between depth intervals 2712.568 - 2715.158 m with sandstone content higher than or equal 0.75 or 75%.

Depth (m)	GR (API)	RHOB (g/cm^3)	DT (µs/ft)	CALI (inch)	SS	SH	COAL	PEF (barns/ê)	NPOR
2712.568	52.982	2.639	58.01455	8.681	**0.763**	0.213	0.000	2.804	0.017
2712.720	62.598	2.654	57.20000	8.664	**0.789**	0.202	0.000	2.802	0.018
2712.872	78.418	2.671	56.52848	8.647	**0.813**	0.181	0.000	2.588	0.023
2713.025	87.323	2.673	56.24939	8.653	**0.827**	0.169	0.004	2.064	0.021
2713.177	86.188	2.571	59.87485	8.633	**0.792**	0.208	0.000	1.466	0.038
2715.158	40.300	2.568	62.95364	8.602	**0.793**	0.173	0.000	2.389	0.021

The data were analyzed, with the determination of the average, minimum, maximum and standard deviation value, and are shown in Table 3.2. From Table 3.2, shale has a higher average value of natural gamma ray than sandstone and coal because shale normally composed with radioactive material. The maximum value of natural gamma ray for shale is about 293.660 API, sandstone is 144.225 API and coal is 258.101 API. The minimum value of shale is about 32.000 API, sandstone is 27.675 API and 10.722 API for coal. The standard deviation value of shale is about 26.350; sandstone is 12.572 and 40.767 for coal. A low standard deviation indicates that the data points tend to be very close to the mean value, whereas high standard deviation indicates that the data are spread out over a large range of values.

The average bulk density of shale is about 2.677 g/cm^3 higher than sandstone 2.571 g/cm^3 because sandstone has additionally porosity, which decreases the bulk density. Coal has the lowest bulk density value with about 1.351 g/cm^3, which is similar to data reported in Schoen (1996). The maximum bulk density of shale is about 2.837 g/cm^3, lower than the maximum bulk density of sandstone, which is 2.964 g/cm^3. The maximum bulk density of coal is 2.62 g/cm^3, which is likely related to additional quartz content. The minimum bulk density value of shale is about 1.506 g/cm^3, sandstone is about 2.393 g/cm^3, and 1.351 g/cm^3 for coal. Standard deviation of bulk density for shale is about 0.175, sandstone is about 0.073 and coal is about 0.238.

Table 3.2 Average, maximum, minimum and standard deviation value for shale, sandstone and coal formation which lithology content ≥75%. STDEV is standard deviation.

	GR (API)	**RHOB (g/cm^3)**	**DT (us/ft)**	**MSFL (Ωm)**	**LLd (Ωm)**	**LLs (Ωm)**	**CALI (inch)**	**PEF (barns/e)**	**NPOR (vol/vol)**
SHALE									
Average	149	2.67	65.8	50	111	91	7.1	3.7	0.14
Maximum	293	2.83	121.6	218	793	776	13.1	6.7	0.55
Minimum	32	1.50	55.3	0	12	12	5.9	1.0	0.01
STDEV	30	0.17	8.0	30	80	80	1.0	0.6	0.05
SANDSTONE									
Average	50	2.57	63.7	28	72	54	8.4	2.6	0.03
Maximum	14	2.96	82.1	142	416	289	15.4	4.3	0.24
Minimum	27	2.39	51.4	0	7	5	5.9	0.9	0.00
STDEV	10	0.07	4.0	20	40	40	1.0	0.3	0.01
COAL									
Average	48	1.58	111.2	2	79	39	8.8	1.7	0.39
Maximum	258	2.62	127.5	35	1478	299	11.0	7.0	0.62
Minimum	10	1.35	60.0	0	14	9	6.4	0.9	0.11
STDEV	40	0.23	10.0	5	160	40	0.9	1.1	0.10

The average delta time of shale is 65.8 ± 8.0 μs/ft, of sandstone 63.7 ± 4.0 μs/ft and of coal 111.2 ± 10.0 μs/ft. This can be explained that although sandstone has a higher porosity than shale but the matrix velocity of sandstone is higher than of shale. On the other hand the delta time of coal is longer than of sandstone and shale because coal is weaker and can easily break by the drilling process. The maximum delta time

of shale is 121.6 μs/ft, of sandstone 82.1 μs/ft, and 127.5 μs/ft for coal. The minimum delta time of shale is 55.3 μs/ft, for sandstone 51.4 μs/ft, and 60.0 μs/ft for coal. The standard deviation of the delta time for shale is about 8.0, for sandstone about 4.0 and for coal about 10.0.

The average borehole size in shale formation is about 7.139 inch; in sandstone is about 8.410 inch and in coal is about 8.891 inch. The caliper log somehow reflects the mechanical properties of a rock formation. The average data of the borehole size show that coal has bigger borehole sizes than sandstone or shale because of lower mechanical properties, easier to break during the drilling process.

The maximum holes size in shale formation is 13.1 inch, in sandstone formation is 15.4 inch, and in coal formation is 11.0 inch. The minimum borehole size in shale formation is 5.9 inch; in sandstone formation is 5.9 inch and in coal formation is 6.4 inch. The standard deviation for shale is 1.0, for sandstone 1.0, and for coal is about 0.9.

The average photoelectric absorption factor is about 2.6 barns/ê for sandstone and 3.7 barns/ê for shale and coal shows a very low photoelectric absorption factor of 1.7 barns/ê, this is because carbon has a relatively low atomic number. The maximum photoelectric absorption factor is about 4.3 barns/ê for sandstones and 6.7 barns/ê for shale and 7.0 barns/ê for coal. The minimum photoelectric absorption factor is about 0.9 barns/ê for sandstones, and 1.0 barns/ê for shale and coal shows 0.9 barns/ê. The standard deviation of photoelectric absorption factor for sandstone is about 0.3, for shale 0.6, and 1.1 for coal.

The average neutron porosity for shale is about 0.14, for sandstone is about 0.03 and 0.39 for coal. The neutron porosity is the measure of hydrogen ion concentration in a formation, where the hydrogen ion can be the component in water, oil and gas. When a pore filled with gas rather than oil or water, neutron porosity will be lowered. This occurs because there is less concentration of hydrogen in gas compared to oil or water. The maximum value of the neutron porosity is 0.55 for shale, about 0.24 for sandstone and 0.62 for coal. The minimum value of neutron porosity is 0.01 for shale, about 0.00 for sandstone and 0.11 for coal. Standard deviation of neutron porosity is about 0.05 for shale, sandstone is about 0.01, and 0.10 for coal.

The average value is the petrophysical signature of the formation without fractures. For example, DT of sandstone without fracture is about 63.7μs/ft, and if DT is longer than this the mean physical property of this rock was changed maybe by open fractures. On the other hand if DT is lower than the average value it is possible that there can be a close fracture filled with mineral that have a higher density.

3.2 Characterization of sandstone formations with different porosity

The sandstone formations are the main target formation of this study. However, sandstone can exhibit different porosities, which have an effect on the petrophysical signature. Therefore, the sandstones are separated in three different porosity classes: less than 5%, between 5 and 10%, and greater 10%. In Table 3.3 the results are shown with the average, maximum, minimum and standard deviation value of sandstone according to the different porosity classes.

Table 3.3 Minimum, maximum, average and standard deviation values of sandstone formation with different porosity. STDEV is standard deviation.

	GR (API)	**RHOB (g/cm^3)**	**DT (us/ft)**	**MSFL (Ωm)**	**LLd (Ωm)**	**LLs (Ωm)**	**CALI (inch)**	**PEF (barns/e)**	**NPOR**
porosity < 5%									
Average	57	2.62	60.4	39.3	84.9	66.6	7.8	2.7	0.03
Maximum	121	2.80	81.7	142.3	416.1	289.3	15.4	4.2	0.24
Minimum	30	2.39	51.4	0.1	11.3	7.0	5.9	1.0	0.00
STDEV	10	0.05	4.0	20.0	60.0	50.0	1.3	0.3	0.02
5% ≤ porosity ≥ 10%									
Average	45	2.53	65.9	21.4	65.3	46.6	8.8	2.6	0.03
Maximum	144	2.79	77.1	102.5	317.4	234.1	15.2	4.3	0.16
Minimum	27	2.43	55.6	0.3	7.6	6.3	8.3	1.1	0.00
STDEV	10	0.04	2.0	10.0	30.0	20.0	1.0	0.3	0.01
porosity >10%									
Average	42	2.51	70.4	13.2	39.7	23.7	9.6	2.5	0.04
Maximum	54	2.96	82.1	57.9	100.7	60.2	13.2	3.4	0.08
Minimum	29	2.42	58.1	2.1	9.2	5.7	8.4	0.9	0.02
STDEV	5	0.11	4.0	10.0	20.0	10.0	1.8	0.5	0.01

From Table 3.3, the average GR of sandstone formation with 0%≤porosity≤5% is about 57 API, with 5%<porosity≥10% is 45 API and with

porosity>10% is 42 API. This sandstone formation contains small parts of clay inside. With increasing porosity, which means less matrix volume, the absolute amount of shale decrease, however, the shale percentage could be the same. The maximum GR for 0%≤porosity≤5% is about 121 API, for 5%<porosity≥10% is about 144 API and porosity>10% is 54 API. The minimum GR for 0%≤porosity≤5% is about 30 API, for 5%<porosity≥10% is about 27 API and porosity>10% is 29 API. The standard deviation of GR for 0%≤porosity≤5% is about 10, 5%<porosity≥10% is about 10, and porosity>10% is about 5.

The average RHOB of the sandstone formation for 0%≤porosity≤5% is about 2.62 g/cm^3, 5%<porosity≥10% is 2.52 g/cm^3 and porosity>10% is 2.51 g/cm^3. When the porosity increases the bulk density decreases. The maximum bulk density for 0%≤porosity≤5% is about 2.80 g/cm^3, for 5%<porosity≥10% is about 2.79 g/cm^3 and porosity>10% is 2.96 g/cm^3. The minimum GR for 0%≤porosity≤5% is about 2.39 g/cm^3, for 5%<porosity≥10% is about 2.43 g/cm^3 and porosity>10% is 2.429 g/cm^3. The standard deviation of RHOB for 0%≤porosity≤5% is about 0.05, 5%<porosity≥10% is about 0.04, and porosity>10% is 0.11.

Average slowness of sandstone formation for 0%≤porosity≤5% is about 60.5 μs/ft, and 5%<porosity≥10% is 66.0 μs/ft and porosity>10% is 70.4 μs/ft. These data reflect the relationship between porosity and slowness of the waves; if porosity increases the slowness also increases, respectively, the wave velocity decreases. Maximum slowness for 0%≤porosity≤5% is about 81.7 μs/ft, 5%<porosity≥10% is about 77.1 μs/ft and porosity>10% is about 82.1 μs/ft. Minimum slowness for 0%≤porosity≤5% is about 51.4 μs/ft, for 5%<porosity≥10% it is about 55.6 μs/ft and porosity>10% is about 58.1 μs/ft. The standard deviation of the slowness for 0%≤porosity≤5% is about 4.0, for 5%<porosity≥10% is about 2.0, and porosity>10% is 4.0.

The average borehole size of the sandstone formation for 0%≤porosity≤5% is about 7.8 inch, for 5%<porosity≥10% is 8.8 inch and porosity>10% is 9.6 inch. When porosity in the sandstone increase the mechanical properties often change and the rock is becomes weak and is more easily to break by the drilling process, which might be a cause of the large borehole size. Maximum borehole size of sandstone formation for 0%≤porosity≤5% is about 15.4 inch, 5%<porosity≥10% is 15.2 inch and

porosity>10% is 13.2 inch. Minimum borehole size of sandstone formation for 0%≤porosity≤5% is about 5.9 inch, for 5%<porosity≥10% it is 8.3 inch and porosity>10% is about 8.4 inch. Standard deviation of borehole size for 0%≤porosity≤5% is about 1.3, for 5%<porosity≥10% is about 1.0, and porosity>10% is about 1.8.

The average photoelectric value of sandstone formation for 0%≤porosity≤5% is about 2.7 barns/ê, for 5%<porosity≥10% it is 2.6 barns/ê and porosity>10% is 2.5 barns/ê. This means that the photoelectric absorption is in reverse sense with the porosity of the sandstones. The maximum photoelectric value of sandstone formation for 0%≤porosity≤5% is about 4.2 barns/ê, for 5%<porosity≥10% is 4.3 barns/ê and porosity>10% is 3.4 barns/ê. Minimum photoelectric value of sandstone formation for 0%≤porosity≤5% is about 1.0 barns/ê, for 5%<porosity≥10% is 1.1 barns/ê and porosity>10% is about 0.9 barns/ê. The standard deviation of the photoelectric value for 0%≤porosity≤5% is about 0.3, for 5%<porosity≥10% the standard deviation is about 0.3, and porosity>10% is 0.5.

The average neutron porosity value of sandstone formation with 0%≤porosity≤5% is about 0.03, for 5%<porosity≥10% the value is 0.03 and porosity>10% is about 0.04. The maximum neutron porosity value of sandstone formation for 0%≤porosity≤5% is about 0.24, for 5%<porosity≥10% it is 0.16 and porosity>10% is about 0.08. Minimum neutron porosity value of sandstone formation with 0%≤porosity≤5% is about 0.00, for 5%<porosity≥10% it is 0.00 and porosity>10% is about 0.02. The standard deviation of neutron porosity for 0%≤porosity≤5% is about 0.02, for 5%<porosity≥10% it is about 0.01, and porosity>10% is about 0.01.

3.3 Qualitative modeling of logging response to formation and fractures

The qualitative modeling of the logging response to formation and fractures applies the average formation data in topic 3.2, the measurement technique of the tool, the borehole environment outlined in topic 1.3 and the fracture parameter explained in topic 2.2.3. In the following the logging response for the different logging tools are presented and explained.

3.3.1 Resistivity log fracture response

In order to model the response of resistivity logs a transition profile of the formation and fractures in the sandstone formation have been established. Sandstones with different porosity values are separated as their petrophysical signature is different. The transition model combines the borehole, the flushes zone, invaded zone and the virgin formation beyond the invaded zone. The absolute depth of all zones mentioned before depend on the porosity and permeability of the formation and also on the drilling process as well as the pump pressure while drilling. The mud resistivity of the well is used and a general brine resistivity of 0.3 Ωm. The transition model includes the formation resistivity with some uncertainty depending on the data in topic 3.2 (average with standard deviation), and the resistivity profile of brine and hydrocarbon (HC) filled fractures; for example see Figure 3.1.

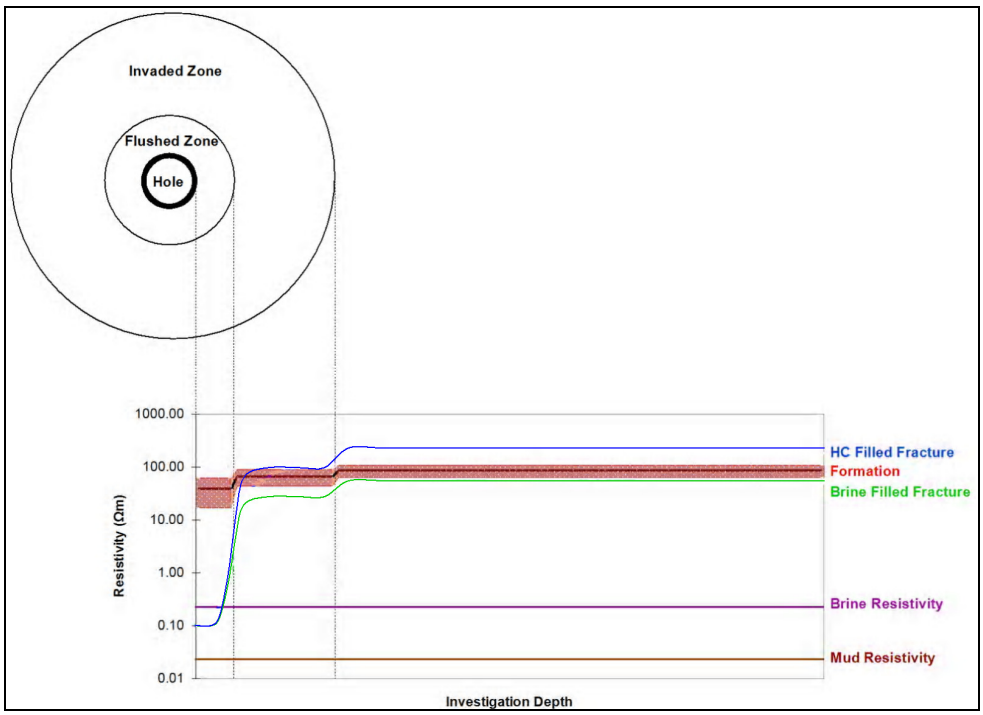

Figure 3.1 Qualitative transition profile of sandstone formation with porosity < 5%.

Figure 3.1 shows the formation resistivity obtained by the average value of resistivity for sandstone with less than 5% porosity. This value represents the mean resistivity reading from MSFL, LLs and LLd in a non-fracture zone of a sandstone formation with porosity less than 5%.

If a hydraulic fracture is filled with brine or hydrocarbon in this layer and the hydrostatic mud pressure is higher than the formation pressure then the mud, which has resistivity about 0.025-0.038 Ωm (highly conductive), can fill the fracture in the flushed zone so that the resistivity of the flushed zone should be reduced and the MSFL log will read a lower value than the formation value even the fracture is filled with high resistive hydrocarbon (Figure 3.1). The mud will penetrate also somehow further into the invaded zone, but less pronounced, so that the resistivity values increase significantly with further distance form the borehole, where the LLs and LLd will measure their resistivity values.

The transition profile also shows that there is a difference between a resistive and conductive fracture, however mainly in the invaded and virgin zone resistivity (Figure 3.1). If the resistivity of the invaded and virgin zone is higher than the formation without fracture value or normal trend, this mean it is resistive fracture filled with hydrocarbon. On the other hand if the resistivity value of invaded and virgin zone is lower than normal, this mean a conductive fracture filled with brine.

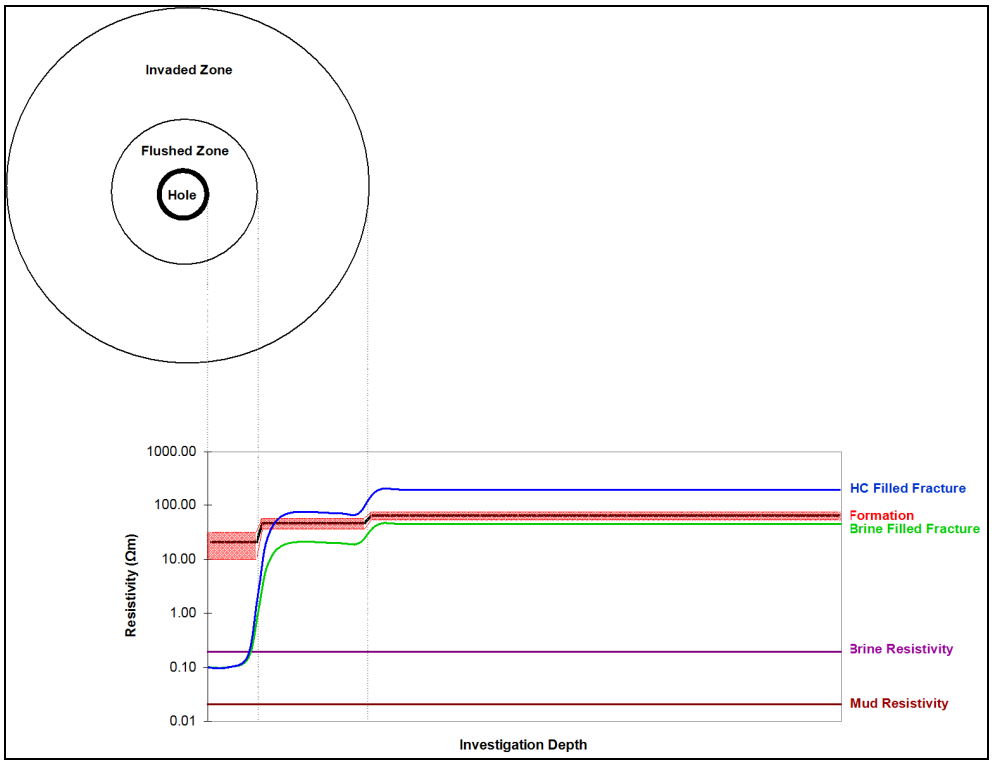

Figure 3.2 Schematic illustration of the transition profile of sandstone formation which 5% ≤ porosity ≤10%.

The transition profiles for formations with 5% ≤ porosity ≤10% and with a porosity > 10% the model will be similar to the one with less than 5% porosity. However, the trend of the formation resistivity is lower if the porosity increases; this mean that the mud can invade deeper into the formation when the porosity and permeability increases (see Figure 3.2 and 3.3).

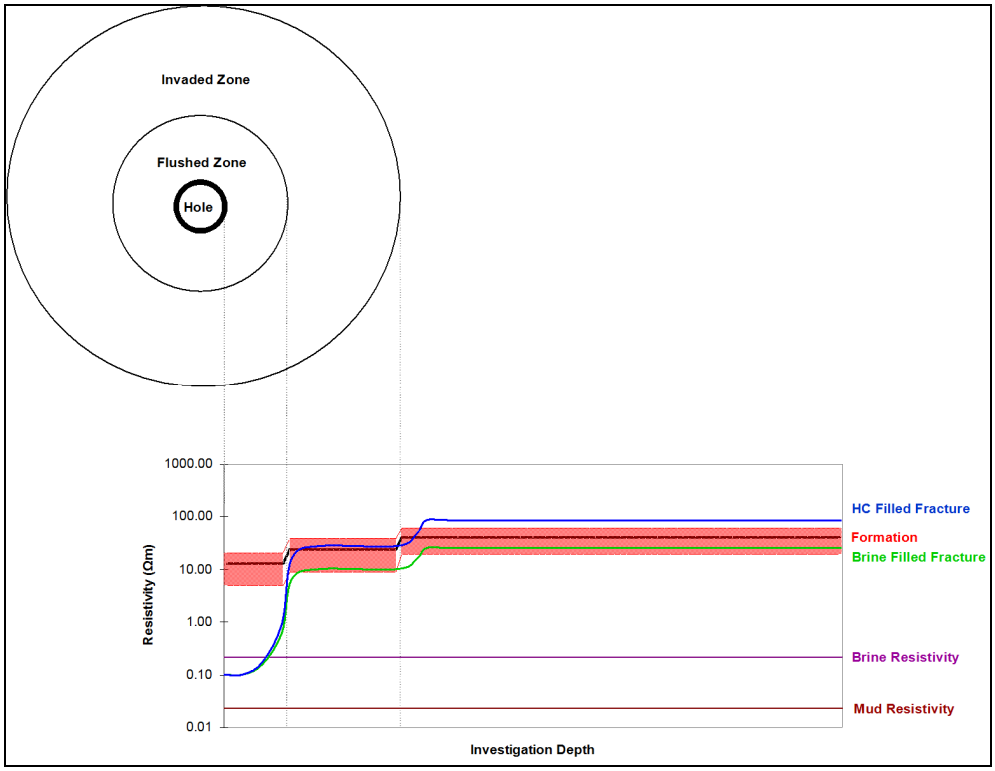

Figure 3.3 Schematic illustration of the transition profile sandstone formation with porosity > 10%.

From three qualitative transitions profiles shown above it can be seen that the MSFL tend to read the resistivity value close to mud resistivity. When break out occurs in front of a fracture or fracture zone and the mud flows inside the fracture the very shallow resistivity reading tool has the clear response to the fracture (see Figure 3.4).

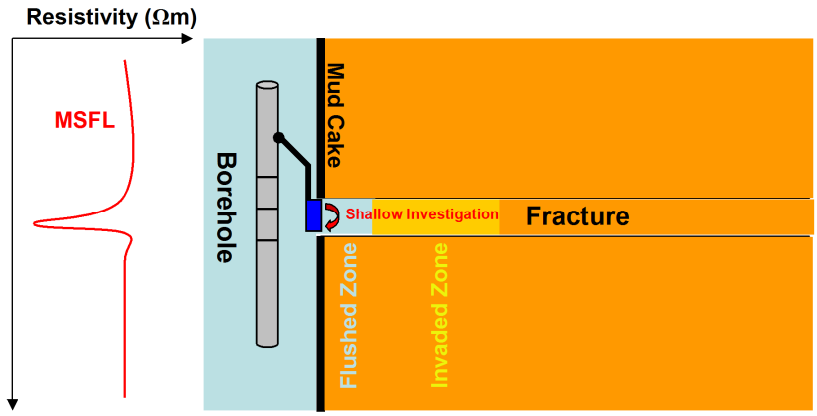

Figure 3.4 Schematic illustration of a hydraulic fracture zone filled with low resistivity mud and the response of an MSFL tool to the open fracture.

3.3.2 Sonic log fracture response

Table 3.4 shows that both ΔTc and ΔTs of shale are longer than of sandstone or the sonic compressional and shear wave velocity of shale is lower than those of a sandstone formation. The baseline or unfractured zone of shale is about 65.9 µs/ft and sandstone is about 63.8 µs/ft for compression slowness; shear slowness is about 105.3 µs/ft for shale and 101.9 µs/ft for sandstone. If a fracture occurs ΔTc and ΔTs are both increased called cycle skipping (see Figure 3.5 and 3.6).

Table 3.4 Average value of ΔTc, ΔTs, and ΔTs/ΔTc for sandstone and shale formation (lithology content ≥75%).

	ΔTc (µs/ft)	**ΔTs (µs/ft)**	**ΔTs/ΔTc**
Shale	65.9	105.3	1.5979
Sandstone	63.8	101.9	1.5972

The ΔTs/ΔTc ratio can be expressed in terms of properties that can be measured in the field, including velocities of P-waves and S-waves. ΔTs/ΔTc ratio can be computed from shear wave and compressional wave velocities or traveling time. Rocks with a high ΔTs/ΔTc ratio are more likely to have fractured zones than those with a low ΔTs/ΔTc. Thus, some insight into the likelihood of fracturing can be obtained from ΔTs/ΔTc ratio (see Figure 3.5 and 3.6).

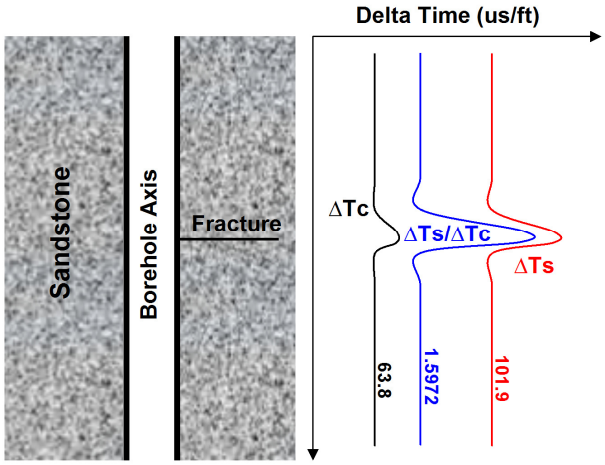

Figure 3.5 Qualitative models of ΔTc, ΔTs log and ΔTs/ΔTc ratio response to a horizontal fracture.

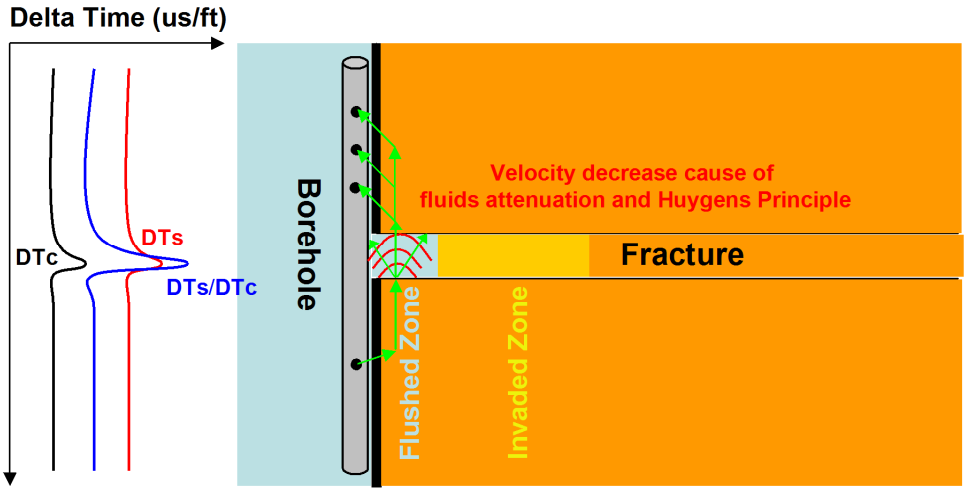

Figure 3.6 Schematic illustration of the response of a hydraulic open and fluid filled fracture to sonic log.

The ΔTs/ΔTc ratio of shale is about 1.5979 µs/ft is slightly higher than of sandstone with is about 1.5972 µs/ft. If ΔTs/ΔTc is increased or higher than the baseline the occurrence of fractures are likely as shown in Figure 3.5 and 3.6.

3.3.3 Photoelectric log fracture response

The photoelectric value of shale is about 3.7 barns/ê and 2.6 barns/ê for sandstone formation (see Table 3.5).

Table 3.5 Average photo electric absorption value of sandstone and shale formation (lithology content ≥75%).

	Pe (barns/ê)
Shale	3.7
Sandstone	2.6

The drilling mud, here water based mud, is usually mixed with barite, which has a very large photoelectric cross section, 267 barns/ê (Crain, 2003). The formation data of this well have comparable low values, i.e. 3.7 barns/ê for shale and 2.6 barns/ê for sandstone. Therefore, the PE curve will exhibit a very sharp peak in front of a fracture filled with barite loaded mud cake as shown qualitatively in Figure 3.7 and 3.8.

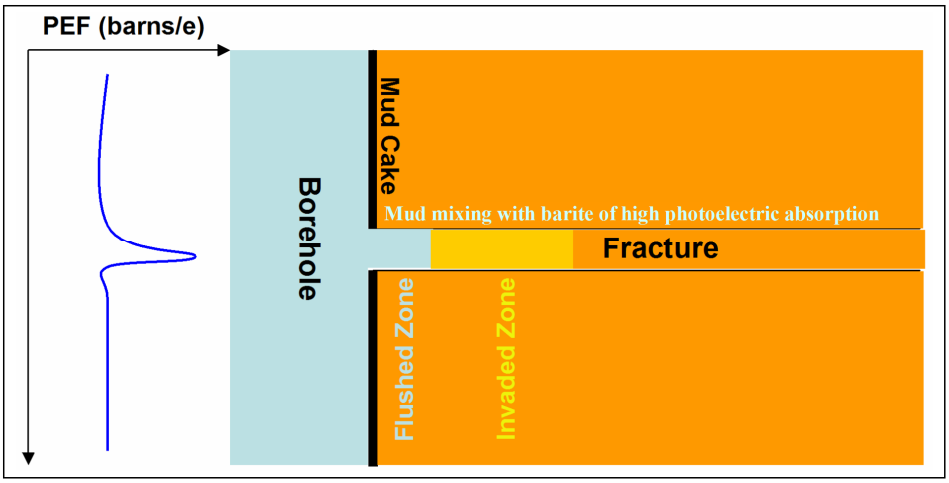

Figure 3.7 Qualitative illustration of the hydraulic fracture zone filled with water based mud (incl. barite) and the response of the photoelectric log to an open fracture.

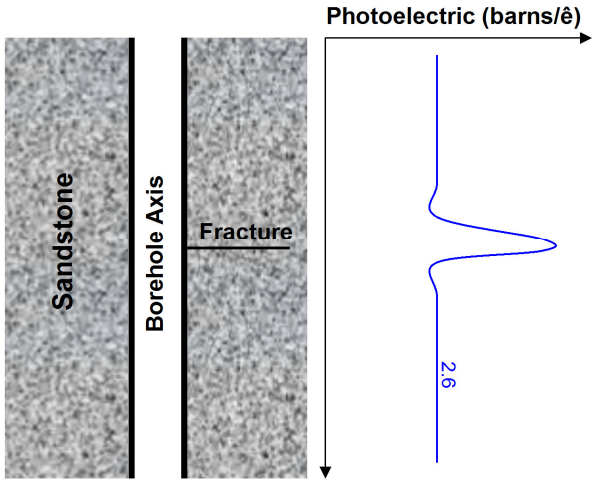

Figure 3.8 Qualitative model of the photoelectric log response to an open fracture.

3.3.4 Bulk density log fracture response

The average bulk density of the shale formation is 2.68 g/cm^3 and sandstone is 2.57 g/cm^3. In the present of fracture, the bulk density log shows a sharp drop in front of the fracture (see Figure 3.9 and 3.10).

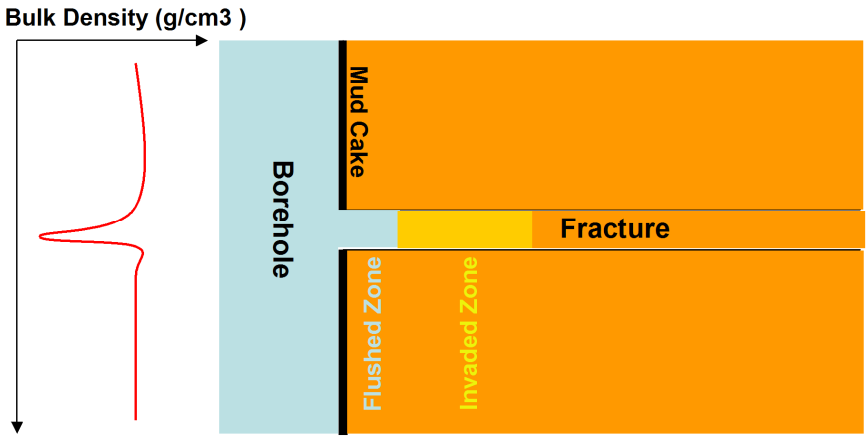

Figure 3.9 Qualitative illustration of the hydraulic fracture zone filled with water based mud and the response of the bulk density log.

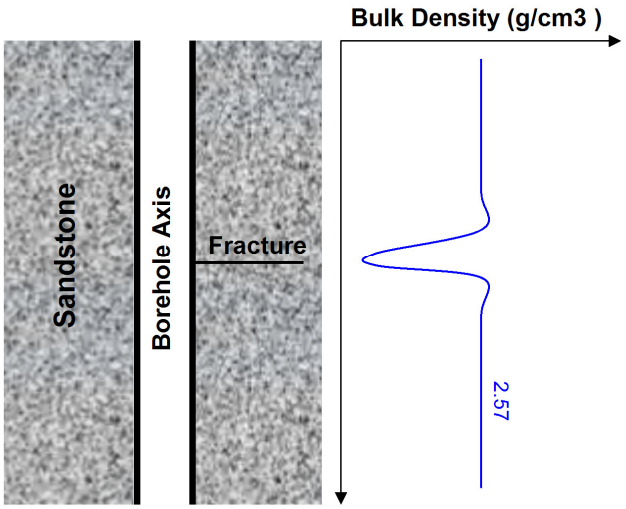

Figure 3.10 Qualitative model of the bulk density log response to an open fracture.

3.4 Fracture response in conventional logging data

For this study fracture data from FMS including depth of fracture, dip angle, azimuth angle, and resistive or conductive fracture were available. These data were used as a reference for fracture locations in the well. However, the main parameters used in this study are depth and “conductive” or “resistive” parameter. Azimuth and dip angle carry some uncertainty as the borehole orientation is not known.

Then the conventional logging data were combined with the FMS fracture data were applied the qualitative modeling of the different logging tool responses (see Figure 3.11). All available logging data were used in the analysis, but only representative examples are shown here.

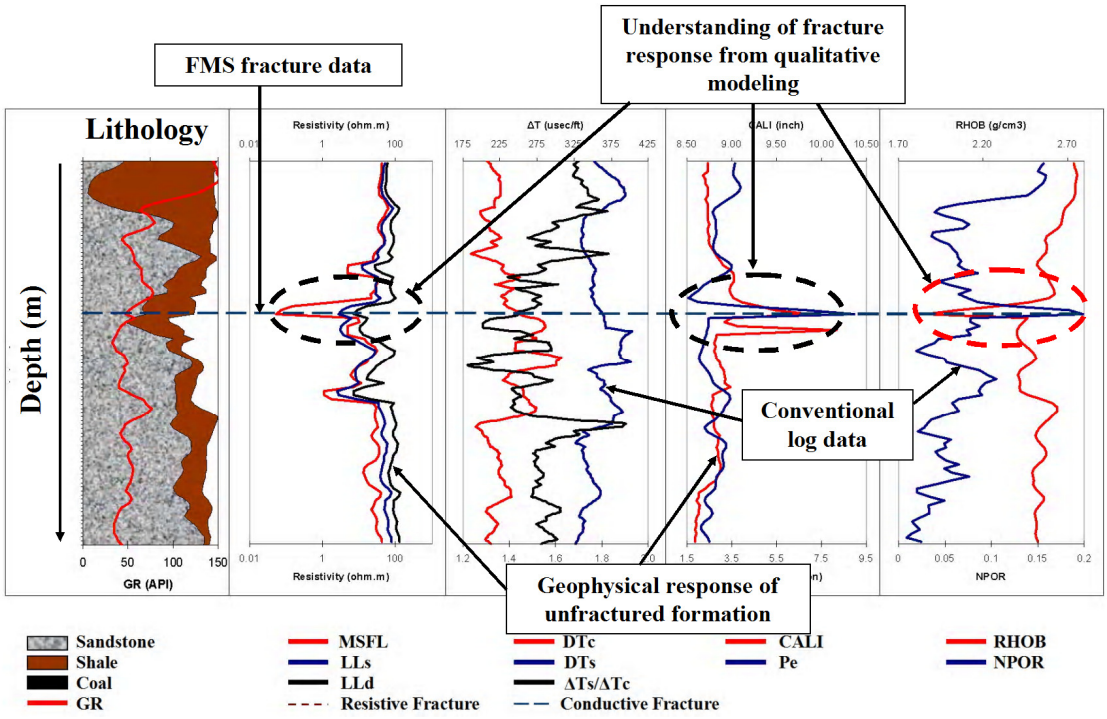

Figure 3.11 Schematic diagram showing the combination of the different data and information for fracture characterization.

3.4.1 Single fracture response

Figure 3.12 shows four single fracture data from FMS and convention logging data between depth 3385.719 – 3394.863 m. Consider single fracture A, at depth 3389.224 m where the formation is sandstone (71.6%) and shale (27.1%) with a porosity of 1.3%. It has a good response to different conventional logging tools: the very shallow resistivity log MSFL reads very low resistivity of about 27.547 Ωm because of lose pad contact to the borehole wall; shallow resistivity (LLs) is reading about 45.05 Ωm, and 57.15 Ωm for deep resistivity (LLd). Compression slowness is about 195.079 µs/m or 59.115 µs/ft due to the unconformity of the formation. Photoelectric absorption is about 3.391 barns/ê caused by the mud, as barite the main component is filled into the fracture. Bulk density shows a lower than normal trend with 2.636 g/cm^2. Single fracture B in Figure 3.12 at depth 3390.748 m has a good response to very shallow resistivity log MSFL reading is about 22.555 Ωm, LLs is about 47.834 Ωm, and LLd is about 58.603 Ωm. Compression slowness is about 194.423 µs/m. This single fracture shows a not good response to the photoelectric absorption and bulk density log. Single fracture C in Figure 3.12, a resistive fracture,

at depth 3391.814 m has a good response to very shallow resistivity log MSFL reading is about 30.458 Ωm, LLs is about 60.989 Ωm, and LLd is about 74.056 Ωm. Compression slowness is about 194.948 µs/m. This single fracture shows not a good response to the photoelectric absorption and bulk density log.

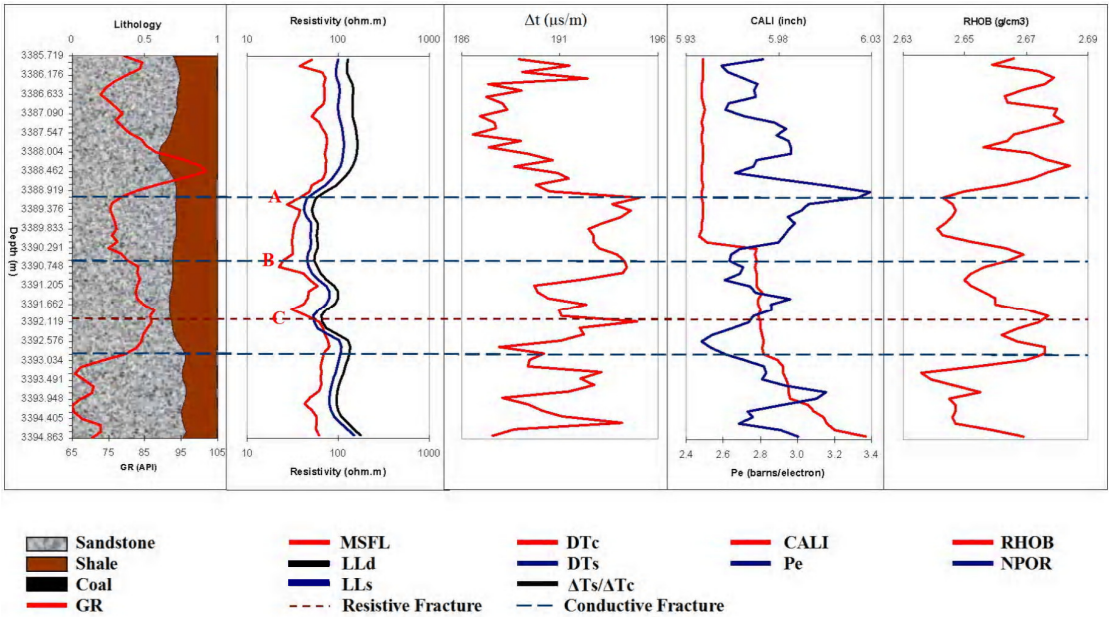

Figure 3.12 Fracture analyses between depths 3385.719 – 3394.863 m.

The single fracture D in Figure 3.13 is at depth 2716.378 m in a formation with 72.5% sandstone, 27.1% shale content and 0.4% porosity. The log data show that the very shallow resistivity log MSFL reads a low value of about 13.848 Ωm. The Poisson's ratio ΔTs/ΔTc is higher than the formation with 1.73, and the photoelectric absorption is about 3.201 barns/ê. Bulk density log is not significantly changed by this single fracture.

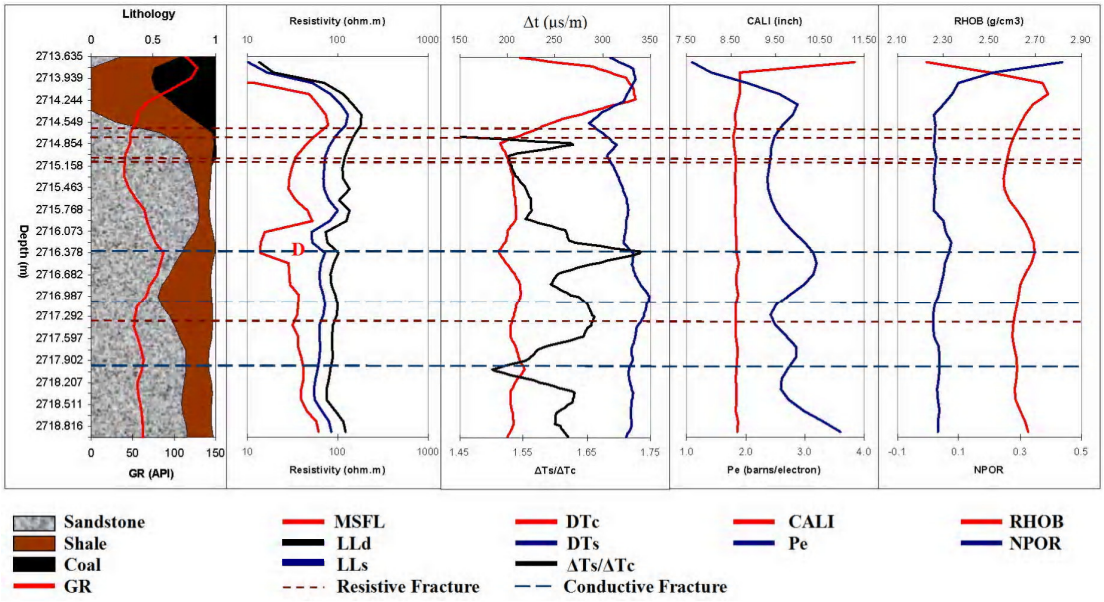

Figure 3.13 Fracture analyses between depths 2713.635 – 2718.816 m.

The single fracture E in Figure 3.14 is at depth 2751.430 m where the formation is 82.8% sandstone, 11.6% shale content and has a porosity of 5.6%. The very shallow resistivity tool MSFL reading is about 82.348 Ωm, which is in contrast to the shallow resistivity reading LLs with 64.465 Ωm and 97.502 Ωm for the deep resistivity log LLd. Both P– and S–wave slowness are increasing to 233.720 µs/ft and 352.600 µs/ft, respectively, but the Poisson's ratio ΔTs/ΔTc is reduced to 1.450. The photoelectric absorption is not changed significantly by this single fracture but the bulk density log shows a very low reading result with 1.85 g/cm^3 and neutron porosity is about 0.2.

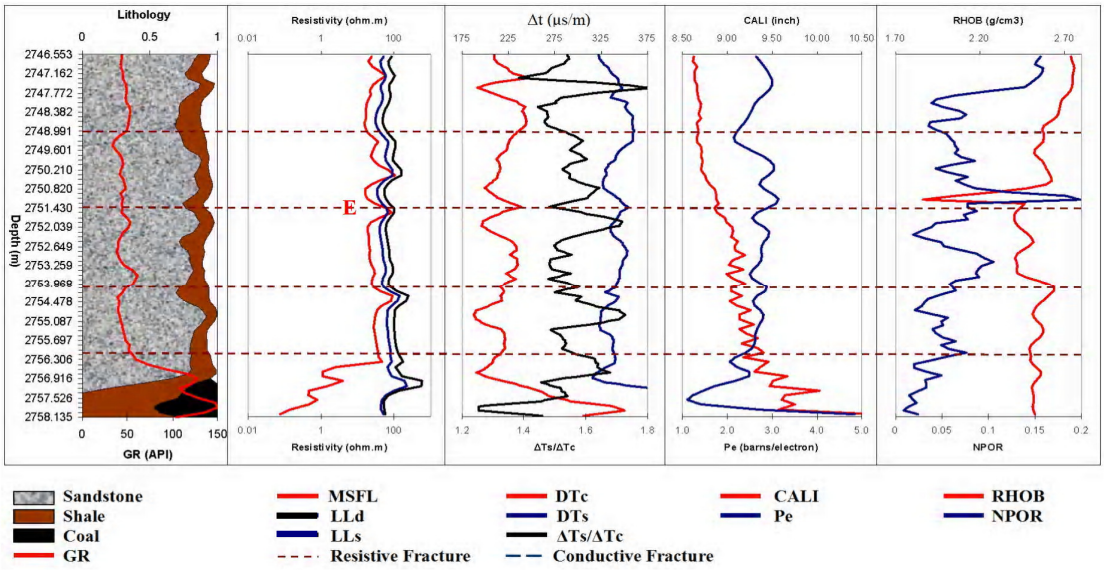

Figure 3.14 Fracture analyses between depths 2746.553 – 2758.135 m.

In Figure 3.15 the single fracture F at a depth of 2830.068 m is in a formation with 82.3% sandstone, 14.7% of shale and a porosity of 3.0%. The MSFL reading very low resistivity with 3.738 Ωm, LLs is about 66.45 Ωm, and LLd is about 76.887 Ωm. The compressional and shear wave slownesses are 202.093 μs/m and 334.000 μs/m; both are not significantly affected by this fracture. However, the Poisson's ratio ΔTs/ΔTc shows a higher value with 1.68. The photoelectric absorption is not affected by this single fracture but the bulk density show a lower value is 2.516 g/cm^3.

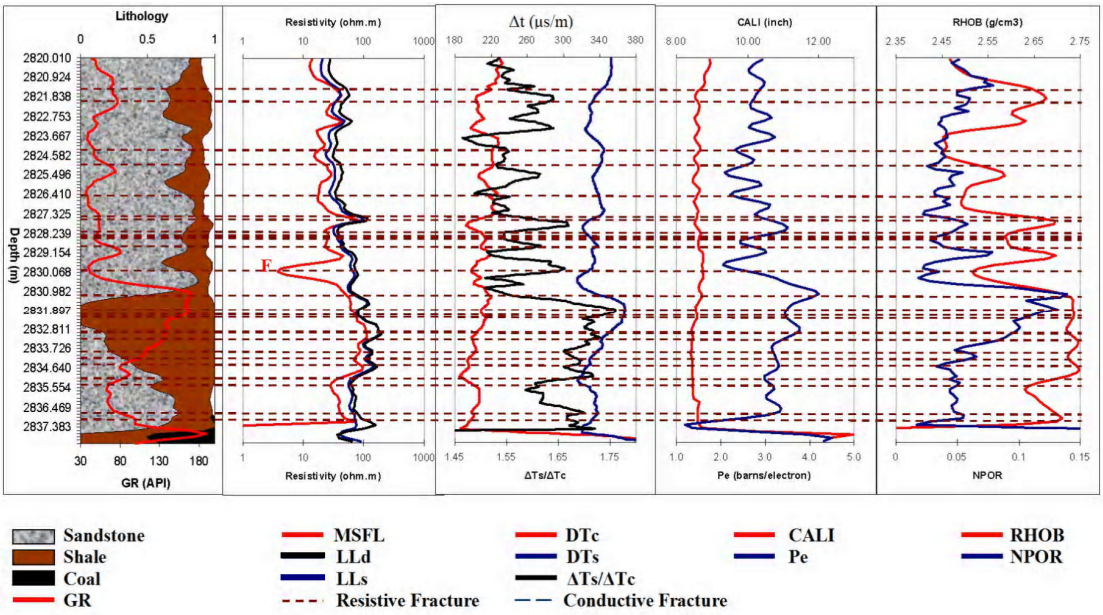

Figure 3.15 Fracture analyses between depths 2820.010 – 2837.383m.

In the depth interval shown in Figure 3.16 many fractures are detected by the FMS, but not significantly changed the conventional logging data. One interesting fracture (fracture R) is at depth 2722.820 m where the lithology is sandstone (76.8%), shale (19.8%) with a porosity of 3.4%. The ΔTs/ΔTc is about 1.61, which is higher than the baseline related to the fracture–free formation. However, the same effect can be seen at depth 2721.900 m where the FMS did not detect any fracture.

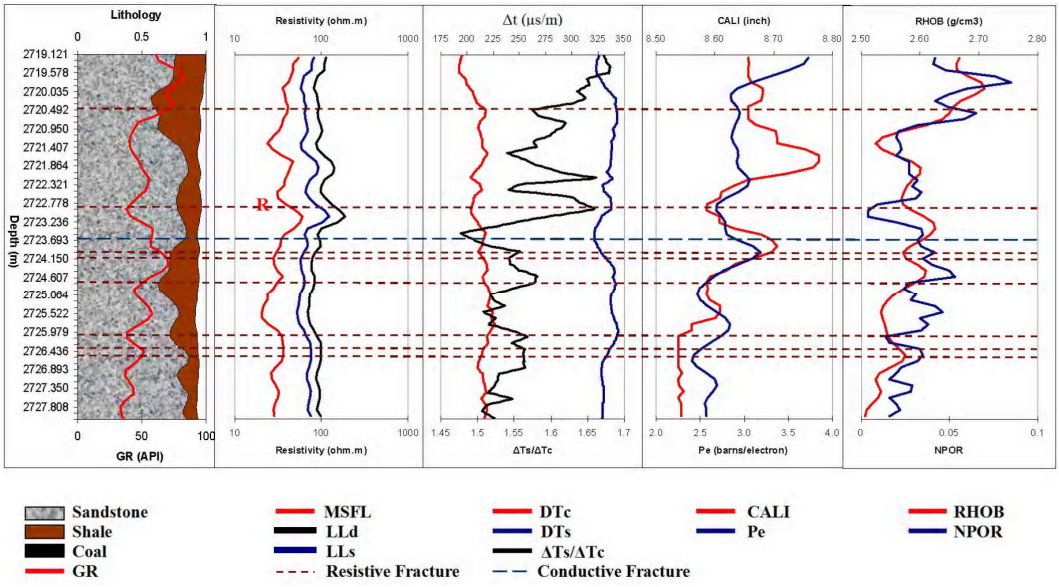

Figure 3.16 Fracture analyses between depths 2719.121 – 2727.808 m.

The single fracture M (Figure 3.17) is at a depth of 2793.560 m where the lithology is 76.9% sandstone, 13% shale with 10.1% porosity. The resistivity log close above this fracture shows with MSFL 2.831 Ωm, LLs 9.571 Ωm, and LLd 16.448 Ωm. The photoelectric absorption is about 3.461barns/ê. At depth 2804.410 m is the lithology 85.8% sandstone, 6.0% shale with 8.2% porosity. Single fracture plane N is indicated by a photoelectric absorption value of about 3.524barns/ê.

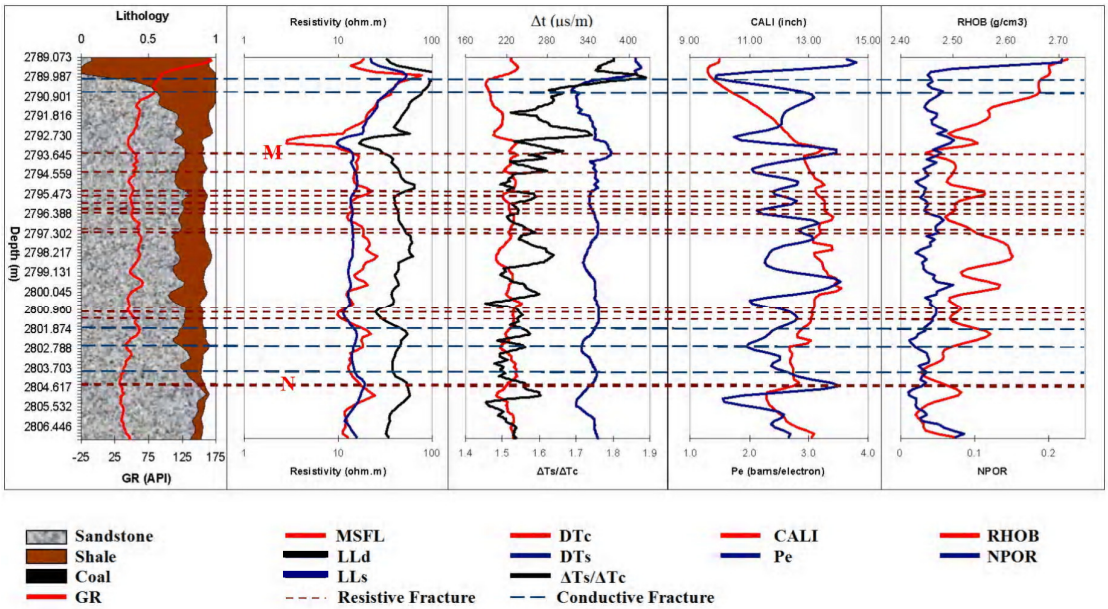

Figure 3.17 Fracture analyses between depths 2789.073 – 2806.446 m.

Single fracture plane O (see Figure 3.18) is at 2810.560 m. The lithology is 70.3% sandstone, 28.6% shale with 1.1% porosity. The fracture plane does not a clear response to many conventional logging data but significantly to Poison's ratio ΔTs/ΔTc, which is about 1.75.

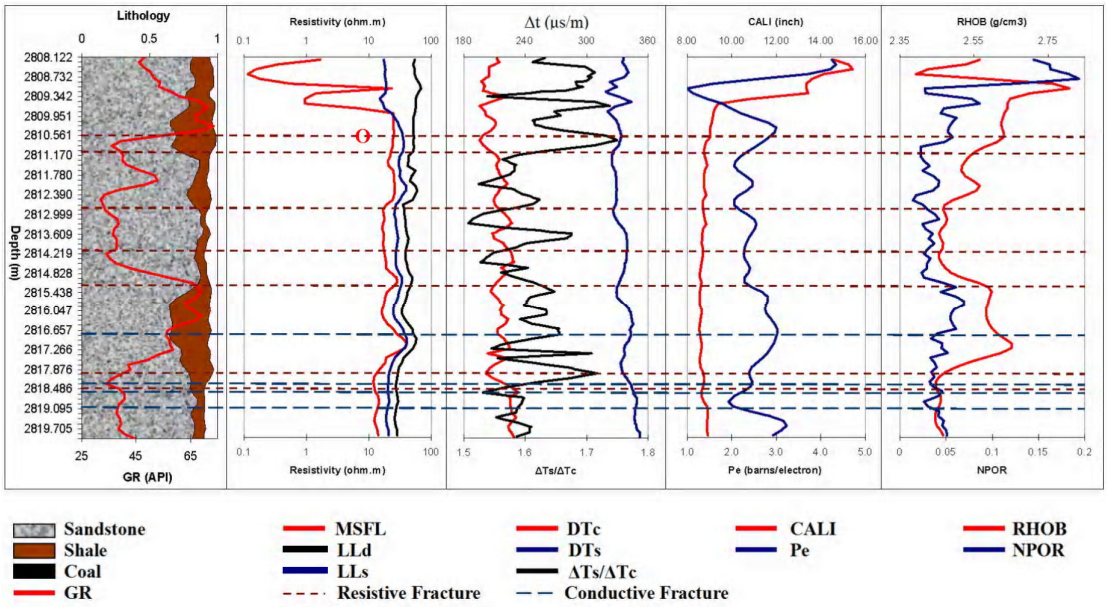

Figure 3.18 Fracture analyses between depths 2808.122 – 2819.705 m.

Single fracture plane Q in Figure 3.19 is at depth 3167.090 m where the lithology is 55.9% sandstone, 36.2% shale with 7.9% porosity. This fracture has a good response to compression slowness, about 233.064 μs/m, which is much larger than the data above and below. MSFL reading for this fracture is about 16.657 Ωm, LLs is 43.973 Ωm, and LLd is 53.911 Ωm; all show some clear decrease.

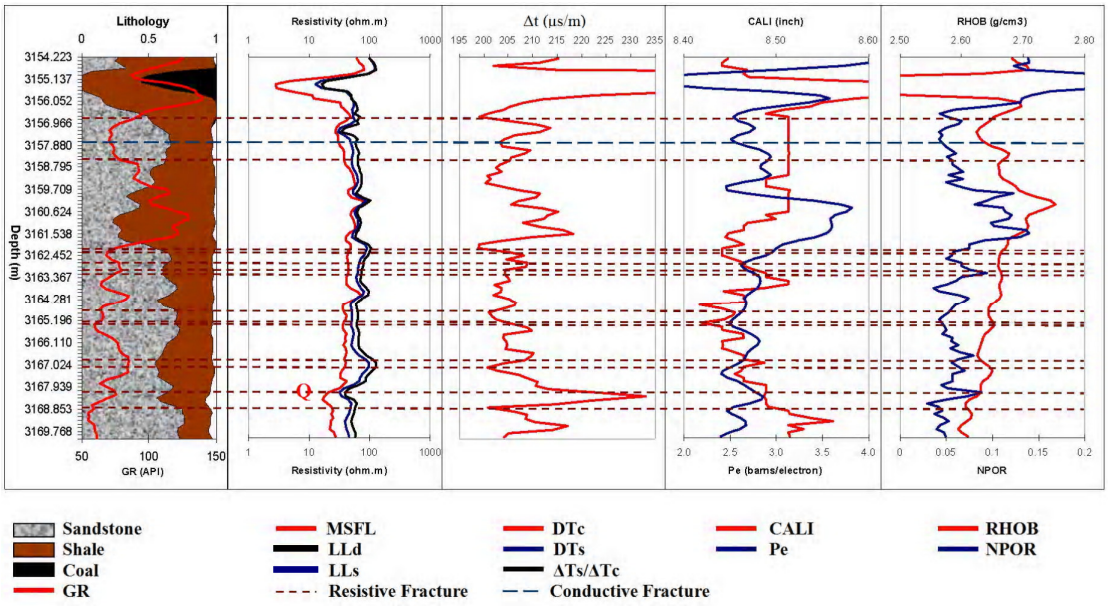

Figure 3.19 Fracture analyses between depths 3154.223 – 3169.768 m.

Single fracture plane R in Figure 3.20 is at depth 3266.650 m where the lithology is 55.8% sandstone, 39.0% shale with 5.2% porosity. This fracture plane has a good response to compression slowness of 226.897 µs/m, a value that is much higher then the above and below. The caliper log shows a larger average borehole diameter with 8.561 inch. The bulk density is reduced to 2.597 g/cm^3, while the neutron porosity shows a higher value with 0.113.

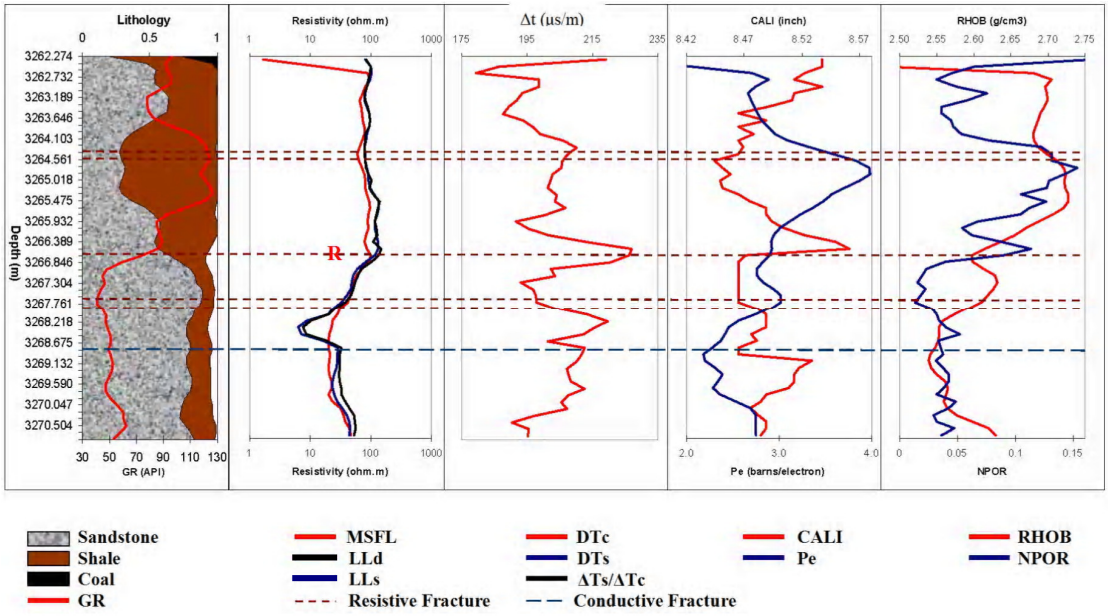

Figure 3.19 Fracture analyses between depths 3262.274 – 3270.504 m.

Single fracture T in Figure 3.21 is at depth 3325.880 m where the lithology is 62.0% sandstone and 38.0% shale. The MSFL resistivity log reading decreases due to the fracture down to 31.676 Ωm, whereas LLs with 57.644 Ωm and LLd with 74.730 Ωm seems to be unaffected. Other logs do not show any significant change.

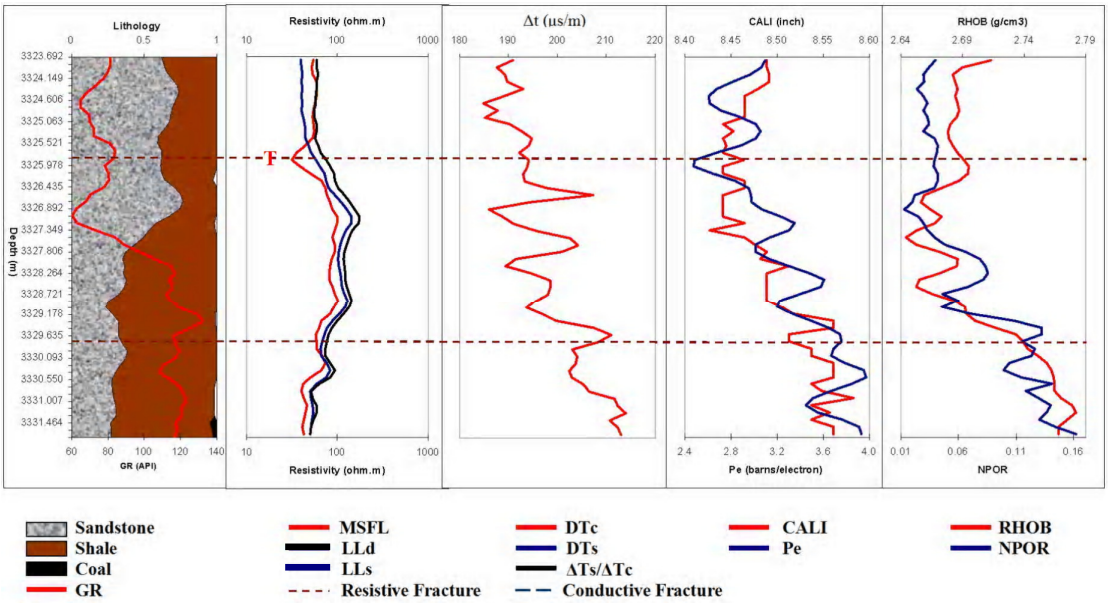

Figure 3.21 Fracture analyses between depths 3323.692 – 3331.464 m.

Single fracture W in Figure 3.22 is at a depth of 3427.800 m where the lithology is composed of sandstone (53.2%) and shale (46.8%). This single fracture response to the resistivity log with a lower MSFL reading of 40.255 Ωm, whereas LLs with 62.823 Ωm and LLd with 76.842 Ωm seems unaffected. The compressional slowness reading increases to about 199.803μs/m.

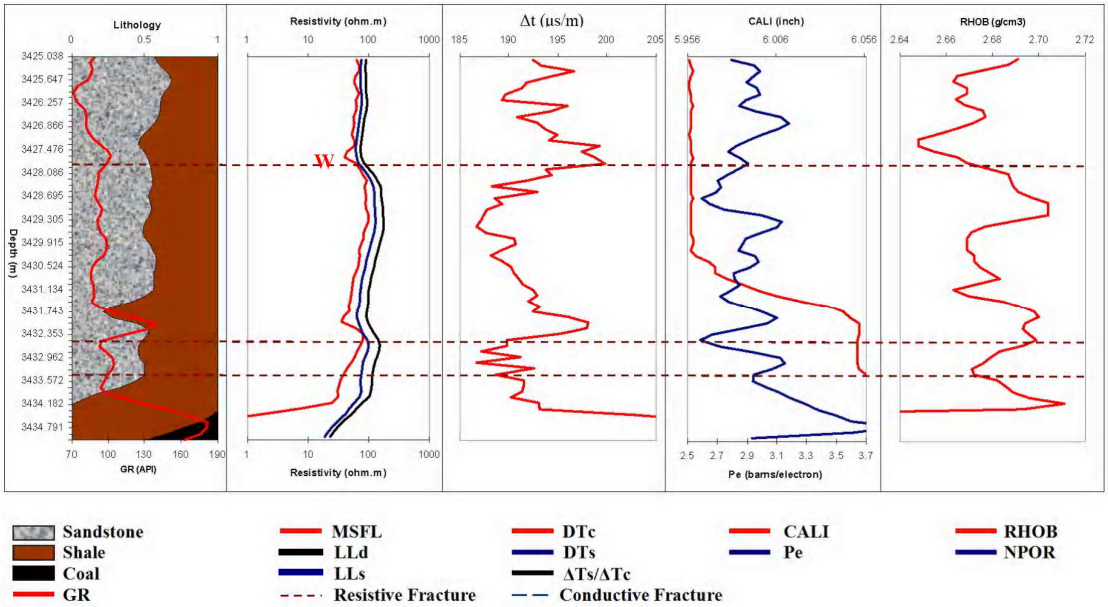

Figure 3.22 Fracture analyses between depths 3425.038 – 3434.791 m.

Single fracture S in Figure 3.23 is at 3626.250 m depth where the lithology is composed of sandstone (55.8%) and shale (44.2%). This single fracture does not have a significant response to most of the logging tools, except the compression slowness that is significantly higher with 192.257 µs/m.

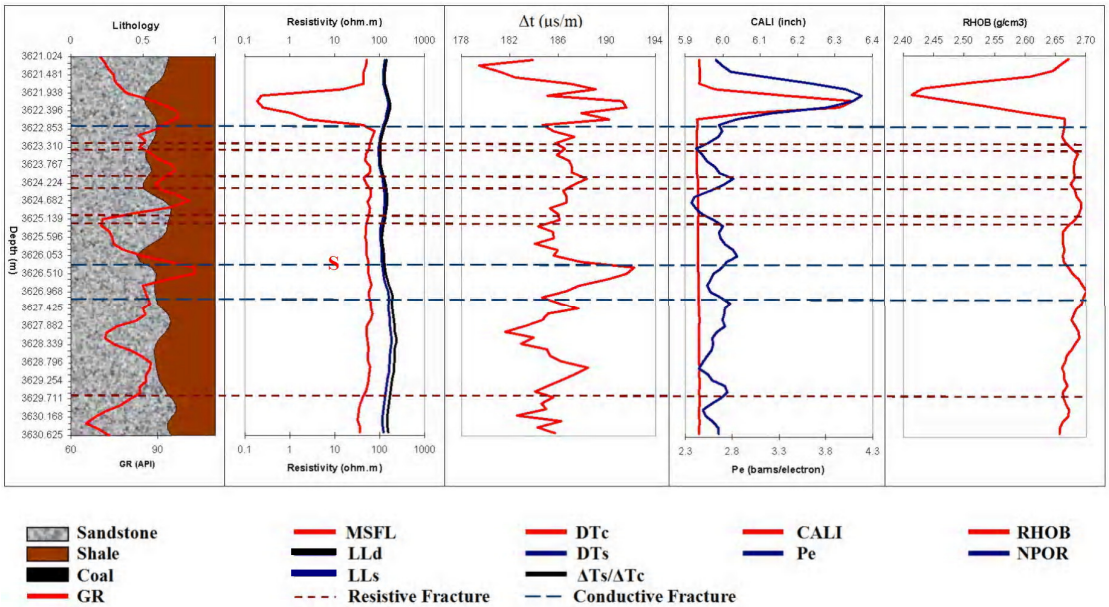

Figure 3.23 Fracture analyses between depths 3621.024 – 3630.625 m.

Single fracture T in Figure 3.24 is at depth 3687.510 m where the lithology is composed of sandstone, 29.3%, and shale, 70.7%. This single fracture has a good response to the MSFL resistivity log with a reading lower than above and below 34.526 Ωm. LLs with 118.571 and LLd with 123.609 Ωm are not affected by the fracture.

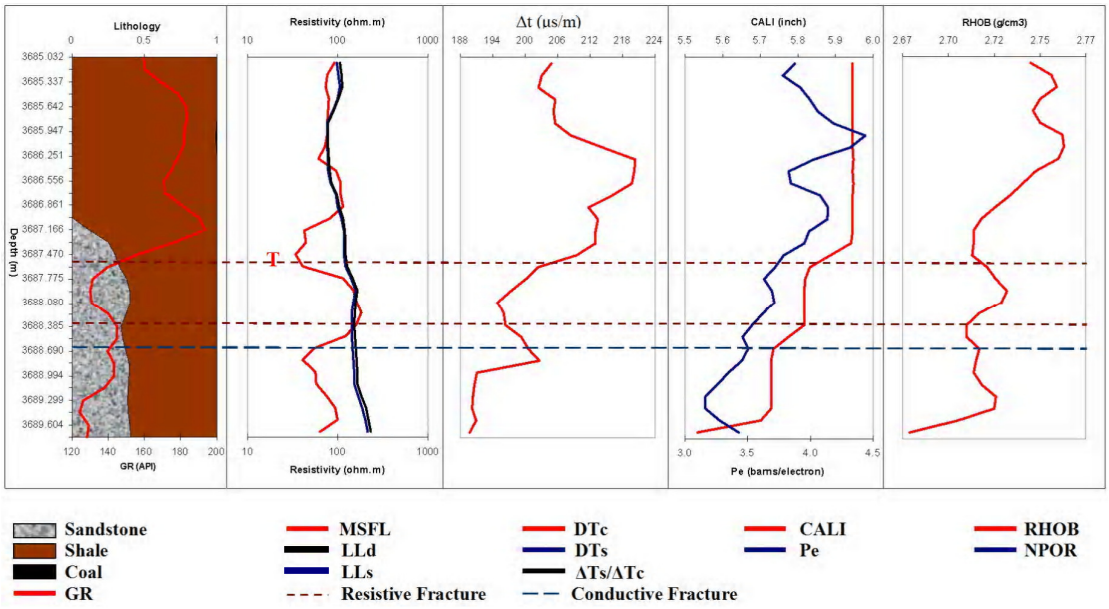

Figure 3.24 Fracture analyses between depths 3685.032 – 3689.604 m.

3.4.2 No response to single fracture

In the data logging available not all single fractures responded to the conventional logging measurements. In Figure 3.25 a conductive single fracture was measures by FMS at a depth of 3665.460 m, but there is not response to any conventional logging data.

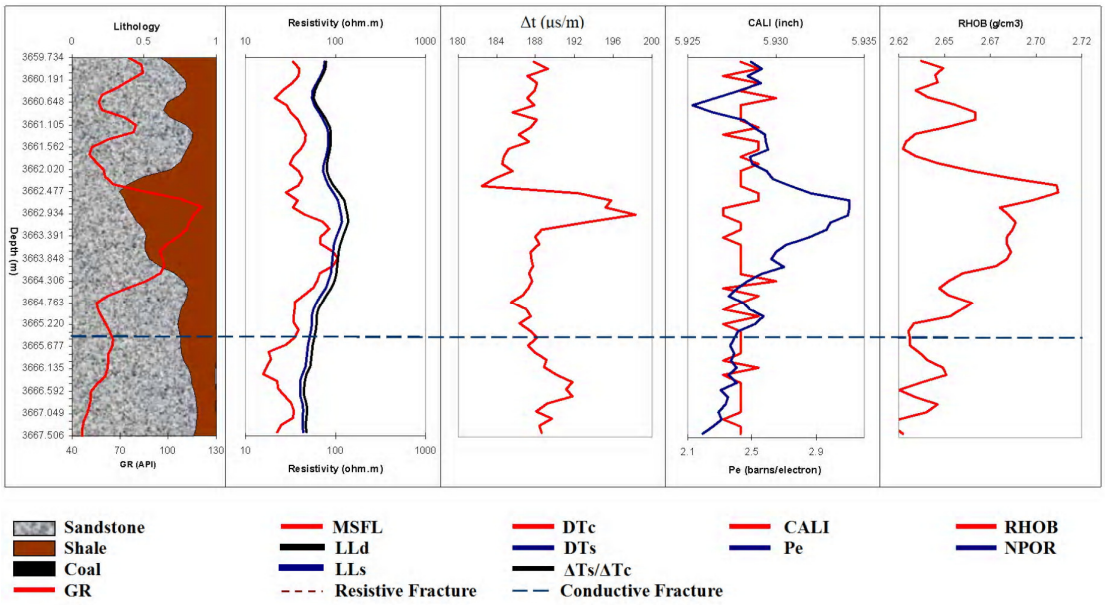

Figure 3.25 Fracture analyses between depths 3659.734 – 3667.506 m.

A resistive single fracture was determined by the FMS measurements at 3590.210 m depth, see Figure 3.26, but there is not response in the conventional logging data.

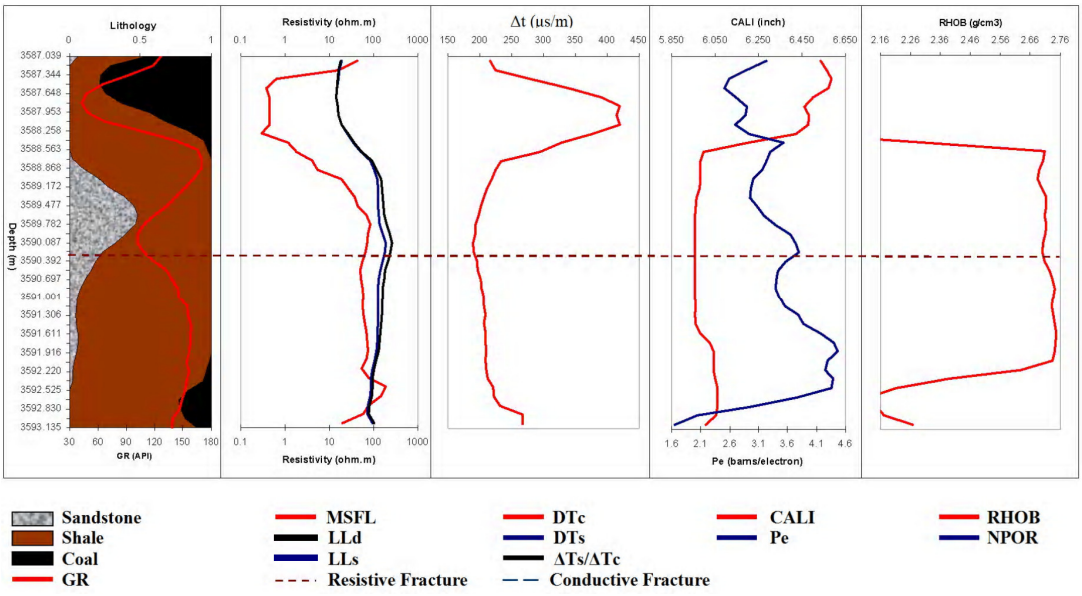

Figure 3.26 Fracture analyses between depths 3587.039 – 3593.135 m.

The FMS data show a resistive single fracture at 3513.860 m (see Figure 3.27), but there is not response seen in the conventional logging data.

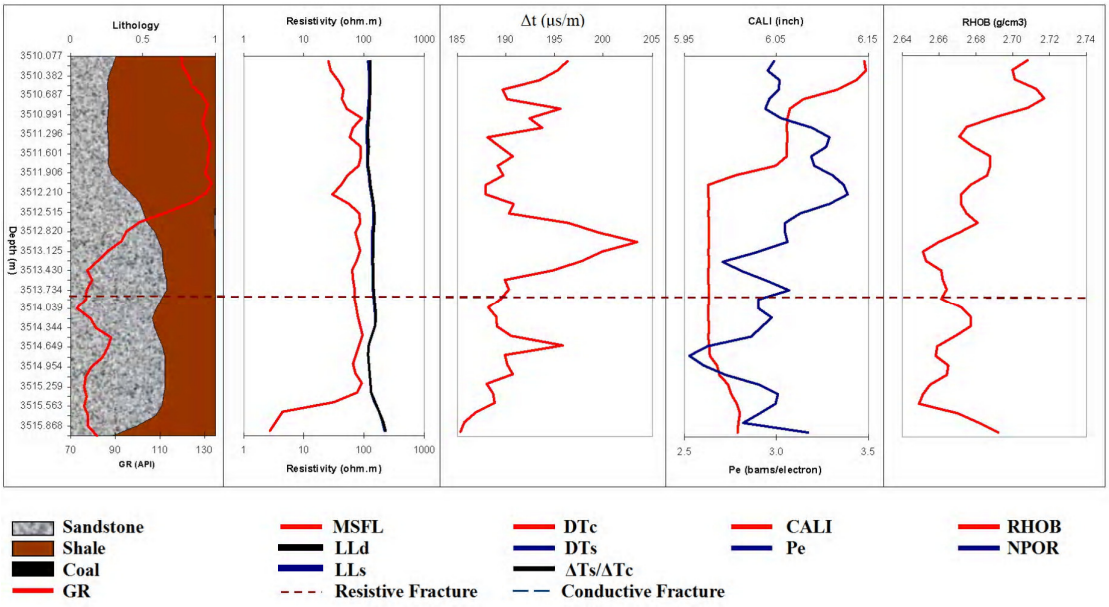

Figure 3.27 Fracture analyses between depths 3510.077 – 3515.868 m.

A conductive single fracture was determined by the Formation Microscanner at 3598.730 m (see Figure 3.28), but there is not response to conventional logging data.

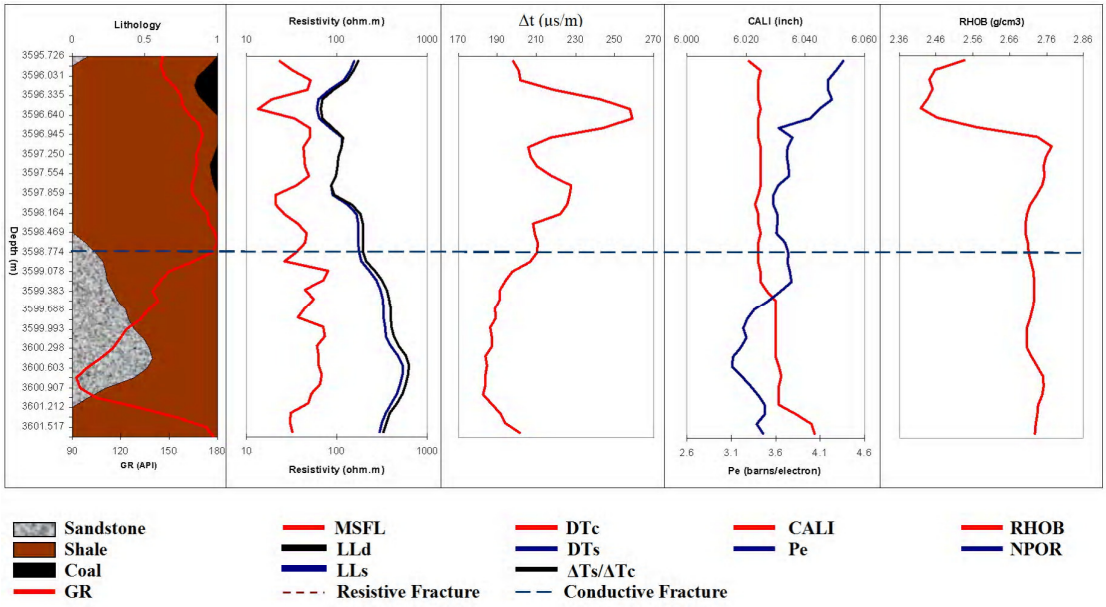

Figure 3.28 Fracture analyses between depths 3595.726 – 3601.517 m.

3.4.3 Fractures zone response

Figure 3.29 shows a fracture zone with FMS and convention logging data between depth 3373.984 – 3385.566 m. Fracture zone G, where the formation is sandstone (72.3%) and shale (26.9%) with a porosity of 0.8% has a good response to many conventional logging data: very shallow resistivity log MSFL reads very low resistivity values of about 21.369 Ωm, as the pad loose contact to the borehole wall; shallow resistivity log LLs reading is about 57.071 Ωm, and 77.824 Ωm for deep resistivity log LLd reading. Compressional wave slowness is higher, about 201.28 µs/m or 60.993 µs/ft, due to the unconformity of the formation caused by the fractures. The photoelectric absorption is about 3.193 barns/ê caused by the mud where barite is the main component filled into the fractures. The bulk density is lower than the normal trend with 2.60 g/cm^2.

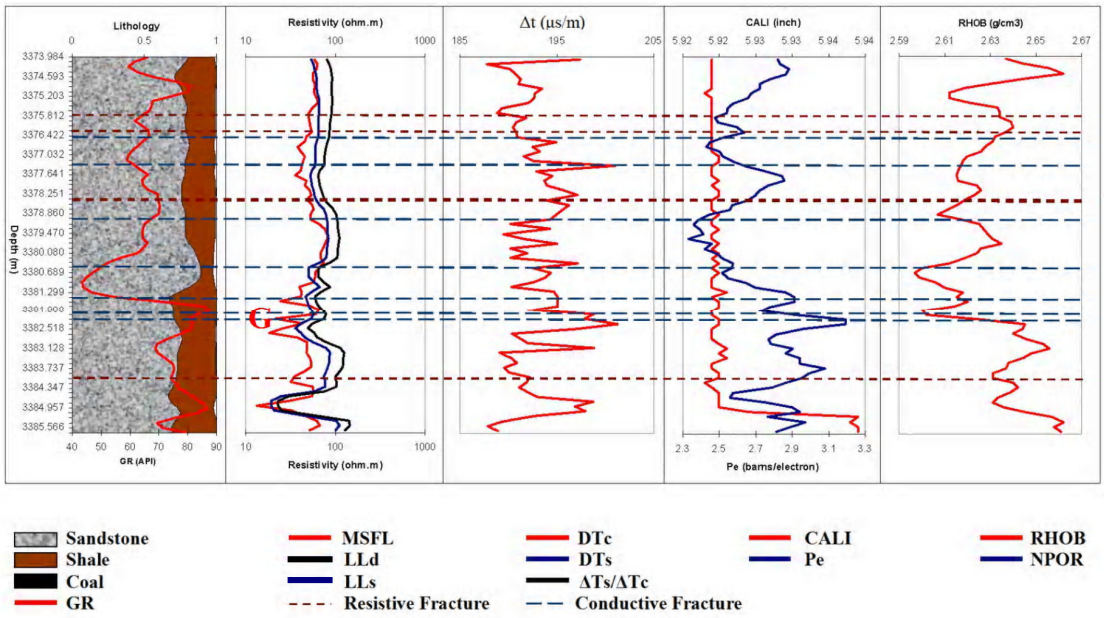

Figure 3.29 Fracture analyses between depths 3373.984 – 3385.566 m.

Fracture zone H in Figure 3.30 at depth around 3203.905 where the formation is sandstone (70.0%) and shale (23.7%) with a porosity of 6.3%. The MSFL reading is about 7.23 Ωm, LLs is 17.622 Ωm, and LLd is 19.943 Ωm, all are lower than the data above an below. The compressional wave slowness is 215.472 μs/m, and therefore higher than the surrounding formation. The photoelectric absorption is 2.919 barns/ê and the bulk density is 2.603 g/cm^2. NPOR log shows that the hydrogen index of this fracture zone is 0.063.

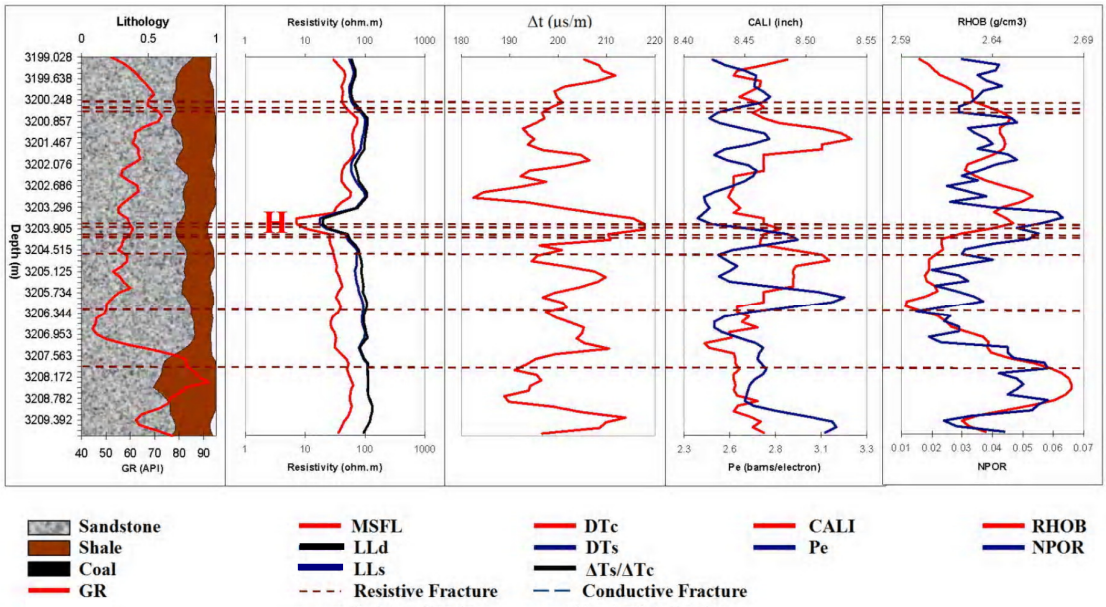

Figure 3.30 Fracture analyses between depths 3199.028 – 3209.392 m.

In Figure 3.31 fracture zone I is in a formation of sandstone (73.6%) and shale (24.4%) and a porosity of 2%. The MSFL reading is 4.023 Ωm, LLs is 17.917 Ωm, and LLd is 17.195 Ωm, all are lowered by the fracture presence. The compressional slowness is not significant changed by this fracture zone, but the photoelectric absorption is good evidence with a higher reading of about 3.26 barns/ê and a bulk density of 2.615 g/cm^2.

Fracture zone J is in a formation of 71.5% sandstone and 28% shale and about 0.5% porosity (Figure 3.31). This fracture zone shows a MSFL reading of about 10.937 Ωm, LLs is about 19.525 Ωm, and LLd is about 23.327 Ωm, all lowered by the fracture zone presence. This fracture zone has not a good response with both the compressional slowness and bulk density. The photoelectric absorption has a good response to this zone by showing a higher value of 3.415 barns/ê.

Fracture zone K has a lithology content of 72% sandstone and 27.7% shale and 0.3% porosity (Figure 3.31). Resistivity readings for this zone are 11.456 Ωm for MSFL, 18.806 Ωm for LLs, and 24.088 Ωm for LLd, all of them lower than the baseline Compressional slowness and bulk density are not significant affected by this fracture zone, but photoelectric absorption is. Photoelectric absorption for this fracture zone is with 3.228 barns/ê significant higher.

The formation of fracture zone L has 78.1% sandstone, 19.7% shale and 2.2% porosity (Figure 3.31). MSFL reading is 15.798 Ωm, LLs 16.051 Ωm, and LLd 21.549 Ωm; all three are lower, with LLs and LLd significant lower. Compressional slowness has a good response to this fracture zone by reading a significant higher value of 302.26 µs/ft. Photoelectric absorption also shows an increase with 2.896 barns/ê and the bulk density is only slightly lower with 2.596 g/cm^2.

Fracture zone M is in a formation with 73.2% sandstone content, 25.6% shale content and 1.2% porosity (Figure 3.31). MSFL reading is about 8.085 Ωm and with this quite significantly lower, LLs is 14.289 Ωm, and LLd is 19.976 Ωm, both also lower than the values above and below. Compressional slowness is not significant different for this fracture zone. Photoelectric absorption shows a higher value with 3.573 barns/ê and the bulk density is also increased with 2.683 g/cm^2.

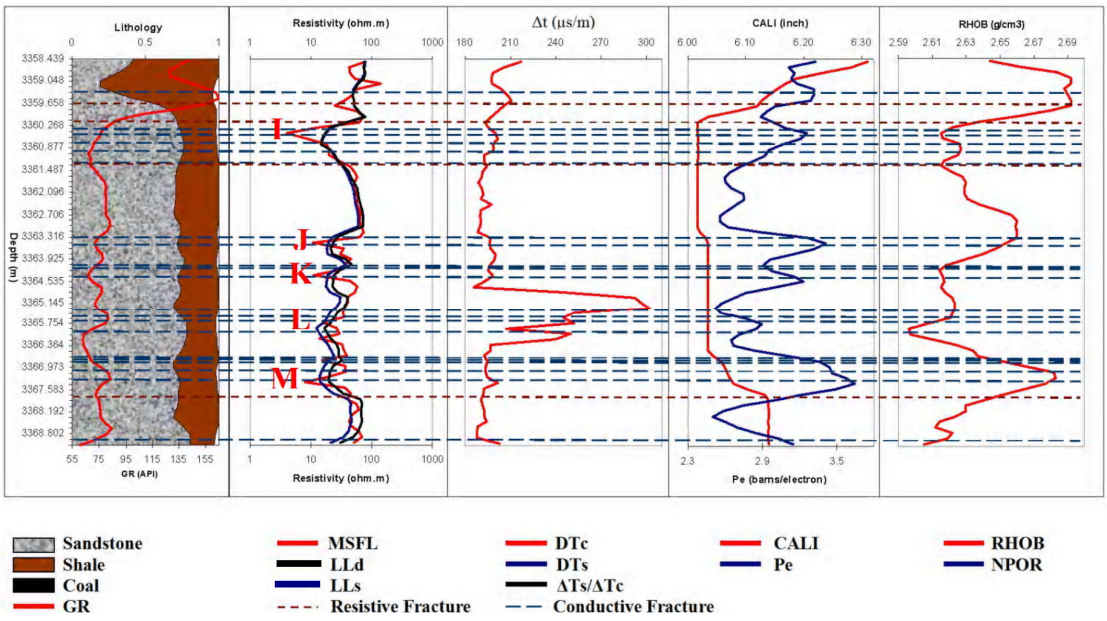

Figure 3.31 Fracture analyses between depths 3358.439 – 3368.802 m.

Figure 3.32 shows the fracture zone N, where the formation includes sandstone (49.6%) and shale (40.9%) with a porosity of 9.5%. MSFL reading is significantly lower with 21.775 Ωm, LLs with 30.692 Ωm and LLd is 36.926 Ωm also lower. Compressional wave slowness and bulk density are not significance changed

by this fracture zone. Photoelectric absorption provides here good fracture evidence by reading higher value with about 3.059 barns/ê.

Fracture zone O is in a formation with 64.7% sandstone and 32.9% shale and has 2.4% porosity (Figure 3.32). MSFL reading is 55.352 Ωm and by this higher. The FMS indicates here a resistive and conductive fracture; however the MSFL reading should be in both cases lower (see Chapter 2). LLs reading is 25.562 Ωm and LLd 29.535 Ωm, both slightly lower. Compressional slowness has a good response to this fracture zone by reading a significant higher value of 209.4 µs/m. Photoelectric absorption is about 2.932 barns/ê and by this also increased. Bulk density is not significantly changed by this fracture zone.

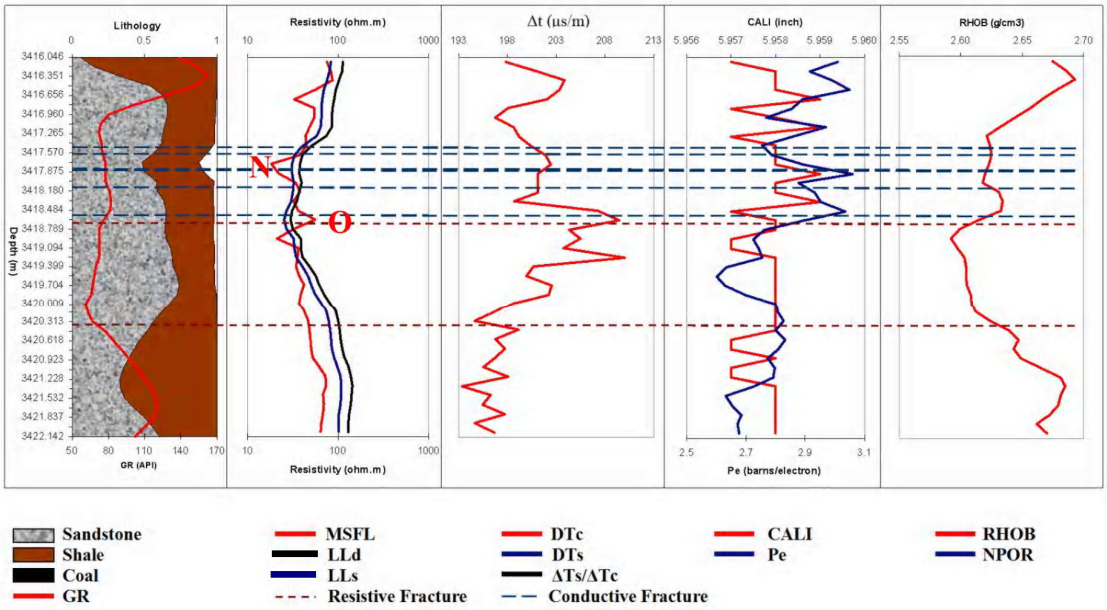

Figure 3.32 Fracture analyses between depths 3416.046 – 3422.142 m.

Figure 3.33 shows the fracture zone P in a formation of sandstone (18.2%) and mainly shale (81.8%) with no porosity (0%). MSFL reading is significant lower with 6.76 Ωm; LLs with 56.717 Ωm and LLd with 83.415 Ωm are also lower. Compressional slowness is with 210.165 µs/m higher, but the baseline is also higher. Bulk density and photoelectric absorption are not significantly changed by this fracture zone.

Fracture zone Q is at depth 3409.645 m where the formation is sandstone (55.4%) and shale (44.6%) with no porosity (0%). The MSFL reading is with 5.585 Ωm significantly lower, whereas LLs with 24.222 Ωm and LLd with 31.593 Ωm are lower but not so significantly. The compressional wave slowness is significantly higher with 200.323µs/m. The photoelectric absorption is slightly higher with 4.132barns/ê, but does not really show a peak. The bulk density is with 2.667 g/cm^2 slightly higher.

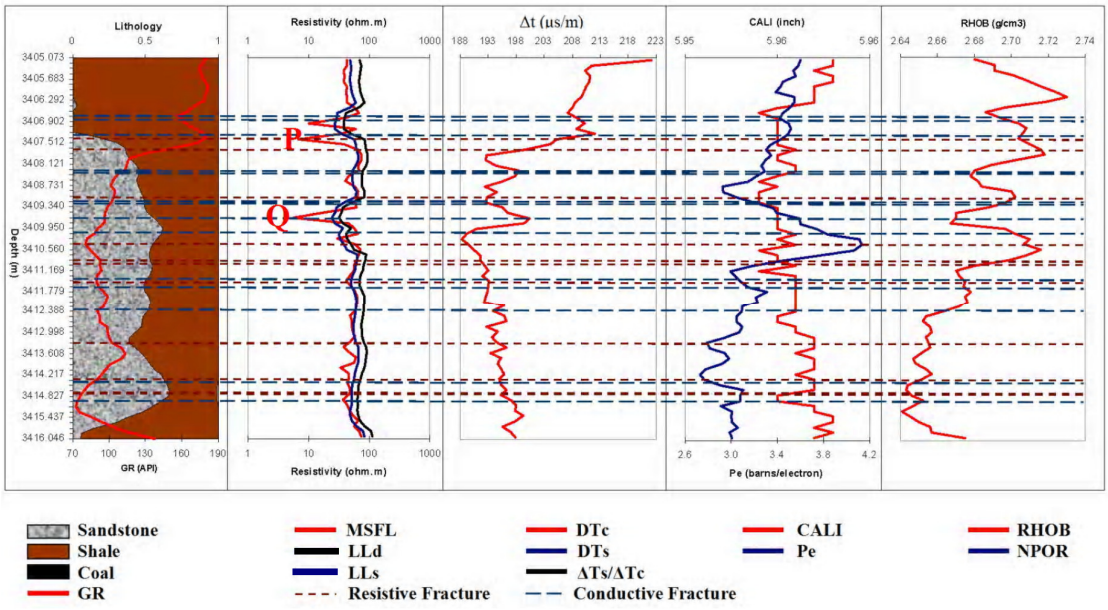

Figure 3.33 Fracture analyses between depths 3405.073 – 3416.046 m.

Fracture zone P in Figure 3.34 is in a formation mainly within shale (91.9%) and 3% sandstone, and a porosity of 5.1%. The compressional slowness for this fracture is about 235.065µs/m and by this higher than the formation above and below. The photoelectric absorption value is 3.956barns/ê, which is higher, but not significantly higher than the formation below and above.

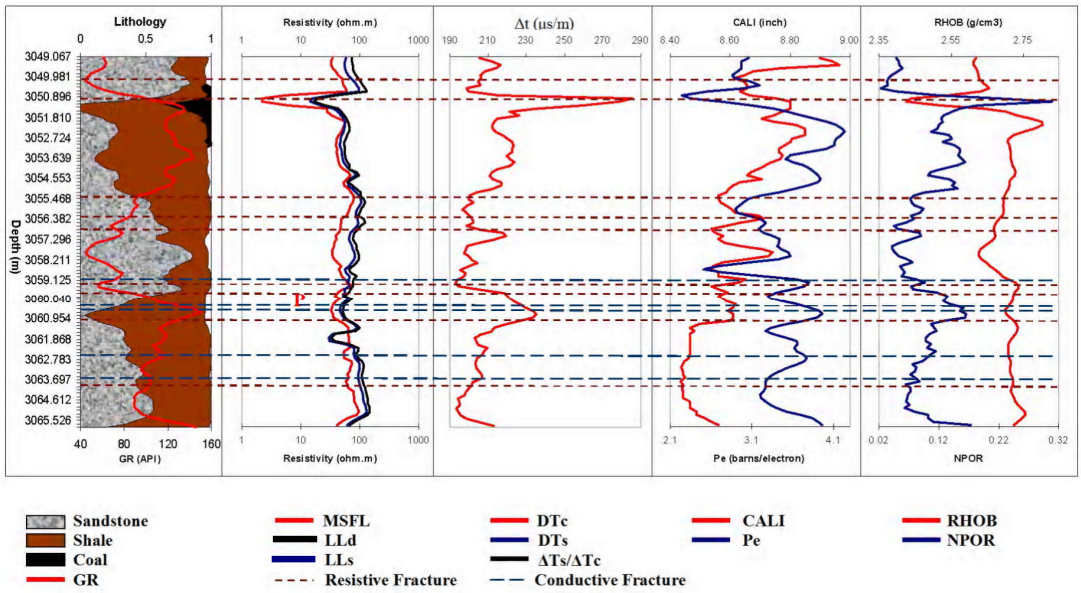

Figure 3.34 Fracture analyses between depths 3049.067 – 3065.526 m.

Fracture zone S in Figure 3.35 is at a depth of 3313.430 m to 3313.500 m which a lithology content of 74.0% sandstone and 20.9% shale and 5.1% porosity. This fracture zone has affected the resistivity log, with all three logs significantly lower; MSFL is 4.536 Ωm, LLs is 12.230 Ωm, and LLd is 19.829 Ωm. The compressional slowness shows a value of up to 231.721μs/m, by this also significant higher. The bulk density shows a lower value with 2.612 g/cm^3.

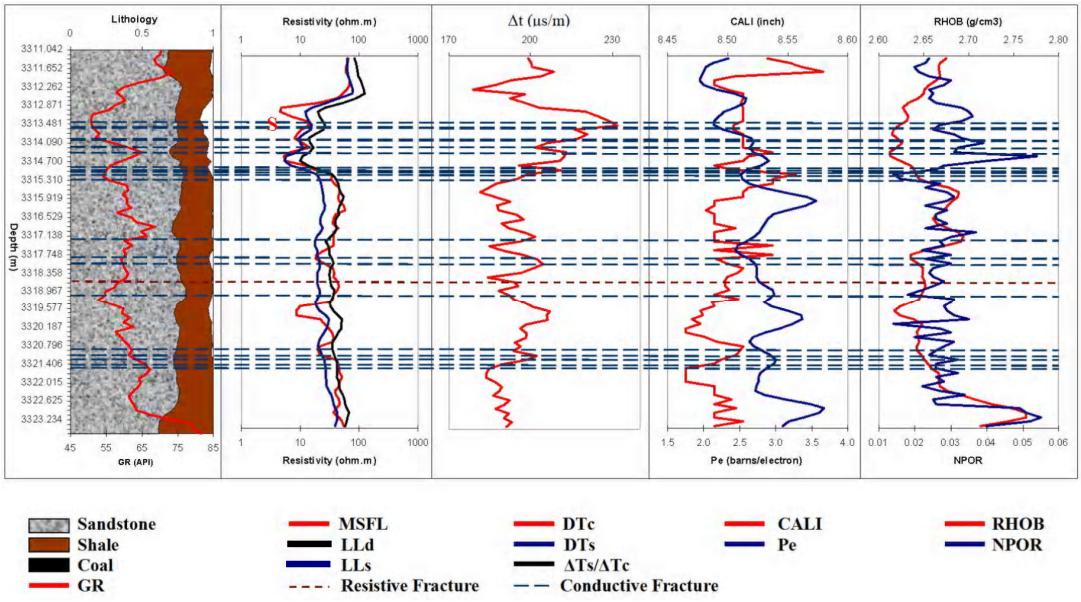

Figure 3.35 Fracture analyses between depths 3311.042 – 3323.234 m.

Fracture zone U in Figure 3.36, at a depth of 3417.810 m, is in a formation with a lithology of 48.3% sandstone and 39.3% shale and a porosity value of 12.4%. Only the resistivity log react to this fracture zone, mainly with a significant lower value of the MSFL reading, down to 18.398 Ωm. LLs is 31.093 Ωm and LLd is 37.782 Ωm, both lower but less significant.

In Figure 3.36 the fracture zone V is at depth 3418.590 m and 3418.650 m, which a lithology of 64.7% sandstone and 32.9% shale and a porosity of 2.4%. The MSFL reading is with 55.352 Ωm slightly higher, whereas the LLs with 25.562 Ωm, and LLd wit 29.535 Ωm are slightly lower. Compressional slowness also has a good response to this fracture zone by reading a higher value of 209.4 µs/m.

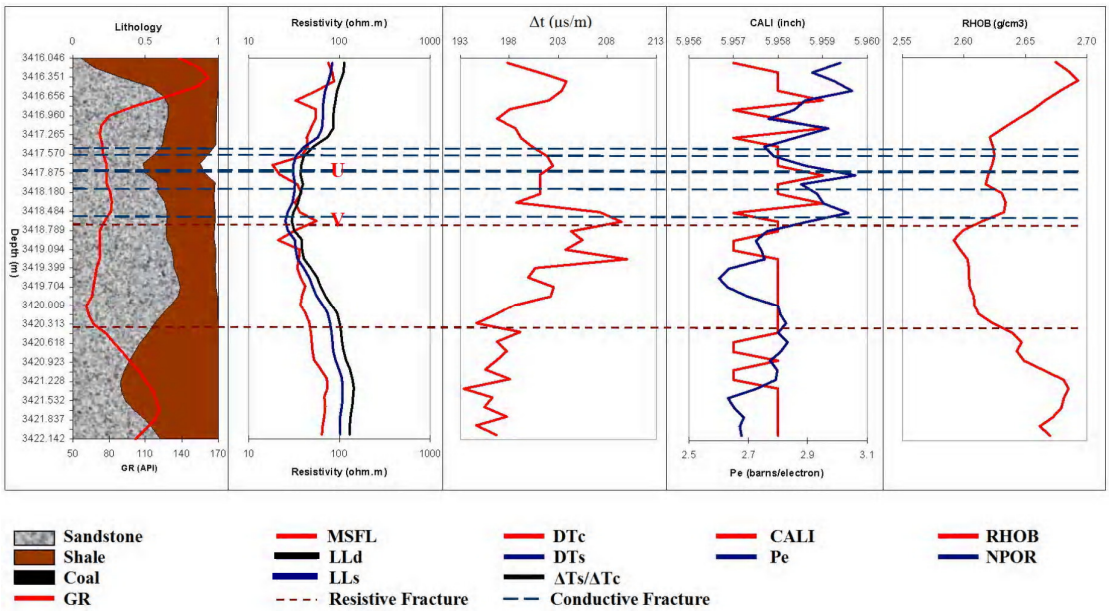

Figure 3.36 Fracture analyses between depths 3416.045 – 3422.142 m.

3.4.4 No response to fractures zone

Some fracture zones have been detected by the FMS tool but they are not seen by the conventional logging tools. In Figure 3.37 is fracture zone W, which is indicated as a conductive fractures; all logging data reading are not significantly changed by this fracture zone.

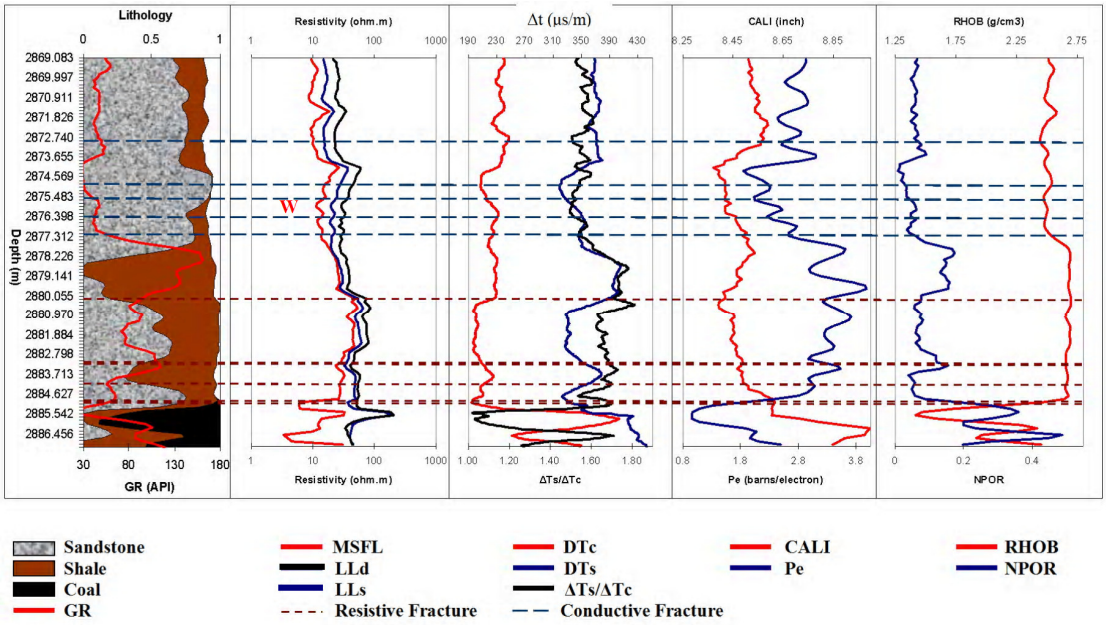

Figure 3.37 Fracture analyses between depths 2869.083 – 2886.456 m.

Fracture zone W in Figure 3.38 shows a resistive fracture zone, but there are not significant changes in any of the conventional logging data.

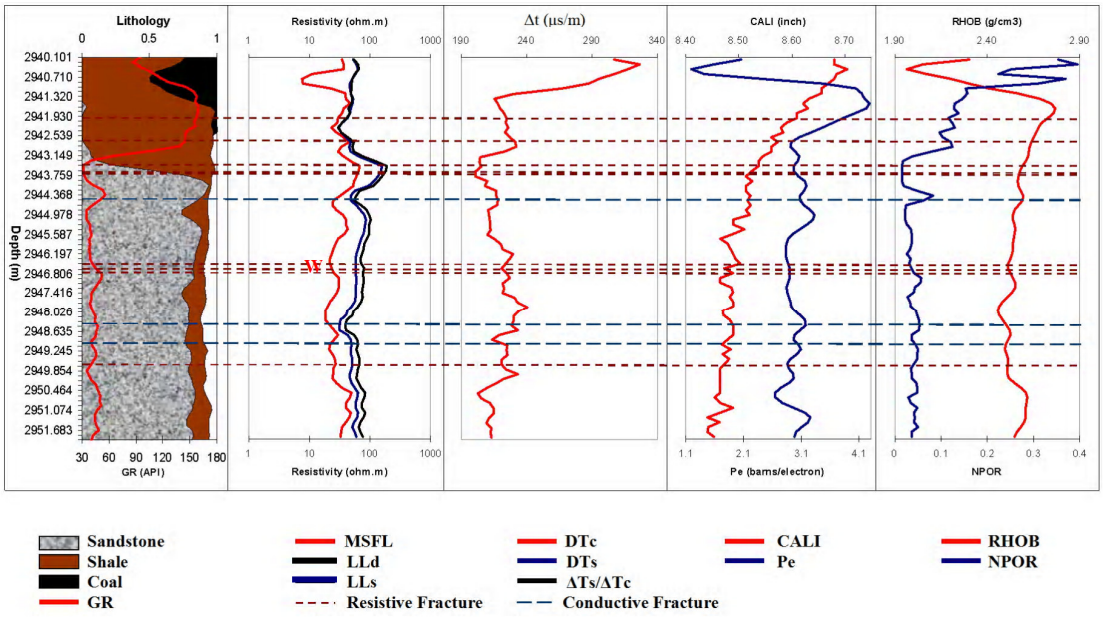

Figure 3.38 Fracture analyses between depths 2940.101 – 2951.683 m.

Fracture zone X (Figure 3.39) is according to the FMS data a resistive fracture zone, but there are not significant deviations in any of the conventional logging parameters.

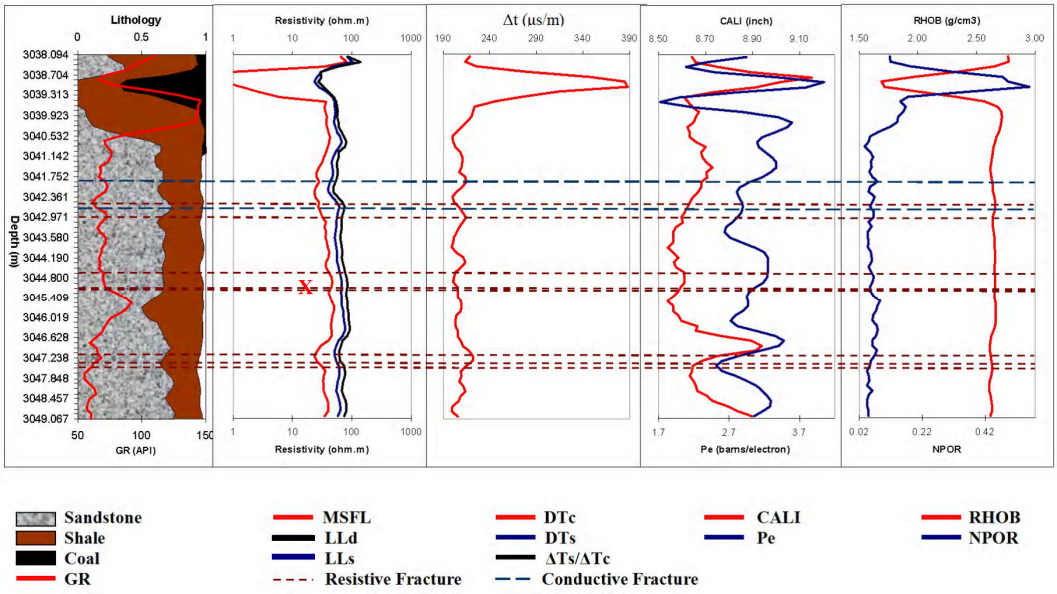

Figure 3.39 Fracture analyses between depths 3038.094 – 3049.067 m.

In Figure 3.40 fracture zone Y is designated as a conductive fracture zone, but also here there are no significant changes in the conventional logging data.

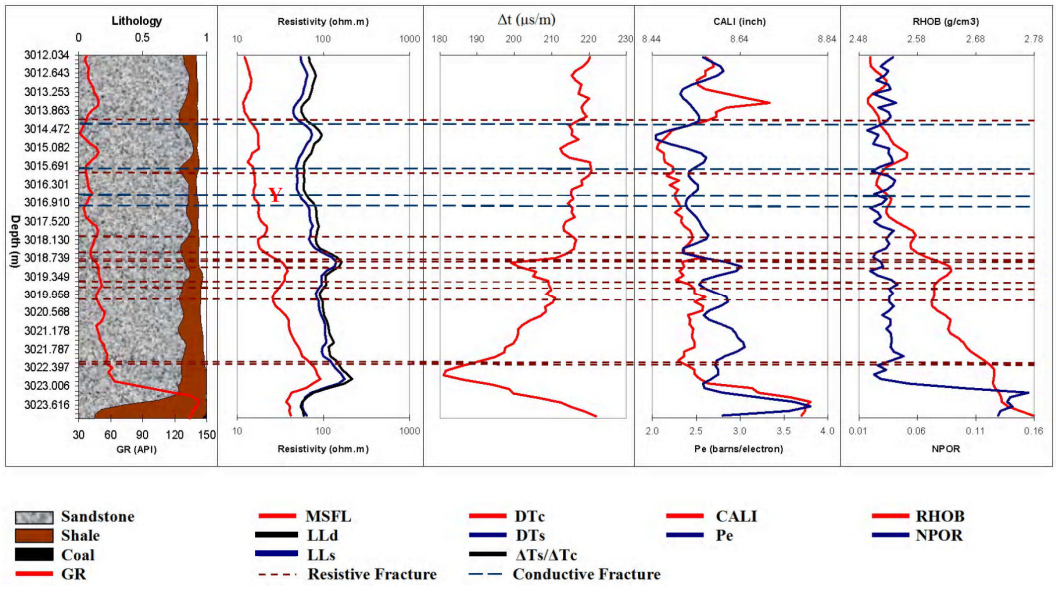

Figure 3.40 Fracture analyses between depths 3012.034 – 3023.616 m.

3.4.5 Fluid filled fracture response

The resistivity logs are used for formation resistivity determination, but fractures filled with conductive or resistive fluid maybe ignored by the resistivity tool, because the fractures are quite small compared with the bulk rock investigated by the current input of the resistivity tools. However, if the fracture aperture is large enough or in case the fluids in the fracture zone are filled with resistive fluids then the contrast between formation resistivity and fracture resistivity might be large enough to see in the LLs and LLd a deviation of the resistivity from the normal trend.

In Figure 3.41 fractures zone AA is a resistive fracture according to FMS data. The resistivity readings are all higher than the normal trend, with MSFL is 68.366 Ωm, LLs is 155.659 Ωm, and LLd is 190.275 Ωm. This fracture zone can be a mineral sealed fracture or closed fracture. Other tools do not show any significant change.

Fractures zone AB in Figure 3.41 comprises conductive fractures with all resistivity readings lower than normal trend, MSFL is 24.446 Ωm, LLs is 47.649 Ωm, and LLd is 54.810 Ωm. This fracture zone possible can be the opened fractures filled with water because the NPOR log reading shows a spike value of 0.082; this mean hydrogen index is higher than the normal trend.

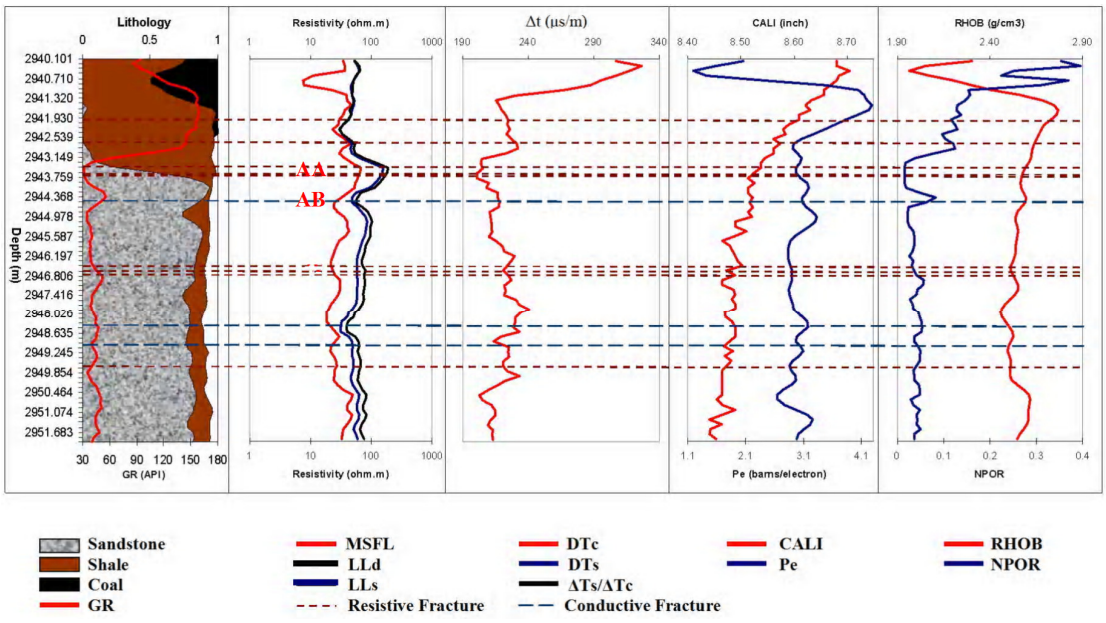

Figure 3.41 Fracture analyses between depths 2940.101 – 2951.683 m.

Fractures zone AC in Figure 3.42 is a resistive fracture because all the resistivity readings are higher than normal trend, with MSFL is 33.129 Ωm, LLs is 140.067 Ωm, and LLd is 161.452 Ωm.

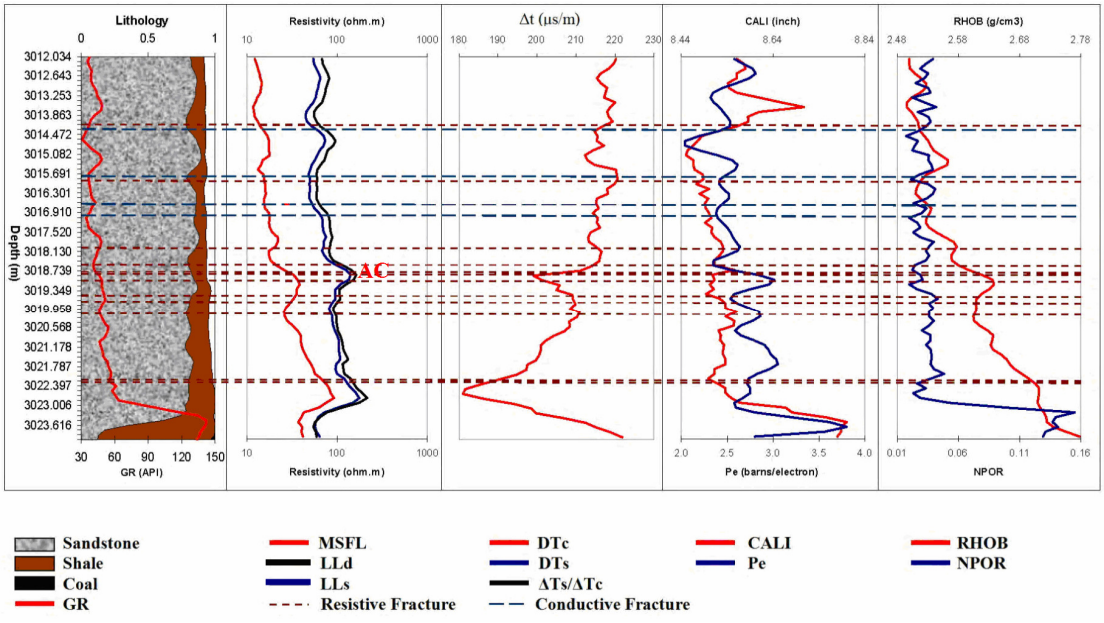

Figure 3.42 Fracture analyses between depths 3012.034 – 3023.616 m.

This fractures zone can be a mineralized fracture with a higher compaction; because the trend of the compressional slowness is lower than the normal trend with a reading of 199.038 µs/m.

CHAPTER 4

Discussion and conclusions

4.1 Discussion

Conventional well logs respond in some way to the presence of fractures as shown in Chapter 3. Several examples have been shown where some fractures respond to only one log and some respond to more than one. Each conventional log type with response to fracture is discussed in the following sections.

4.1.1 Fracture identification from bulk density log

In front of an open fracture or fracture zones the pad of the density tool contacts to the fracture and it reads a lower density as compared with the average values of 2.68 g/cm^3 for shale, 2.57 g/cm^3 for sandstone, and 1.59 g/cm^3 for coal (see Figure 4.1, 3.19, and 3.28).

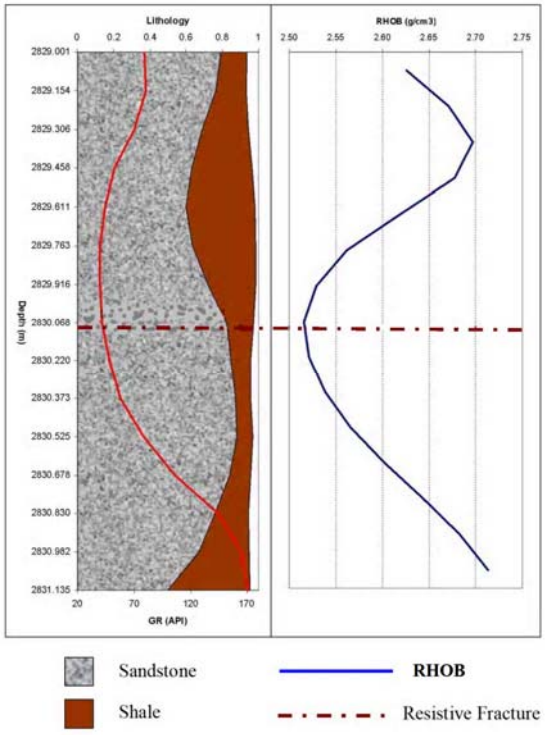

Figure 4.1 Fracture data from FMS and convention logging data between depths 2746.553 – 2758.135 m.

4.1.2 Fracture identification from resistivity logs

Three main resistivity tools, MSFL, LLs, and LLd tools are available for this research. MSFL indicates fractures by showing low resistivity spikes opposite open fractures or borehole break out in front of fractures (see Figure 4.2 and 4.3). From Figure 4.2, the width of the MSFL deviations is around half a meter. This is not the fracture aperture but it is the width of borehole break out opposite the fracture. In this research MSFL can detect the fracture with the same response in many fracture zones such as fracture plane A, B and C (see Figure 3.11 in Chapter 3). Even MSFL has been successfully used to aid fracture detection but it is not good to identify different type of fluids filled in hydraulic fracture, because of both resistive and conductive hydraulic fractures give the same response in the MSFL, see Figure 3.12 in Chapter 3. The results show that A, B are conductive fractures, C is a resistive fracture but all showing low resistivity spikes in the MSFL. For some fractures the fluids filled inside can be detected by using LLs and LLd.

Hydraulic opened fractures filled with fluids can be both resistive fractures if hydrocarbon flows inside and conductive fracture if brine filled inside. If the fracture aperture is large enough or in case the resistivity of the fracture zone and the resistivity of the fluid filled fracture has a larger contrast LLs and LLd might be able to provide a resistivity deviated from the normal trend (see Figure 4.2 and 4.3).

From Figure 4.3, a single fracture at depth 2716.340 m is conductive because the resistivity reading by LLs and LLd is lower than the normal trend. This fracture zone can be hydraulic open fracture filled with brine (also see fracture F, Figure 3.14, Chapter 3).

From Figure 4.4, a single fracture at depth 2830.070 m is a resistive one because the resistivity reading by LLs and LLd is slightly higher than the normal trend. This fracture zone can be a hydraulic open fracture filled with hydrocarbon.

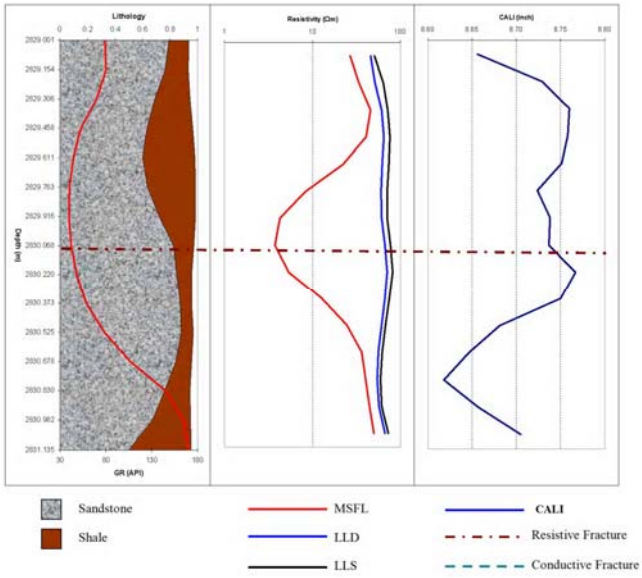

Figure 4.2 MSFL reads low resistivity spikes opposite a resistive open fracture at 2830.070 m depth.

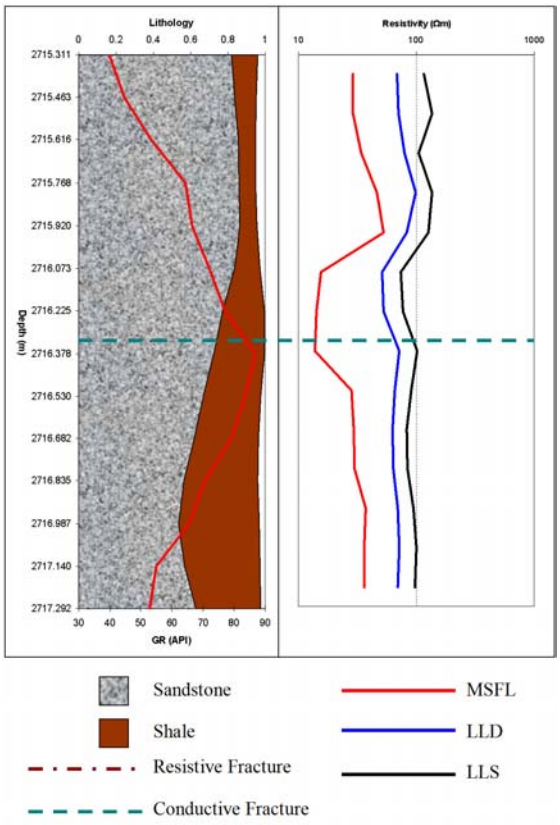

Figure 4.3 Illustrated MSFL reading low resistivity spikes opposite the conductive opened fracture at depth 2716.340 m and the small reduction of resistivity reading by LLs and LLd.

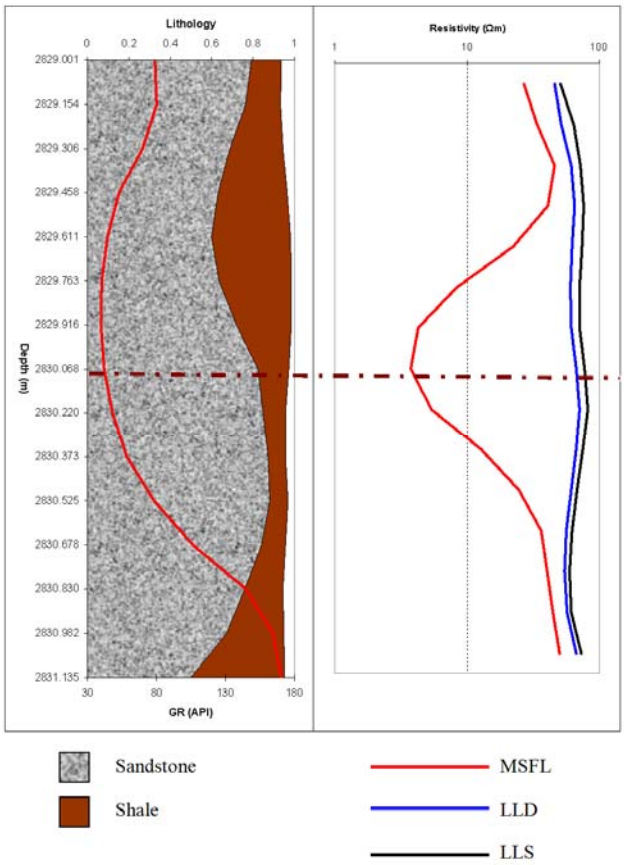

Figure 4.4 MSFL reads a low resistivity spike opposite a resistive open fracture at depth 2830.070 m and a small increase of the resistivity reading by LLs and LLd.

4.1.3 Fracture identification from sonic log

The sonic log is quite successful for fracture characterization because the sonic compressional and shear slownesses show an increase in the delta (Δt) time in front of an open fracture and a decrease of the delta (Δt) time in front of the sealed fractures with higher compaction (see Figure 4.5). Fracture Q in Figure 3.18, for example, also shows the same response by compression wave delta time**.**

The delta time of shear wave is also effected by fracture occurrence by showing an increase of the shear wave slowness or transit time of the shear wave, especially in fluid filled fractures (see Figure 4.6).

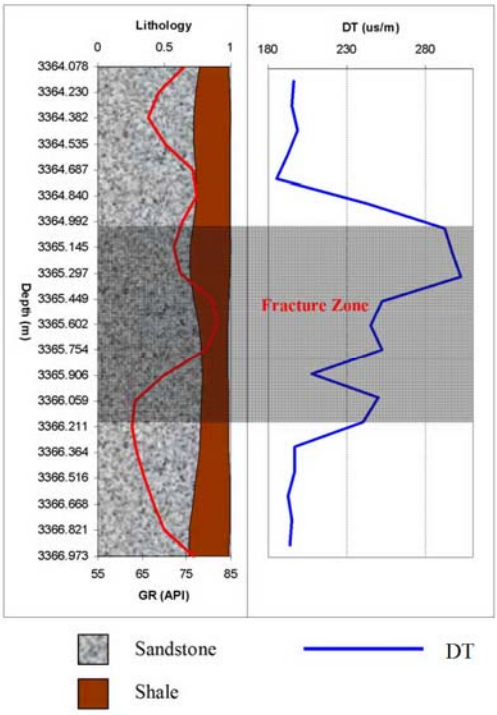

Figure 4.5 Compressional wave slowness increases at a fracture zone at 3364.992 – 3366.211 m depth.

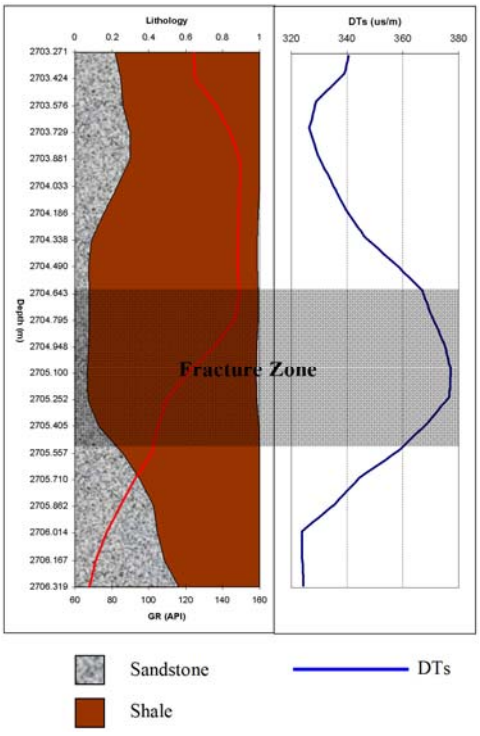

Figure 4.6 Shear wave slowness increases at the fracture zone at depth 2704.643 – 2705.550 m.

Fluids and fluid filled fractures do not transmit shear waves as well as P–waves, and the shear arrivals are strongly attenuated in fractured zones. Hence, the delta time of shear wave strongly increase at fluid filled fractures. Then the ratio of Vp/Vs or t_S/t_C or $\Delta t_S/\Delta t_C$ is significant to the fluid filled fractures by showing a higher value. Because some fracture or fracture zones only slightly affect the compressional waves but affect more the shear waves (see Figure 4.7 and 3.17).

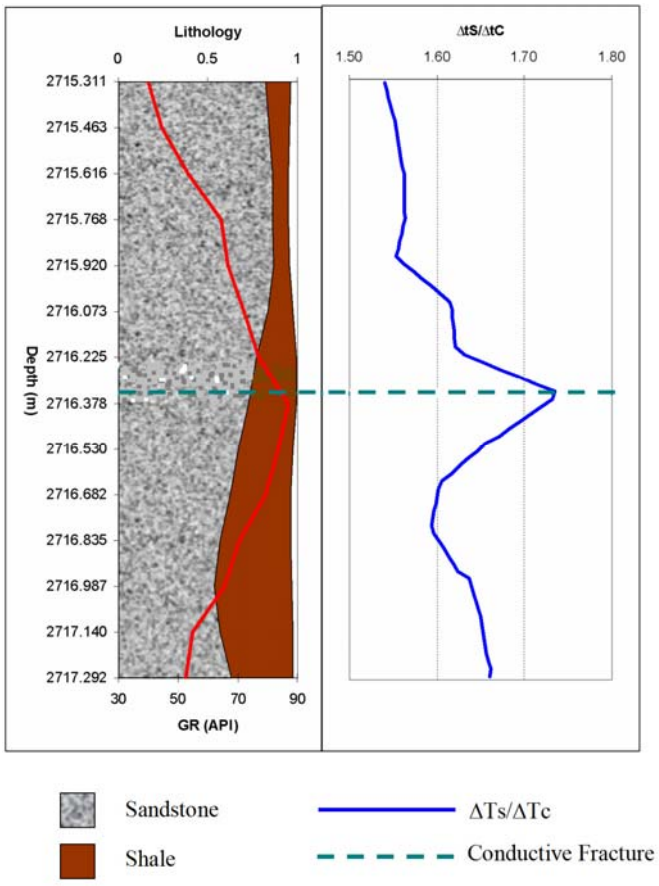

Figure 4.7 Fracture data from FMS and convention logging data between depths 2713.635 – 2718.816 m and the response of the sonic log, here as $\Delta t_S/\Delta t_C$.

4.1.4 Fracture identification from caliper log

Some fractures or fracture zones can be detected by caliper log if the borehole will become oblong by the drilling when it intersects a fracture. This looks like a borehole washout, but rough, large, or irregular borehole in otherwise competent rock

usually indicates fractures (see Figure 4.8). Single fracture R (see Figure 3.19) is a good example for fracture characterization by caliper log.

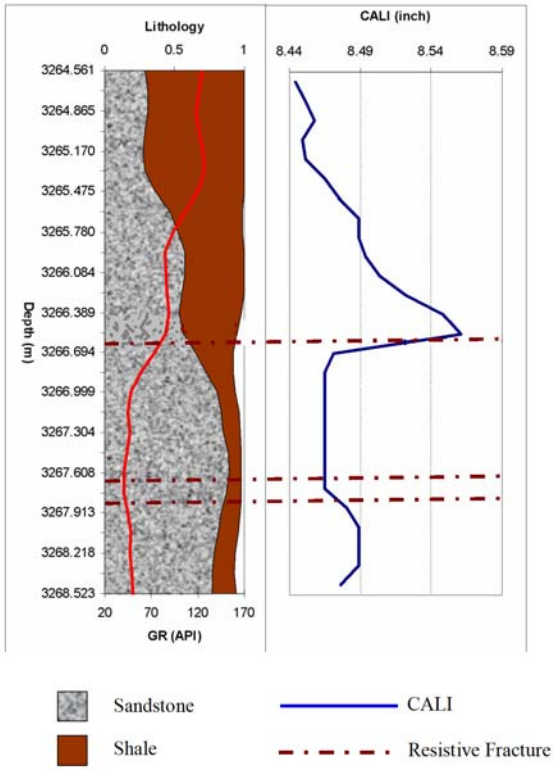

Figure 4.8 Fracture data from FMS and convention logging data between depths 3262.274 – 3270.504 m and the response of the caliper log.

4.1.5 Fracture identification from photoelectric log

The photoelectric absorption log is quite successful for fracture characterization. The PE curve exhibits a very sharp peak in front of a fracture filled with barite loaded mud cake, especially when weighted mud are used, which then is a fracture indicator (see Figure 4.9). Figure 3.28 and 3.29 also show the same results, higher values of photoelectric absorption in front of the fracture.

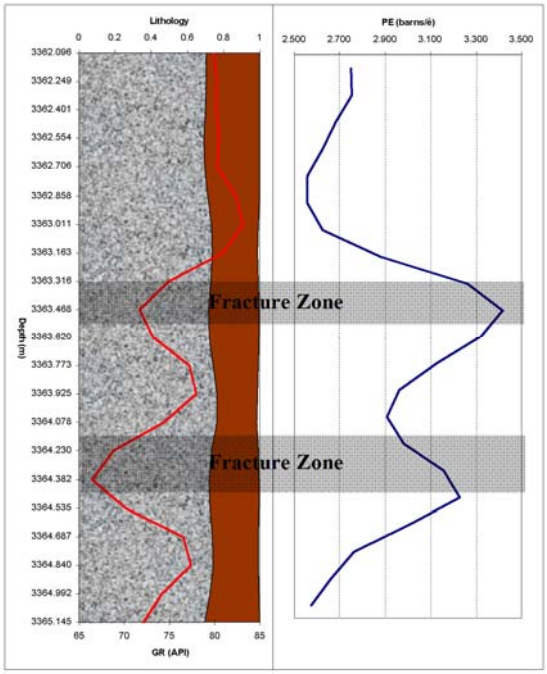

Figure 4.9 Fracture data from FMS and convention logging data between depths 3358.439 – 3368.802 m and the response of the photoelectric absorption log.

4.1.6 Fracture identification from log combination

In fracture characterization no single conventional well log provides reliable characterization of the fractures in the wellbore, hence a combination of different logs with a review of all available log curves together provides the best coherent results available. In the following main log combination are discussed.

Fracture or wash out

In some cases the MSFL resistivity reading is very low and close to the mud resistivity but there is no fracture present according to FMS, but borehole breakout occurred (see Figure 3.23). This is an ambiguous result whether it is a fracture or borehole breakout response of the MSFL and other logging data.

Considering Figure 4.10 the washout occurred at a depth interval around 2621.938 – 2622.396 m, and it affected all logging data in the same way as it would be a fracture: with a resistivity reading from MSFL very low, a compressional wave slowness increased, caliper log reading higher than normal, photoelectric absorption

higher due to barite in the drilling mud, and a bulk density reading very low. In this case it can be decided sure that a fracture is present if the caliper log shows a stable borehole size (see Figure 3.12).

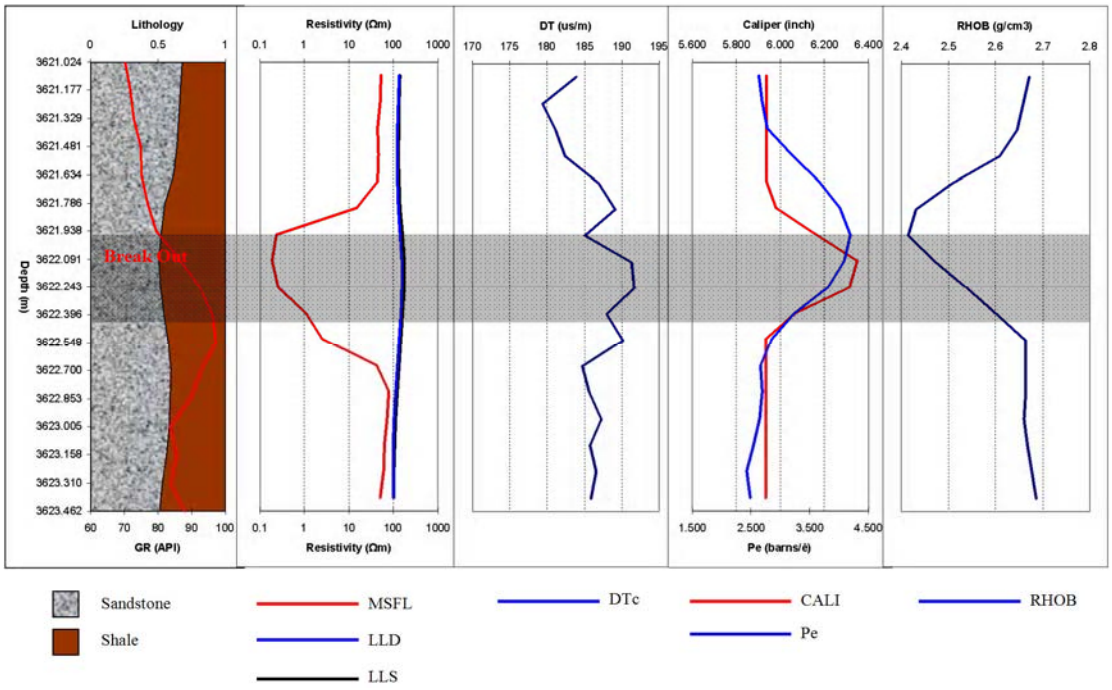

Figure 4.10 Borehole breakout zone at a depth between 2621.938 – 2622.396 m and the response of the conventional logging data.

Closed or open fractures

In case closed fractures occur, then normally they are resistive fractures with high resistive minerals sealing. This type of fracture might be not characterized by only one logging tool, but all logs should be under consideration. From Figure 4.11 mineralized fractures present and response to logging data by MSFL, LLd and LLs showing higher resistivity reading than the normal trend. The bulk density shows a high value, the compressional slowness decreases because of high compaction, and the borehole size is not much changed (also see Figure 3.13).

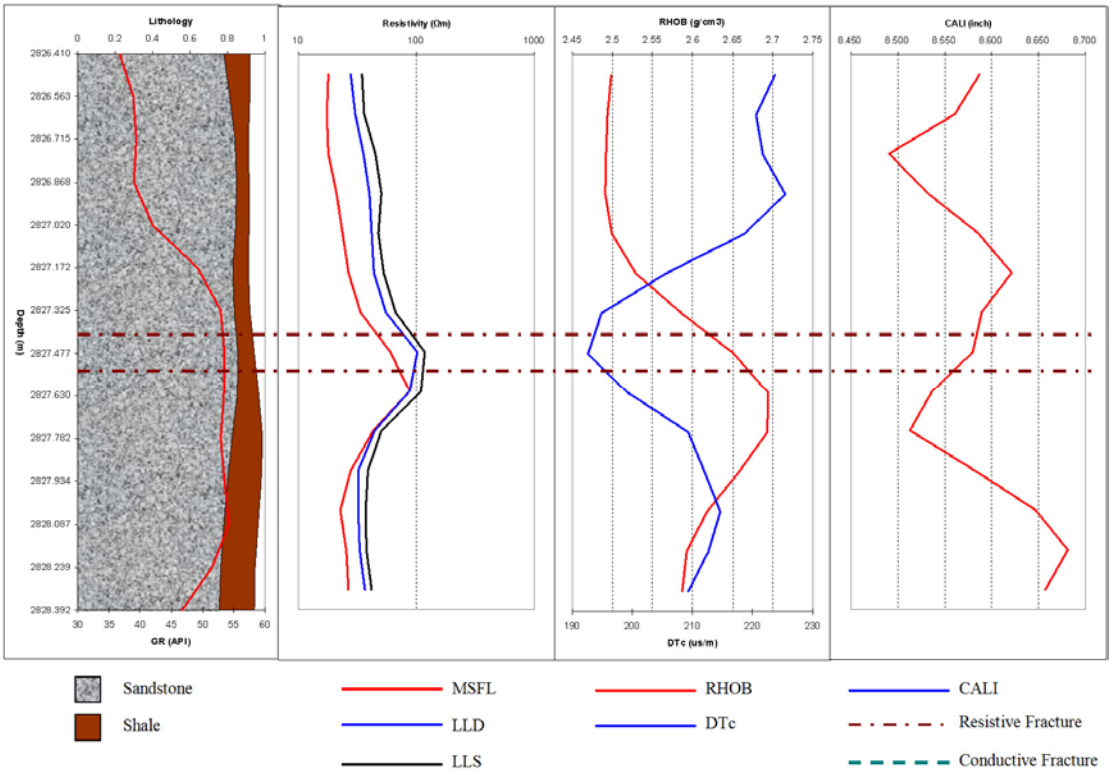

Figure 4.11 Closed or sealed fracture at depth 2827.390 and 2827.520 m with the response to the resistivity log, density log, sonic log, and caliper log.

Coal content

Coal content is also making an ambiguous response to the fracture characterization because the mechanical weaker coal can easier break during the drilling process and its response to conventional logging data is similar to fractures and wash out. However, the photoelectric absorption of coal in this well is relatively low with around 1.78 barns/ê, so that this data can be used to reliably separate between coal and natural fractures.

Figure 4.12 shows at a depth of around 3100.426 m the response of logging data: the MSFL resistivity reading is low, the compressional wave slowness is increased, caliper log measure the borehole size bigger than normal, and bulk density reading is very low while neutral porosity is increased as coal can generate some gas. However, the photoelectric absorption with around 1.45barns/ê identified this as a coal seam and not a natural fracture.

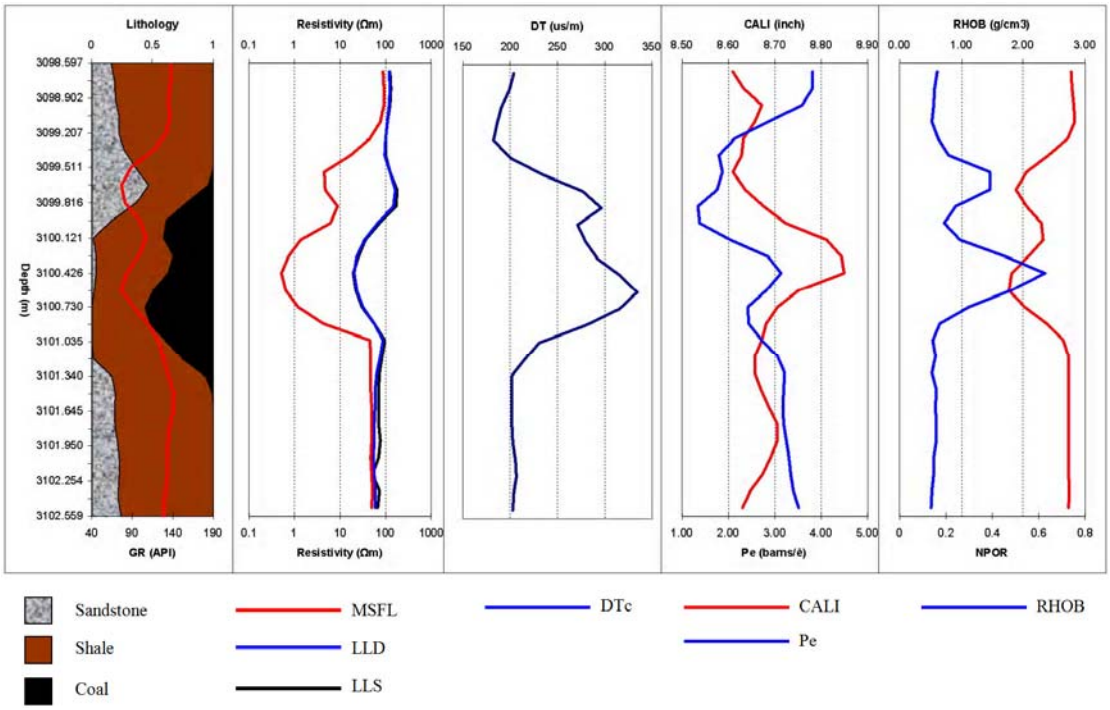

Figure 4.12 Illustrated the coal content zone at depth between 3399.816 – 3101.340 m response to convention logging data.

4.1.7 Conventional logging correlated with FMS

FMS is a very specific and high resolution tool used for detailed structural interpretation such as fractures size, orientation and the resistivity of fluids filled (see Figure 1.8 and 1.9) by using a running speed very low to get the sampling interval around 0.25 cm. The objective of conventional tool runs is to identify productive zones, depth and thickness of zones, to distinguish oil, gas or water in a reservoir, and to estimate hydrocarbon reserves. Because of this conventional logging data do not need high resolution sampling intervals as the FMS tool.

This research used conventional logging data with a sampling interval of 15.2 cm for the logging data set 1, and 2.5 cm for the logging data set 2. Because of this the conventional logging data have some limitations in detecting fractures compared to FMS. First, single fractures or fracture zones should be large enough or somehow larger than the sampling interval, because if they are smaller than the sampling interval the tools might not see them (see Figure 3.25-3.28). Second, conventional tools cannot see the orientation of fracture planes, which is often also not necessary, but they can determine the changes a possible fracture has on the conventional tools.

Therefore, open fractures can be detected because of the drilling mud flows into the fractures and by this affecting the MSFL reading, or even the LLs and LLd data. For the closed or sealed fracture is more difficult to identify them with conventional tools because, for example, LLd and LLs integrate resistivity over a bulk rock mass, hence a small compacted fracture may have little effect to the resistivity. Some times a small group of tight but closely spaces fractures can affect porosity or water saturation sufficiency to give rise to a small anomaly on an electrical resistivity or density log. However, closed fractures are not of primary importance in reservoir fracture characterization.

Although both FMS and MSFL are resistivity tools they are different in data acquisition and interpretation. Therefore, in this research a success rate for fracture characterization between the FMS and conventional logging data cannot be given. FMS sees more or less all fractures, with different aperture and different fluid or mineral content. However, with examples here from many single fractures and fracture zones it could be shown that conventional logging methods with known limitations can be used successfully to evaluate and identify fractures in a well drilled in a fractured reservoir as discussed above.

4.1.8 Checklist for fracture identification

In the following a checklist is given that can be used as a guideline for fracture identification using conventional logging data. There is a potential range of conventional logs that can be used to interpret qualitatively the presence of fractures. Table 4.1 is a summary of fracture responses from conventional logs.

Table 4.1 Qualitative fractures characterization by conventional logging data.

Logging data	Open fracture		Sealed fracture		Washout
	Brine filling	HC filling	Radioactive mineralized	Non-radioactive mineralized	
1. GR	Decrease	Decrease	Increase	Decrease	Decrease
2. RHOB	Decrease	Decrease	Increase	Increase	Decrease
3. DTc	Increase	Increase	Decrease	Decrease	Increase
4. DTs	Increase	Increase	Decrease	Decrease	Increase
5. DTs/DTc	Increase	Increase	Stable	Stable	Increase
6. MSFL	Decrease	Decrease	Stable/ Increase	Stable/ Increase	Decrease
7. LLs	Decrease	Increase	Stable/ Increase	Stable/ Increase	Decrease
8. LLd	Decrease	Increase	Stable/ Increase	Stable/ Increase	Decrease
9. CALI	Increase	Increase	Stable	Stable	Increase
10. PEF	Increase	Increase	Stable	Stable	Increase
11. NPOR					

From Table 4.1 it can be seen that the steps of fractures characterization for fractures filled with HC and brine are similar, but only LLs and LLd is different. If an open fracture is hydraulic then mud can fill inside the fracture, therefore both HC filling and brine filled fractures show lower MSFL reading. This is caused by the mud that pushed the formation fluids into the formation and almost the entire flushed zone is filled with conductive mud. However, LLs and LLd, which measure deeper formation resistivity, both or one can detect the fluids filling the fractures by showing a small anomaly. If both or one of them do not show any change in the signal then fractures filling can not be characterized. Other logging data should be considered to confirm the fracture, especially sonic log, DTs, which is more affected by liquid filling; it should be decreased, and DTs also the same but less effect than DTc. Hence, the ratio of DTs/DTc is significant to fluids filling fractures because of DTs is more attenuated than DTc. PEF is also used for more reliable analysis of a fracture presence by showing a higher value in front of open fractures filled with mud which composed of barite. RHOB is decreased if a fracture is present because of the fractures induced secondary porosity and density decreased inverse to the porosity increase. In some cases CALI shows a bigger borehole in front of open fractures caused by drilling break but; however a wash out also shows the same result; in this case FMS fracture data is more reliable.

Sealed fractures normally are mineralized with higher compaction and therefore they are mainly resistive. Hence, MSFL, LLs and LLd should be reading higher resistivity values than the normal trend, but if the resistivities contrast between

mineralized fractures and normal formation is not much they might not see it. However, for this type of fracture with high compaction the DTc and DTs should be decreased because the velocity of sonic wave can perform faster and RHOB should be reading higher in front of this fracture. In some cases fractures are sealed with radioactive mineralization and then the gamma ray log show higher GR reading, but this phenomenon mostly occur in metamorphic rocks.

4.1.9 Fracture index

The various log derived fracture indicators can be merged which allows a wide variety of inputs. The input curves are assigned a threshold value, a median value, and a maximum probability as a fracture detector. In addition, each input is weighted according to its correlation to natural fracturing in the specific area (Crain, 2003).
In this study, the weighting is assigned to the MSFL, DTc, RHOB, CALI and PEF. The output is a fracture probability curve or fracture index. Figure 4.13 and 4.14 shows the result of fracture index by using the fracture index equation below, which was developed for this study:

Fracture index = ((DTc>Average+Stdev)+(MSFL< Average-Stdev)+(RHOB< Average-Stdev)+(CALI> Average+Stdev)+(PEF> Average+Stdev))/N (4.1)

where Stdev = Standard Deviation and N = number of thresholds tested. For the thresholds all curves have equal weight and the amount of excursion of a curve beyond its threshold is not considered. The result is normalized between 0.0 and 1.0 by the number of thresholds tested.

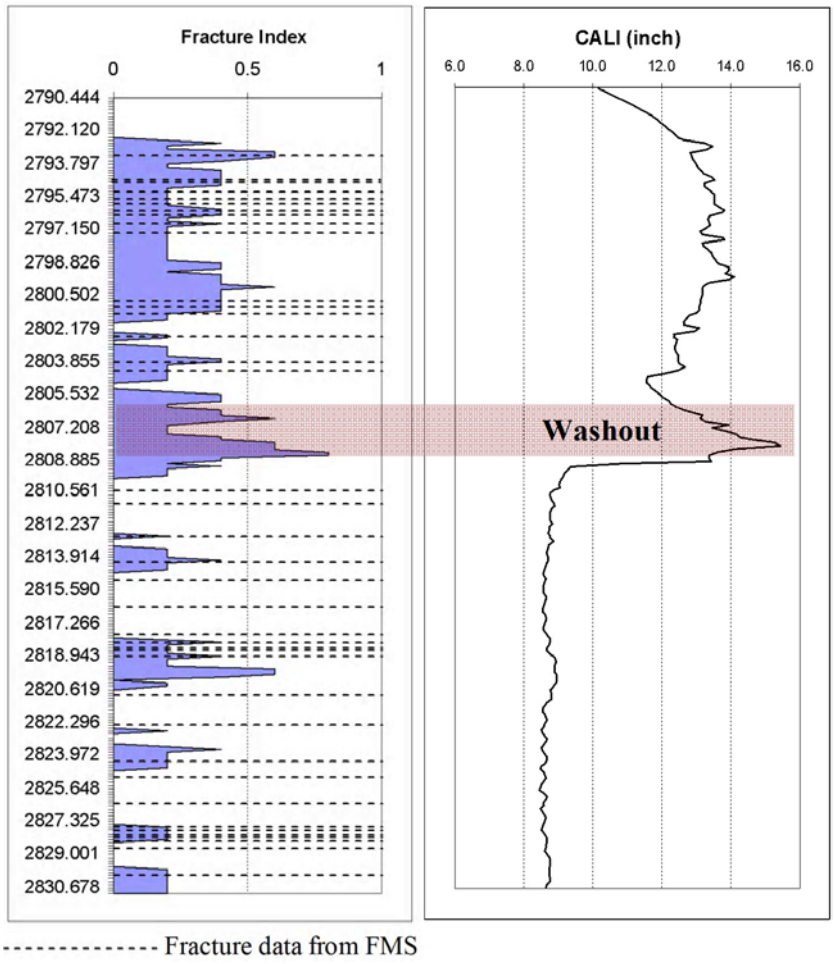

Figure 4.13 Fracture index correlated with fracture data from FMS between depths 2790.444 and 2830.678 m.

Figure 4.13 and 4.14 shows the result for selected sandstone layers, where the fractures index is correlated to fracture data from FMS, especially focusing on fracture zones. In general the fracture index shows higher values in the fracture zones and also for selected single fractures. However, some calculated results such as on Figure 4.13, at depths between 2805.500 and 2809.000 m show a high fracture index but no fractures present in FMS data because this zone is effect by borehole enlargement or washout

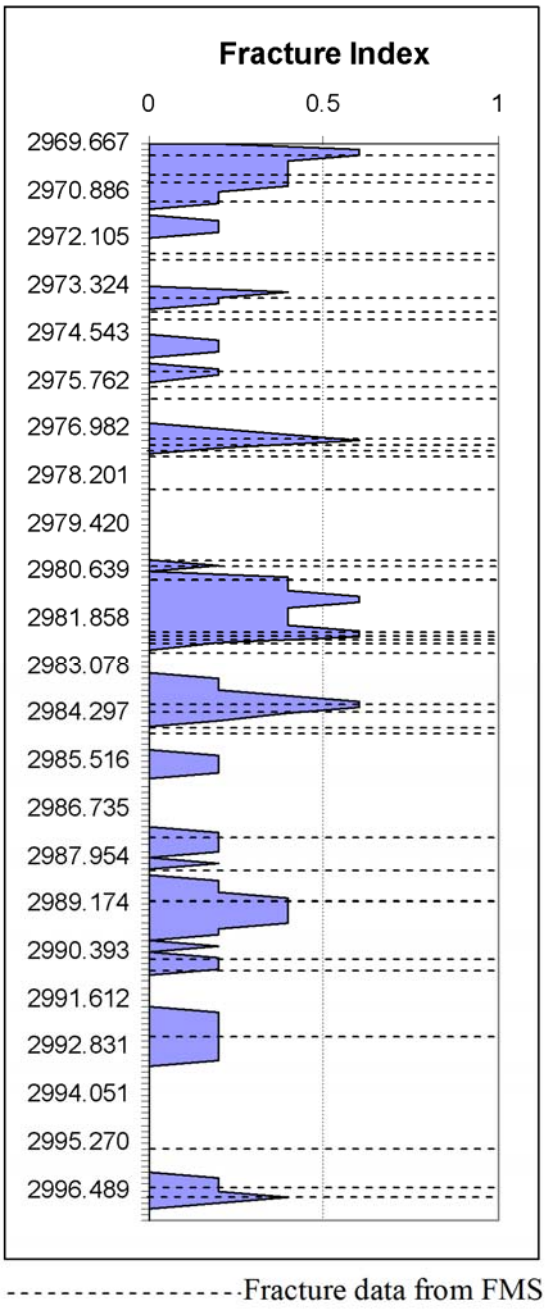

Figure 4.14 Show the fracture index correlated with fractures data from FMS between depths 2969.667-2997.251 m.

4.2 Conclusions

Fracture characterization in hydrocarbon reservoirs is today and likely in the future still an important issue, not only for clastic reservoir but also for carbonate reservoirs. From the result shown in Chapter 3 and the discussion above it can be

concluded that conventional logging data can be successful applied for fracture characterization by separate the response signal into two different types of fractures.

First, when open fracture occur, the RHOB is reading lower than normal in front of the present open fracture while DTc, DTs and the ratio of DTs/DTc is increasing. MSFL show low reading value close to mud resistivity, LLs and LLd may be affected by showing a very small anomaly which can be identify by the resistivity of fluid filled fracture. The PEF increases because of mud composed with barite filled inside open fractures. However if the caliper log shows bigger hole size it might be possible to have washout but not fracture present. Photoelectric log is also the good tool to separate between fracture and coal content because if mud filled inside the fracture or washout the photoelectric absorption shows a higher peak than normal but it shows a very low value if a coal layer is interbeded.

Second, when sealed or mineralized fracture occurs, the RHOB, DTc, DTs and the ratio of DTs/DTc show higher values than normal because of high compaction. This type of fracture is normally filled with resistive minerals and possible can be detect by resistivity log by MSFL, LLd and LLS showing a very small increase. However some fracture or fracture zone can not see by conventional logging data because of maybe fracture aperture smaller than sampling interval. To avoid this lower speed of measurements might be achieved to get smaller sampling intervals.

Third, a more general fracture checklist for the identification was established based on the relationships identifies and learned from the qualitative fracture response of conventional logging tools and the correlation with FMS data. This checklist might be used also for other wells with similar lithology (clastic reservoirs).

Fourth, a fracture index was established and determined for this well by using threshold and input weight of the conventional logging data. The correlation of the fracture index with the FMS especially for the fracture zones is quite good. The fracture zones probably are mainly hydraulic fractures and contribute to the overall fluid flow system more than single fractures.

Finally, this study has confirmed that conventional logging has a good potential to be used in fracture reservoir characterization. For further work it would be preferable to have core data for a correlation as cores would provide a realistic picture of the fracture size and properties.

REFERENCES

Antonellini, M. and Aydin, A., 1995. Effect of faulting on fluid flow in porous sandstones: geometric properties. American Association of Petroleum Geologists Bulletin 79, p. 642-671.

Barton, C.A. and Zoback, M.D., 1990. Self-similar distribution of macroscopic fractures at depth in crystalline rock in the Cajon Pass scientific drillhole. In: Rock Joints, Rotterdam ISBN 90 6191 109 5, p. 163-170.

Bates, R.L. and Jackson, J.A., 1980. Glossary of Geology, 2d ed. Falls Church, Va. American Geological Institute.

Bassiouni, Z., 1994. Theory, Measurement, and Interpretation of Well Logs, SPE Textbook Series, Vol. 4.

Boggs, J.R., 2000, Principles of sedimentology and stratigraphy, 3rd ed. Toronto: Merril Publishing Company.

Crain, E.R., 2003. Crain's Petrophysical Handbook. Publications.

Crampin, S., 1981. A review of wave motion in anisotropic and cracked elastic media. Wave Motion, p. 343-391.

Crampin, S., 1986. Anisotropy and Transverse Isotropy, Geophysical Prospecting 34, p. 96-99.

Crampin, S., 1989. Suggestions for a consistent terminology for seismic anisotropy, Geophys. Prospect., 37, p. 753–770.

Crampin, S., Holmes, G.M. and Young, P., 1993. Preliminary analysis of shear-wave splitting in granite at the underground research laboratory, Manitoba: Can. J. Expl. Geophys. 29, p. 140-152.

Czubek, J.A., 1983. Advances in gamma–gamma logging. In: C.G. Clayton, Editor, Nuclear Geophysics, Selected Papers on Applications of Nuclear Techniques in Mineral Explorations, Mining and Process Control, Pergamon Press, Exeter, p. 153–172.

Dershowitz, W. and LaPointe, P., 1995. Discrete Fracture Approaches for Oil and Gas Applications. Proceedings, NARMS '94, Northern American Rock Mechanics Symposium, Austin, TX. Balkema, Rotterdam.

Ekstrom. G., Dziewonski, A.M. and Woodhouse, J.H., 1987. Centroid-moment tensor solutions for the 51 IASPEI selected earthquakes, 1980-1984, Phys. Earth Planet, Inter., 47, p. 62-66.

Ellis, D.V., 1987. Well logging for earth scientists. Elsevier, Amsterdam.

Fertl, W.H., 1979. Gamma ray spectral data assists in complex formation evaluation. Log Analyst, v. 20, no. 5, p. 3-37.

Fertl, W.H. and Rieke, 1979. Gamma ray spectral evaluation techniques identify fractured shale reservoirs and source rock characteristics. Society of Petroleum Engineers, of the American Institute of Mining, Metallurgical, and Petroleum Engineers Paper SPE 8454, p. 14.

Fletcher, R.C. and Pollard, D.D., 1981. Anticrack model for pressure solution surface. Geology, p. 419–424.

Haggas, S., Brewer, T.S., Harvey, P.K. and Iturrino, G., 2001. Relocating and orienting cores by the integration of electrical and optical images: a case study from Ocean Drilling Program Hole 735B. J. Geol. Soc. (London, U.K.), 158, p. 615–623.

Holmes, G.M., Crampin S. and Young R.P., 1993. Preliminary analysis of shear-wave splitting in granite at the Underground Research Laboratory, Manitoba. Can. J. Expl. Geophys., 29, p. 140-152.

Holstein, E.D., 2007. Petroleum Engineering Handbook, Volume V. Reservoir Engineering and Petrophysics.

Howard, K.W.F., 1990. Geophysical well logging methods for the detection and characterisation of fractures in hard rocks. In: S.H. Ward, Editor, Investigations in Geophysics, No. 5 Geotechnical and Environmental Geophysics vol. I, Society of Exploration Geophysicists, p. 287–307.

Hudson, J.A., 1981. Wave speeds and attenuation of elastic waves in material containing cracks, Geophys. J. R. astr. SOC., 64, p.133-150.

Hughes, D., 2002. An Overview of the Caltrans Borehole Geophysical Logging Program. Geophysics and Geology Branch, California Department of Transportation, Sacramento, California.

Hyne, N.J., 2001. Nontechnical Guide to Petroleum Geology, Exploration, Drilling, and Production. PennWell Corporation.

Jakobsen, P.R. and Rosenbom, A.E., 2004. Infrared Thermography and Fracture Analysis of Preferential Flow in Chalk. Vadose Zone Journal, Vol. 4 No. 2, p. 271-280.

Keys, W.S., 1988. Borehole geophysics applied to ground water investigations. U.S. Geological Survey.

Keys, W.S., 1990. Borehole Geophysics Applied to Ground-water Investigations, Techniques of Water Resources Investigations of the U.S. Geological Survey, Book 2, Chapter E2.

Kierstein, R.A., 1984. True location and orientation of fractures logged with the acoustic televiewer including programs to correct fracture orientation. U.S. Geological Survey Water Resources Investigations Report 83-4275. 42 pp.

Kokesh, F.P., Schwartz, R.J., Wall, W.B. and Morris, R.L., 1965. A new approach to sonic logging and other acoustic measurements. Petrol. Technology, v.17, p. 282-286.

Kuhfal, D., Lacazette, A. and Thomas, A.R., 2007. Fracture Development in Salt Dome Caprock, Hardin County, Texas. Search and Discovery Article.

Lacazette, A., 2001. NaturalFractures.com. LLC, Houston, TX.

La Pointe, P.R. and Dershowitz, W.S., 1994. Discrete Fracture Approaches for Oil and Gas Applications. Proceedings: 1st North American Rock Mechanics Symposium, The University of Texas at Austin, p. 19-30.

Lau, J.S.O., 1983. The determination of true orientations of fractures in rock cores. Canadian Geotechnical Journal 20 (3), p. 221– 227.

Licht, W. and Dublin, T., 2005. The Face of Decline: The Pennsylvania Anthracite Region in the Twentieth Century. Cornell University Press.

Lovell, M.A., Harvey, P.K., Brewer, T.S., Williams, C., Jackson, P.D. and Williamson, G., 1998. Applications of FMS images in the Ocean Drilling Program. Geological Society [London] Special Publication No. 131, p. 287-303.

Luthi, S.M. and Souhaite, P., 1990. Fracture apertures from electrical borehole scans. Geophysics 55, p. 821-833.

National Academy of Sciences, 1996. Rock fractures and fluid flow. Commission on Geosciences, Environment and Resources.

Pollard, D.D. and Segall, P., 1987. Theoretical displacements and stresses near fractures in rock: with applications of faults, joints, veins, dikes, and solution surfaces in Fracture Mechanics of Rock. B. K. Atkinson, ed. London: Academic Press, p. 277–349.

Rider, M.H., 1986. The geological interpretation of well logs. John Wiley & Sons, Inc., New York, p. 175.

Rosenbom, A.E. and Jakobsen, P.R., 2004. Infrared Thermography and Fracture Analysis of Preferential Flow in Chalk. Vadose Zone Journal, Vol. 4 No. 2, p. 271-280.

Schafer, J.N., 1979. A practical method of well evaluation and acreage development for the naturally fractured Austin Chalk formation, paper U, in 20th Annual Logging Symposium Transactions: Society of Professional Well Log Analysts, p. 25.

Schlumberger, 1999. Log Interpretation Principles / Applications.

Schlumberger, 1989. Log Interpretation Principles/Applications. Schlumberger Educational Services. Houston, Texas, 250 pp.

Schlumberger, 1991. Log Interpretation Principles/Applications. Schlumberger Educational Service, Houston, Texas.

Schlumberger, 1995. DSI-Dipole Sonic Imager. Schlumberger Wireline and Testing, SMP-5128.

Schoen, D.A., 1996. Educating the reflective practitioner: Toward a new design for teaching and learning in the professions. San Francisco: Jossey-Bass, Inc.

Secor, D.T., 1969. Mechanics of natural extension fracturing at depth in earth's crust. Geological Survey of Canada Paper 68-52, p. 3-48.

Serra, O., 2004. Well Logging - Data Acquisition and Applications. ISBN.

Serra, O., 1979. Fundamentals of well log interpretation. The acquisition of logging data: Amsterdam, Elsevier, p. 423.

Serra, O., 1984. Fundamentals of well log interpretation. The acquisition of logging data: Amsterdam, Elsevier, p. 423.

Serra, O., 1989. Formation MicroScanner image interpretation. Schlumberger Educational Service, p. 117.

Tracy, R.J., 1996. Petrology: igneous, sedimentary and metamorphic. 2nd ed, Freeman, 281 - 292

Wti, J.S., Tittman, I. and Johnstine, C.W., 1964. The Dual Spacing Formation Density Log. J. Per. Tech.

VITAE

Name Mr. Paitoon Laongsakul

Student ID 4722142

Education

Degree	Name of Institution	Year of Graduation
B.Sc. (Physics)	Prince of Songkla University	1999

Work position and address

Data Engineer at Weatherford KSP Company Limited 555 Rasa Tower, 19th Floor, Phaholyothin Road, Kwaeng Chatuchak Khet Chatuchak Bangkok 10900 THAILAND

List of publication and proceeding

Laongsakul, P. and Dürrast, H., 2010. Characterization of Reservoir Fractures Using Conventional Geophysical Logging. Proceeding of the 5th International Conference on Applied Geophysics, p. 67-76.